ASSESSMENT OF TRANSPARENT LUMINESCENT SOLAR CONCENTRATORS FOR BUILDING INTEGRATED PHOTOVOLTAICS

A THESIS SUBMITTED TO
THE GRADUATE SCHOOL OF NATURAL AND APPLIED SCIENCES
OF
MIDDLE EAST TECHNICAL UNIVERSITY

BY

TIMOTHY BUNOTI

IN PARTIAL FULFILLMENT OF THE REQUIREMENTS
FOR
THE DEGREE OF MASTER OF SCIENCE
IN
BUILDING SCIENCE IN ARCHITECTURE

FEBRUARY 2022

Approval of the thesis:

ASSESSMENT OF TRANSPARENT LUMINESCENT SOLAR CONCENTRATORS FOR BUILDING INTEGRATED PHOTOVOLTAICS

Submitted by **TIMOTHY BUNOTI** in partial fulfillment of the requirements for the degree of **Master of Science** i**n Building Science in Architecture, Middle East Technical University** by,

Prof. Dr. Halil Kalıpçılar
Dean, Graduate School of **Natural and Applied Sciences** _____

Prof. Dr. Fatma Cana Bilsel
Head of the Department, **Architecture** _____

Assist. Prof. Dr. Mehmet Koray Pekeriçli
Supervisor, **Architecture, METU** _____

Examining Committee Members:

Assoc. Prof. Dr. Ayşe Tavukçuoğlu
Department of Architecture, METU _____

Assist. Prof. Dr. Mehmet Koray Pekeriçli
Department of Architecture, METU _____

Assist. Prof. Dr. Aktan Acar
Department of Architecture, TOBB ETÜ _____

Date: 10.02.2022

I hereby declare that all information in this document has been obtained and presented in accordance with academic rules and ethical conduct. I also declare that, as required by these rules and conduct, I have fully cited and referenced all material and results that are not original to this work.

Timothy Bunoti

Signature:

ABSTRACT

ASSESSMENT OF TRANSPARENT LUMINESCENT SOLAR CONCENTRATORS FOR BUILDING INTEGRATED PHOTOVOLTAICS

Bunoti, Timothy
Master of Science, Building Science in Architecture
Supervisor: Assist. Prof. Dr. Mehmet Koray Pekeriçli

February 2022, 178 pages

Despite the recorded increase in the installed capacity of solar energy resources globally, its use in urban areas is still limited and hindered due to the lack of sufficient solar real estate in cities. Irregularity of the city skyline that often results in large shaded areas and the slenderness of high-rise city buildings that limits the available rooftop area for installing conventional solar PV panels have been the main contributors to this phenomenon. Thus, there is a pressing need to devise creative means to harvest solar energy and increase solar real estate in densely populated urban areas.

Converting conventional mono-functional building envelope materials into multi-functional energy harvesting ones is one of the ways solar real estate could be expanded in urban areas. As an emerging technology, Luminescent Solar Concentrators have shown the possibility of transforming the predominantly transparent city building facades into solar energy generators while maintaining transparency and unobstructed vistas for the building occupants. However, LSC technology is still in its infancy despite its foreseen potential to expand solar real

estate in urban areas. Its full growth and quick advancement call for more research efforts to be invested.

Thus, this research seeks to add to the ongoing research in this area of technology by proposing an 8 step framework that can be deployed to determine the electrical output of transparent LSC devices. Computer software is used to demonstrate the framework's application on a selected reference building located in a densely populated urban neighbourhood while considering all potential known benefits of this technology, such as adequately functioning under diffuse lighting. The results showed that though the technology is still in its infancy, it can produce enough electricity to subsidize the actual building energy demand by a rather outstanding value annually.

This thesis also presents a general overview of PV technology and its advancements while highlighting the milestones, especially regarding power conversion efficiencies and material usage achieved to date.

Keywords: Building Integrated Photovoltaics (BIPV), Luminescent Solar Concentrators (LSC), Renewable Energy (RE), Photovoltaics (PV)

ÖZ

ŞEFFAF LÜMİNESAN GÜNEŞ KONSANTRATÖRLERİNİN BİNALARA ENTEGRE FOTOVOLTAİK UYGULAMALARI İÇİN DEĞERLENDİRİLMESİ

Timothy, Bunoti
Yüksek Lisans, Yapı Bilimleri, Mimarlık
Tez Yöneticisi: Dr. Öğr. Üyesi Mehmet Koray Pekeriçli

Şubat 2022, 178 sayfa

Dünya genelinde güneş enerjisi kaynaklarının kurulu gücünde kaydedilen artışa rağmen, bu şehirlerde yeterli güneş enerjisi gayrimenkulünün bulunmaması nedeniyle kentsel alanlarda kullanımı hala sınırlı ve engelleniyor. Genellikle geniş gölgeli alanlara neden olan şehir silüetinin düzensizliği ve konvansiyonel güneş PV panelleri kurmak için mevcut çatı alanını sınırlayan yüksek katlı şehir binalarının inceliği bu fenomene ana katkıda bulunmuştur. Bu nedenle, yoğun nüfuslu kentsel alanlarda güneş enerjisi hasadı ve güneş gayrimenkulünü artırmak için yaratıcı araçlar tasarlamak için acil bir ihtiyaç vardır.

Geleneksel tek işlevli bina kabuğu malzemelerini çok işlevli enerji hasadı malzemelerine dönüştürmek, kentsel alanlarda güneş enerjisi gayrimenkulünün genişletilmesinin yollarından biridir. Gelişmekte olan bir teknoloji olarak, Lüminesan Güneş Yoğunlaştırıcılar, bina sakinleri için şeffaflığı ve engelsiz manzaraları korurken, ağırlıklı olarak şeffaf şehir bina cephelerini güneş enerjisi jeneratörlerine dönüştürme olasılığını göstermiştir. Bununla birlikte, kentsel alanlarda güneş enerjisi gayrimenkulünü genişletmek için öngörülen potansiyeline rağmen, LSC teknolojisi hala emekleme aşamasındadır. Büyümesinin tam meyve vermesi için daha fazla araştırma çabasına yatırım yapılması gerekiyor.

Bu nedenle, bu araştırma, şeffaf LSC cihazlarının elektrik çıkışını belirlemek için konuşlandırılabilecek 8 adımlı bir çerçeve önererek, bu teknoloji alanında devam eden araştırmalara katkıda bulunmayı amaçlamaktadır. Bilgisayar yazılımı, yoğun nüfuslu bir kentsel mahallede bulunan seçilmiş bir referans binada çerçevenin uygulamasını göstermek için kullanılırken, bu teknolojinin yaygın aydınlatma altında yeterli şekilde çalışması gibi bilinen tüm potansiyel faydaları göz önünde bulundurulur. Sonuçlar, teknolojinin henüz emekleme aşamasında olmasına rağmen, gerçek bina enerji talebini yıllık olarak oldukça yüksek bir değerle sübvanse etmeye yetecek kadar elektrik üretebileceğini gösterdi.

Bu tez aynı zamanda PV teknolojisine ve ilerlemelerine genel bir bakış sunarken, özellikle bugüne kadar arşivlenen güç dönüştürme verimlilikleri ve malzeme kullanımı ile ilgili kilometre taşlarını vurgulamaktadır. Son olarak, bu teknolojinin şimdiye kadar tamamlanan gerçek hayattaki uygulamaları, tezin son bölümünde dört örnek olay incelemesinde sunulmaktadır.

Anahtar Kelimeler: Bina Entegre Fotovoltaikler (BIPV), Lüminesan Güneş Konsantratörleri (LSC), Yenilenebilir Enerji (RE), Fotovoltaikler (PV)

TABLE OF CONTENTS

ABSTRACT v

ÖZ vii

TABLE OF CONTENTS ix

LIST OF TABLES xi

LIST OF FIGURES xii

LIST OF ABBREVIATIONS xvi

1 INTRODUCTION 1

1.1 Argument 1

1.2 Aims & Objectives 4

1.3 Procedure 4

1.4 Disposition 5

2 LITERATURE REVIEW 7

2.1 PART 1: Overview of Renewable Energy 7

2.1.1 A Brief Review and Evaluation of Renewable Energy Sources 8

2.1.2 An Argument for Renewables 8

2.2 PART 2: An Overview of Photovoltaic Technology 10

2.2.1 History and Early Evolution of Photovoltaics 10

2.2.2 Operation of Photovoltaic Solar Cells 13

2.2.3 Power Losses in PV Cell Solar Conversions 14

2.2.4 Evolution of Photovoltaic Cell Technology 15

2.2.5 Comparison of Market Share of PV Technologies 16

2.2.6 Concept of the Solar Cell 18

2.3 PART 3: Building Integrated Photovoltaics 53
2.3.1 Definition of Building Integrated Photovoltaics 54
2.4 PART 4: An Overview of Transparent Photovoltaics 74
2.4.1 Types of Transparent Photovoltaics 75
2.4.2 Overview of Solar Concentrator Technology 78
2.4.3 Energy Loss Mechanisms in LSCs 84
2.4.4 Components of a Luminescent Solar Concentrator Device 89
2.4.5 Categories of LSC Technologies 92
2.4.6 Challenges Associated with Wave Length Selective TPV and LSCs: 95
2.5 PART 5: Brief Overview of Energy Storage Technologies 99
3 THE FRAMEWORK 103
4 MATERIALS AND METHODS 121
4.1 Research Materials 121
4.1.1 Selection of Reference Building 122
4.1.2 Solar Energy Harvesting System 125
4.2 Research Aim & Methodology 127
4.2.1 Assessment Methods and Data Sources 128
4.2.2 System Performance Simulation 129
5 RESULTS AND DISCUSSION 147
5.1 Overall System Performance Variables and Simulation Parameters 147
5.2 Evaluation of the Electrical Performance of the System 151
5.3 Summary, Final Thoughts and Recommendations 158
6 CONCLUSION 161
REFERENCES 165

LIST OF TABLES

TABLES

Table 2.1 Various PV Technologies and the Year of the First Research Report. (Subtil Lacerda & Van Den Bergh, 2016). 16
Table 4.1 Summary of the Electrical Simulation Variables and Parameters 129
Table 4.2 Summary of Input Parameters 131
Table 4.3 Summary of Relevant Assessment Specifications and Parameters 139
Table 5.1 Balances and Main Results 149
Table 5.2 Summary of System Performance Values 156
Table 5.3 Building Energy Demand 156
Table 5.4 Summary of the Loss Mechanisms in the PV System 157

LIST OF FIGURES

FIGURES

Figure 2.1 Illustration of the Absorption of Photons in a Semi-conductor Material with Bandgap Width Eg (Oliveti et al., 2014). 15
Figure 2.2 Number of Patents per PV Generation for 2002 and 2010. (Subtil Lacerda & Van Den Bergh, 2016). 17
Figure 2.3 Graphic Illustration of the Different PV Technologies (Jelle *et al*., 2012). 18
Figure 2.4 Conversion Efficiencies of Flexible CdTe and CIGS Solar Cells Fabricated by Low-temperature Processes (Jelle *et al*., 2012). 20
Figure 2.5 Mono-crystalline Cell Wafer. 22
Figure 2.6 Polycrystalline Cell Wafer 23
Figure 2.7 The Relationship Between the Open-circuit Voltage and the Average Grain Size (Bergmann & Werner, 2002). 24
Figure 2.8 Manufacturing Process for Crystalline Silicon Wafers (Oliveti *et al*., 2014). 26
Figure 2.9 Images of Monocrystalline Ingot (Left) and Polycrystalline ingots (Right) 27
Figure 2.10 Monocrystalline Cell with a Dark Smooth Appearance (Left); Polycrystalline Cell with a Scattered Blue Appearance (Right) (Alba Energy, 2018). 28
Figure 2.11 Left: Different tones of Coloured Cells (Left); A coloured Solar Module (Right) 29
Figure 2.12 Silicon-based Solar Panels with Curvature Used on the RA 66 Shuttle Designed by Kopf Solar Design. 29
Figure 2.13 Structure with Multi Subdivisions Used to Achieve Façade Curvature with Silicon-based Solar Panels 30
Figure 2.14 FKI Tower, Designed by Adrian Smith + Gordon, Seoul, South Korea 31

Figure 2.15 Structure of Thin-film Solar Cell (Barry, 2018). 33
Figure 2.16 (left) Example of Typical Red-brown a-Si and Black µm-Si Module; (middle) Different Patterns for Different Transparency Levels, Defined in the PV Accept Project; (right)a-Si Modules in Different Colours, Provided by Onyx Solar (Morini, 2021). 35
Figure 2.17 (Left) Exterior Appearance of Perforated Thin-film and its Interior Lighting Effect (Right) Manufactured by Onyx Solar and Installed on Balenciaga's New Storefront in Miami (Kelly, 2018). 36
Figure 2.18 CIGS Based Modules; Modules Manufactured by Manz Used on Façade of House of the German Team at the 2009 Solar Decathlon (Left). CIGS Modules Manufactured by Sulfurcell Used on the Façade of Ferdinand-Braun-Institut für Höchstfrequenztechnik, Berlin. 38
Figure 2.19 CdTe Solar Cell Configurations: (a) Superstrate and (b) Substrate (Basol & McCandless, 2014) 40
Figure 2.20 An Array of CdTe PV 41
Figure 2.21 Organic Photovoltaic 43
Figure 2.22 OPVs Used on the German Pavilion, Milan Expo. (Left); Heliatek's HQ, Dresden (Right). 44
Figure 2.23 Construction of the Dye-sensitized Nanocrystal Line Solar Cells (Sharma *et al*., 2018). 46
Figure 2.24 ye Sensitised Solar Cells of Different Colours (Morini, 2021) 48
Figure 2.25 Designs on a DSSC Achieved by Varying Colour Layer Thickness .. 49
Figure 2.26 Expected Market Applications of DSSC (Market Analysis Report, 2020). 50
Figure 2.27 PSC (black) have Exponential Growth of the Perovskite Solar Cell's Power Conversion Efficiency Since its Inception Compared to other PV Technologies (Ossila, 2021). 51
Figure 2.28 Maximum Photon Energy Utilisation is also referred to as the Open-circuit Voltage (Voc) divided by the Optical Band-Gap for Common Single-junction Cells. 52

Figure 2.29 A Technical Solution to Reduce the Reflectiveness of Module Covers Using a Micro Structured Pyramidal-shaped Top layer (Gochermann Solar Technology, n.d.).....56
Figure 2.30 Different appearances of macroscopic surface textures.....58
Figure 2.31 Figure of Spectrally Selective Morpho-Colour Structure Located on the Inside of the Front Cover (Kuhn *et al.*, 2020).....59
Figure 2.32 A comparison of Thin-Film-based Technologies' Market Share Growth (Paire *et al.*, 2014).....62
Figure 2.33 Comparison of the Different cell Interconnection Methods.....64
Figure 2.34 Standard Busbar Interconnection.....66
Figure 2.35 A Comparison of Two Module Cell Layouts.....67
Figure 2.36 The Façade of the Z3 Building of Ed. Zublin in Germany.....70
Figure 2.37 Predicted Growth of Cell Technologies (Pickerel, 2018).....74
Figure 2.38 Figure of an Energy Diagram for the Ground State (So) and the Two Lowest Occupied Orbitals (S1, S2) for an Excitonic Material (Traverse *et al.*, 2017).....78
Figure 2.39 Modes of Energy Loss in a Lumogen F305 Dye-doped LSC Device. (Moraitis *et al.*, 2018).....86
Figure 2.40 Illustrative diagram.....89
Figure 2.41 Illustration of a Non-wavelength-Selective Solar Concentrator, Coloured LSCs and a Scattering Concentrator. LSCs (Traverse *et al.*, 2017).....93
Figure 2.42 Display of a Wavelength Selective Luminescent Solar Concentrator Device.....94
Figure 2.43 The Schematic Diagram above is of PV Electrical Storage and Usage System (Akbari *et al.*, 2019).....101
Figure 3.1 Pyranometer *(Z. Li et al., 2021).*.....104
Figure 3.2; UV and NIR selectively harvesting LSC device (Yang & Lunt, 2017).....109
Figure 3.3; Schematic figure of LSC device showing different light parts (W. G. J. H. M. van Sark, 2013).....111

Figure 3.4 Possible losses of photons in an LSC device. (Moraitis *et al*., 2018). 112
Figure 3.5 Diagram of an LSC Device (Weber & John, 1976). 115
Figure 3.6 Comparisons of efficiencies for different edge-mounted PV cells..... 118
Figure 4.1 Rectilinear Façade of the Old YKKS Building. 123
Figure 4.2 Transformation of the Concrete Perforate Wall Façade into a Transparent Facade by TEGET Architecture Office 123
Figure 4.3 Views of the building completed in 2017. North Facing façade (Left); South facing façade (Right). 124
Figure 4.4 Illustration of LSC Window (Meinardi *et al*., 2017). 126
Figure 4.5 Image of the LSC Device Used Showing its Size and Effects of Different Spectral Lighting on the Matrix (Meinardi *et al*., 2017). 127
Figure 4.6 Location of the Site along Istiklal Street 133
Figure 4.7 Sun Path along with the Reference-Building Site. 134
Figure 4.8 Sun Paths (Height / Azimuth diagram)..... 135
Figure 4.9 Solar Radiation Simulation on Building Reference Façade. 136
Figure 4.10 PV Module Layout on Façade 141
Figure 4.11 Typical Layout for a Stand-Alone PV System 144
Figure 5.1; Normalised Electrical Production of the System 152
Figure 5.2 System Performance Ratio and Solar Fraction Measurements 155

LIST OF ABBREVIATIONS

ABBREVIATIONS

AM: Air Mass

BIPV: Building Integrated Photovoltaics

C: Carbon

CdS: Cadmium Sulphide

CO: Carbon Monoxide

EES: Electrical Energy Storage

EQE: External Quantum Efficiency

ETM- Electron Transportation Material

FRET: Förster Resonance Energy Transfer

GHG: Green House Gasses

GW: Giga Watts

HTM: Hole Transportation Material

HOMO: Highest Occupied Molecular Orbital

IAM: Incidence Angle Modifier

IEA: International Energy Agency

In_2O_3:H: hydrogen-doped (hydrogenated) Indium Oxide

IR: Infrared

kW: Kilo Watt

kWh: Kilo Watt Hour

LCOE: Lowest Levelized Cost of Electricity

LQE: Luminescent Quantum Efficiency

LSC: Luminescent Solar Concentrator

LUMO: Lowest Unoccupied Molecular Orbital

NIR: Near Infrared

NREL: National Renewable Energy Laboratory

NSRDB: National Solar Radiation Database

PCE: Power Conversion Efficiency

PMMA: Polymethyl Methacrylate

PV: Photovoltaic

QD: Quantum Dots

QY: Quantum Yield

RE: Renewable Energy

Si: Silicon

SnO_2:F: Fluor-doped tin oxide

$SO_{2:}$ Sulphur Dioxide

STC: Standard-Testing Conditions

TCO: Transparent Conductive Oxide

TCO: Transparent Conductive Oxides

TPV: Transparent Photovoltaics

UV: Ultraviolent

W: Watts

ZnO:Al: aluminium-doped zinc oxide

ZnO:B: boron-doped zinc oxid

CHAPTER 1

INTRODUCTION

This chapter presents an introduction to the various topics that will be discussed in the thesis. The first subsection of the chapter makes an argument for the study while providing the reasons behind the study. The second subsection mentions the objectives and aims of the study, while the third subsection lays out the procedure, and the last subsection consists of the disposition that gives a brief layout of all the thesis's major chapters.

1.1 Argument

Total solar power installations have rapidly increased globally over the past decades. By the end of 2019, a total of 627 gigawatts (GW) of global solar power generation was recorded (NS Energy, 2021). The mentioned figures infer a more than double increase from 300 GW installed by the end of 2016 (Bergren *et al.*, 2018). Despite the rapid growth in installation capacity, solar energy still only accounts for less than 5% of the total energy generation worldwide. In fact, by 2018, only 1% of the energy in remote regions globally could be met from the then installed PVs (Xue *et al.*, 2018). On the other hand, the International Energy Agency (IEA) projects a 27% global domination of solar energy production over other energy forms by 2050. However, Bergren et al. (2018) argue that innovative means of harvesting energy in densely populated urban areas are needed to attain this target. The use of solar energy in urban areas has been limited mainly by a lack of solar real estate, *i.e.* sufficient space for installing solar harvesting equipment. For instance, slender high-rise buildings that generally make a great area of the city fabric lack sufficient rooftop

area for installing PV panels. Thus, electricity used to power such urban structures usually comes from fossil fuels burnt outside the urban districts and then transported to the city centres. Besides putting a demand on the infrastructure, this issue also adds to the cost of electricity in urban areas. Regarding the cost of electricity, in major cities such as New York in the U.S, electricity is estimated to be almost three times higher than the national average (EIA, 2021). Thus, incorporating renewable energy forms as an alternative to fossil fuels could play a major role in cutting electricity costs throughout major cities globally. Building attached silicon-based (Si-PV) conventional PV systems have been the most widely used to convert sun energy into electricity for a long time. However, in highly urbanized city fabrics, where infrastructure development is mainly vertical, the resulting slender tall buildings don't provide enough rooftop area to install these conventional PV systems (Meinardi *et al*., 2017). Thus, this has created an insufficient installation area for the Si-PV type systems. It is argued that with the current state of PV technologies, only 1kW of electricity can be produced from $7m^2$ of the installation area. This is perhaps one of the reasons the 2020 goal of newly constructed buildings in the EU archiving net-zero energy was nearly impossible to achieve. Therefore, there is a pressing need to devise innovative means of increasing the installation area of PV systems without necessarily compromising on both the building aesthetics and occupant comfort. One of these ways solar energy production could be increased is by converting mono-functional building surfaces such as façades into active energy-generating surfaces through the adoption of multi-functional Building Integrated Photovoltaic systems. Building Integrated Photovoltaics (BIPV) allow for electricity production at the point of use, eliminating the need for energy-transportation infrastructure and thus cutting the cost of electricity. One currently developing technology that could help transform these building surfaces into energy harvesters are the Luminescent Solar Concentrators (LSC). These can potentially transform conventional energy-passive glazing systems into semi-transparent solar energy harvesting windows. This is perhaps one of the surest ways urban façades could be transformed into solar energy harvesters.

It has been argued that the integration of solar energy harvesting systems invisibly into the fenestrations of buildings will ultimately increase the chances of their public acceptance as they do not alter the building aesthetics and hinder views to the outside. (Meinardi *et al.*, 2017).

The foreseen potential of this new technology enhancing the use and generation of solar energy in urban areas only reveals the need to increase research efforts that should hasten its advancement and application. Thus, this thesis adds to the already ongoing studies by proposing a framework that can be used to determine the electrical output of a transparent solar system. The proposed framework is further tested on a selected reference building in an urban area in the city of İstanbul, Turkey. For this purpose, computer-based simulations were run using PVsyst software. The results revealed that although the current highest efficiencies recorded for the LSC technology are not sufficient for its commercialisation, *i.e.* to produce enough energy to support the daily operations of the building fully, it could efficiently subsidise the building's electrical loads, thus, cutting on the operational costs of the building annually.

Prior to presenting the proposed framework, a series of background studies on transparent photovoltaics and solar systems, in general, are presented under the literature review section of the thesis. This is intended to build a general understanding of the topics presented in later sections of the methodology, materials and research results.

At the end of the study, the need for more research efforts, especially by practitioners in construction and architectural fields, was made evident based on the existing wide knowledge gap and insufficient tools available to conduct building assessments of the technology. For instance, the lack of computer-based software specific to the simulation and analysis of transparent photovoltaic systems was realised. Future endeavours should also focus on integrating analysis tools for transparent PVs into

existing architectural modelling software to ease their adoption and hasten acceptance in the building industry.

1.2 Aims & Objectives

The main objectives of this thesis will be;

- Provide information on the current advancement in the photovoltaic field in general.
- Give a general understanding of multi-functionality through photovoltaics.
- Suggest a framework for determining the electrical output of a transparent luminescent solar concentrator.
- Test the proposed framework on a selected reference building using computer-based simulations.
- Assess the cost benefits of adopting multi-functional LSC façades in place of conventional energy inactive glass façades.

1.3 Procedure

With regard to the aims and objectives listed above, the thesis first gives a general overview of renewable energy, emphasising its environmental and economic benefits. Next, an in-depth study into the different PV technologies is made, emphasising the different generations of the solar PV technologies mentioning their differences and objectives. The intent of this is to build a general background for understanding the transparent solar systems that are the core focus of the study and are discussed in the sections that will follow. Since this thesis mainly focuses on the transformation of transparent energy passive façades into active energy generators, the focus of the literature review section is on Luminescent Solar Concentrators. An in-depth analysis of their manufacturing, research progress and mode of operation is

presented. Furthermore, a brief discussion on energy storage systems, an essential part of all solar harvesting systems, is presented.

The third chapter presents the proposed framework that could be used to determine the electrical output of any transparent solar façade system that utilises LSC technology. The proposed framework is then tested on a selected reference building in a densely populated urban neighbourhood in the following chapter. For testing purposes, the reference building is remodelled with the existing energy passive glass panels of the reference façade replaced with energy-generating LSC units. Modelling and simulation data were mainly acquired from internet-based sources, research work, and cloud databases. This was supplemented with information acquired from the building's architects. The results are presented and discussed in the fourth chapter. The final chapter consists of a conclusion giving an overview of the materials covered in the thesis while also making recommendations for further research and advancement of the LSC technology.

1.4 Disposition

Overall, this thesis comprises six different chapters;

1. The First Chapter consists of the introduction where an argument for the study is made, aims and objectives listed, a comprehensive description of the procedure is made and finally, a disposition that briefly summarises all the different chapters of the thesis is presented.

2. The Second Chapter gives a general overview of all renewable energy systems, focusing on the current PV technologies through a systematic literature review. The later part of this chapter focuses on Luminescent Solar Concentrator Technology.

3. Chapter Three presents the proposed framework for determining the electrical output of transparent luminescent solar concentrators.

4. Chapter Four of the thesis presents the Materials and methods used for this study.

5. In Chapter Five, the results of the assessments are discussed and recommendations made.

6. Chapter Six presents a conclusion to the thesis making a general overview of all the main points of the thesis and recommendations to further research on LSC technologies.

CHAPTER 2

LITERATURE REVIEW

This chapter, presented in four parts, is intended to provide background knowledge and create a general understanding of the topics under discussion in the thesis. Part one of the chapter provides an overview of Renewable energy sources. Focus is on the essence of the adoption of RE forms. Part two gives an overview of conventional PV technologies at large to create a general understanding of the ensuing topics of discussion. Different important aspects related to solar energy advancements, such as the history of photovoltaics and the different generations as well as milestones reached in the advancement of PV technologies, are discussed. Part 3 discusses the different aspects and advancements regarding Building Integrated Photovoltaics. Multi-functionality through building-integrated photovoltaics is explored. The different design options available for enhancing the aesthetic and applicability of BIPV will also be discussed. Finally, part four of this chapter focuses on transparent solar harvesting systems.

2.1 PART 1: Overview of Renewable Energy

Renewable energy forms are types of energy that are generated from infinite sources. In most cases, the sources of renewable energy naturally exist. Renewable energy sources are sometimes referred to as alternative or sustainable energy sources. The five major types of renewable energy include; solar, geothermal energy, wind energy, biomass, hydroelectric energy. This thesis will solely focus on solar energy systems; thus, other renewable energy forms have been kept out of scope. The ensuing subsections briefly discuss a few aspects related to renewable energy. The

later sections of this part of the chapter will explore the advancements and evolution of PV technologies.

2.1.1 A Brief Review and Evaluation of Renewable Energy Sources

Abolhosseini *et al*., (2014), in their study, noted the increasing adoption of renewable energy (RE) forms. According to the authors, the majority of the countries around the world are currently widely investing in renewables. The increasing adoption of RE energy sources has further been fuelled by the fast advancements in technology, such as the increased power conversion efficiencies recorded for photovoltaics. Such technological advances have resulted in renewable energy forms becoming more cost-efficient.

In its 2014 report, the IEA forecasted an exponential increase in the number of countries producing over 100MW of energy solely from renewable means by 2017. According to Abolhosseini *et al*., (2014), conventional fossil energy sources could be cheaper than renewables; however, the latter has more environmental and social benefits than the former.

According to (Benedek *et al*., 2018), the witnessed advancements and use of renewable energy sources result from government policy. According to the author, such policies aim to ensure “energy security”, curbing climate change and economic development enhancement.

2.1.2 An Argument for Renewables

In a world currently experiencing a population explosion and high urbanisation rates like never seen before, energy security also becomes an extremely critical issue to be ensured. Adopting renewable energy sources has been regarded as one of the surest ways to ensure energy security amongst different communities. This is mainly because RE could potentially help diversify energy generation modes, thus yielding a

more decentralised electricity supply system that could be less prone to disruption (OECD, 2012). However, the expected potentials in the RE sources have fallen back for several reasons. One of the reasons RE sources have not achieved their full expectations is their dependency upon nature, which makes them prone to seasonal fluctuations resulting from the changes in weather conditions.

Generally, policies that advocate for RE usually do so on the basis that these forms of energy have the potential to reduce environmental impacts through reduced greenhouse gas (GHG) emissions that could otherwise result from burning fossil fuels for energy. In this regard, the ways in which energy is currently produced has been seen to be unsustainable and could potentially result in high temperatures globally and other climate associated catastrophes (OECD, 2012). RE sources have been noted to have a lower emission of CO2 compared to energy sources that are not renewable. In a study carried out by the International Energy Agency to assess the GHG emission capability of RE sources in 2011, it was discovered that using RE sources could reduce GHG emissions by an outstanding 1.7 giga tonnes (GT) (OECD, 2012). Effectively, curbing GHG emissions is one of the key ways most countries globally will reach their climate change objective. Thus, taking advantage of the GHG reduction potential offered by RE sources could be one way this could be achieved.

Regarding economic growth, adopting RE sources could offer economic relief to societies from energy-associated expenditures by enabling them to use solar or wind resources in their localities for energy generation instead. The possibility of exporting electricity from renewable energy sources has also been seen as a viable way of contributing to a country's economic growth. For instance, concentrating solar plants have been constructed to generate electricity for export purposes.

Investing in RE has also seen an increase in the jobs created. In 2008, the United Nations Environment Programme (UNEP) reported that RE for each unit of installed

capacity and per dollar generated created more jobs than their fossil counterparts (UNEP *et al*., 2008).

Perhaps some of the biggest beneficiaries from RE endeavours could be rural communities that find it difficult to cope with the upward fluctuating prices of centralised fossil fuel sources. Furthermore, rural communities benefit from the growing use of RE sources as these create jobs and new investment arenas. The installation of RE energy sources could foster the creation of new firms in an area and the emergency of new sectors in an economy (OECD, 2012).

2.2 PART 2: An Overview of Photovoltaic Technology

Photovoltaic technology has been evolving for more than a century since the discovery of the photovoltaic effects by Edmond Becquerel in the 1800s. This subsection explores the revolutionary events and discoveries turning points in PV technology. Furthermore, the main figures that played an important role in the evolution of PV technology are mentioned. The aim is to introduce and descriptively explore key concepts regarding photovoltaic technology to aid a clearer understanding of the main topics of the thesis to be later discussed.

2.2.1 History and Early Evolution of Photovoltaics

The Photovoltaic effect that forms the basis of PV technology was first discovered by 19-year-old French physicist Alexandre-Edmond Becquerel in 1839, who discovered that some materials could produce electricity when exposed to sunlight (Cook *et al*., n.d.). This discovery occurred while Alexandre experimented with platinum electrodes dipped in an electrolyte. An electrolyte, by definition, is any solution capable of conducting electricity. In his case, it was silver chloride that had been dissolved in an acidic solution. When Alexander placed his experimental setup under direct sunlight, his observation was that the current was enhanced.

In the years that followed (1860s -70s), Augustin Mouchot, another French scientist, applied the photovoltaic effect in a solar-powered steam engine. Augustin Mouchot presumed that the main fuel, "coal" that was being used to power steam engineers at the time, was a limited resource that could run out or become increasingly more expensive, thus seeking to turn to solar as an alternative. According to Oliveti *et al*., (2014), this application of solar in a steam engine saw the first application of a parabolic trough solar collector. However, contrary to Augustin's assumptions about the coal resources, coal prices reduced, making it cheaper and solar more expensive, which led the French government to withdraw funding for Augustin Mouchot's project.

Augustin's invention of the solar-powered steam engine was closely followed by a photovoltaic demonstration in England by William Grylls Adams and Richard Evans Day in 1876. Richard was a student to William, who was a natural philosopher. The couple attempted to demonstrate the PV effect on a block of platinum - selenium (semiconductor) based junction but with very poor results. This was followed by another breakthrough by Charles Fritts (An American inventor), who made a "gold-selenium junction" PV device with an efficiency of 1%.

In 1887, Heinrich Hertz, a German scientist, discovered the photoelectric effect, where electrons were discharged from a material that could absorb light of a wavelength shorter than "material-dependent threshold frequency."

In 1905, Albert Einstein wrote a paper that made an elaborate description of the photoelectric effect by assuming that the energy from the light was being transported by photons ("quantised packages of energy").

Jan Czochralski, a chemist from Poland in 1918, devised means of developing "high-quality crystalline." His approach is still relevant today in the production of monocrystalline silicone that is applied in high-end crystalline silicon cells.

After the 1950s, the growth of c-Si technology was seen. Perhaps the real first actual prototypes of a solar cell used in our current day were first produced by Daryl M.

Chapin, Calvin S. Fuller, and Gerald L. Pearson at the Bell Laboratories in the U.S. This Si-based prototype had an efficiency of 6%. The first reports on the cadmium sulphide (CdS), an II-VI semiconductor, were made around the same time.

In the mid of the 50s, corporations such as RCA Corporation and the Hoffman Electronics Corporation became actively engaged in the production of silicon-based solar cells that were to be used in powering the satellites orbiting the earth. The first concentrated solar plant that produced 1MW of electricity was built by Italian scientist Giovanni Francia in 1968.

The 1970s followed with a series of advancements in solar technology, such as the invention of the first gallium arsenide heterojunction solar-based cell by Zhores Alferov. Alferov's invention laid the basis for the III-V semiconductor materials today applied in solar technology. Shortly, after in 1976, the first amorphous silicon-based thin-film was developed at the RCA Laboratories by Dave E. Carlson and Chris R. Wronski. Two years later, SHARP made the first solar-powered calculators in Tokyo.

The 1973 OPEC induced oil crisis sparked an even increased interest in PV technologies leading to a massive investment by many companies in the production of PV systems for space usage.

The first copper sulphide/cadmium-sulphide junction based thin-film solar cell with a conversion efficiency of 10% was developed in 1980 at the University of Delaware. In 1985, another milestone in solar cell efficiencies was reached when crystalline silicon solar cells with more than 20% efficiencies were exhibited in Australia.

Another milestone in PV technology was reached when the first high-efficiency Dye-sensitized solar cell in which a molecular sensitizer-based semiconductor material is placed between a photo anode and an electrolyte was demonstrated in Switzerland in 1991. This was followed by the demonstration of "a concentrator solar cell based on III-V semiconductor materials" in 1994 at National Renewable Energy Laboratory

placed in the U.S. This particular cell reached efficiencies over 30% and was based on indium-gallium- phosphide/gallium-arsenide tandem junction.

2.2.2 Operation of Photovoltaic Solar Cells

The generation of electricity from a PV cell is based on the photovoltaic effect. Photovoltaic effect could be defined as the generation of voltage or electric current in a material by exposure to light. Oliveti *et al*., (2014) defined the photovoltaic effect as the generation of a voltage or potential difference at the junction of two different materials when the materials are exposed to "electromagnetic radiation". The authors relate the photovoltaic effect to the photoelectric effect that causes materials to release electrons when light that has a frequency above the threshold of the "material-dependent frequency" is projected on them. The photovoltaic effect can be witnessed mainly in semi-conductor materials (Singh *et al*., 2021). In his 1905 publication, Albert Einstein explained this phenomenon by making an assumption that light contains well defined "energy quanta" or photons. Following this assumption, Einstein concluded that the energy of such a proton could be given by the following formula;

$$E = h\nu$$

h represents the Planck's constant and whereas ν is the frequency of the light (Oliveti *et al*., 2014).

The photovoltaic effect, as described by Einstein is the basis of the PV cell electricity generation from sunlight. The sun releases a great amount of radiation each minute of the day. Each minute 1367Watts of energy are radiated upon each square meter of the earth's surface (Cook *et al*., n.d.). When this sunlight, which also contains photons (packets of solar energy), strikes the PV cell and is converted into electricity. According to Cook *et al*., (n.d.), the protons in sunlight contain different amounts of energy corresponding to the different "wavelengths of the solar spectrum." When

these protons strike the PV cell, three different phenomena are most likely to occur; reflection, transmission or absorption of the protons. The electricity generated by the PV cell results from the absorption of the protons. The energy of the absorbed photons is then transferred to the electrons of the semiconductor material atoms. This energy exchange between the protons and electrons causes the electron to escape its position in a single atom and join the current flow within the circuit. The electric cell has an inbuilt electric field which provides the required potential difference to move the electricity through the circuit.

2.2.3 Power Losses in PV Cell Solar Conversions

One major downside regarding the electricity generation in single-junction PV cells that has to be addressed is the energy losses. According to Cook *et al*., (n.d.), during the conversion of sunlight into electricity, half of the energy is lost due to the following occurrences;

- Failure to convert photons with energies below the band gap into electricity
- Thermalisation of protons whose energies exceed the bandgap

This phenomenon is illustrated in a diagram in Figure 2.2.1 below. When the energy of the photon E_{ph} is equivalent to the *hv* described above, the electrons will be moved from positions E_i to positions E_f creating a gap at position E_i left to be filled. However, if the photon energy E_{ph} exceeds the bandgap width E_g, part of the energy will be converted into heat energy.

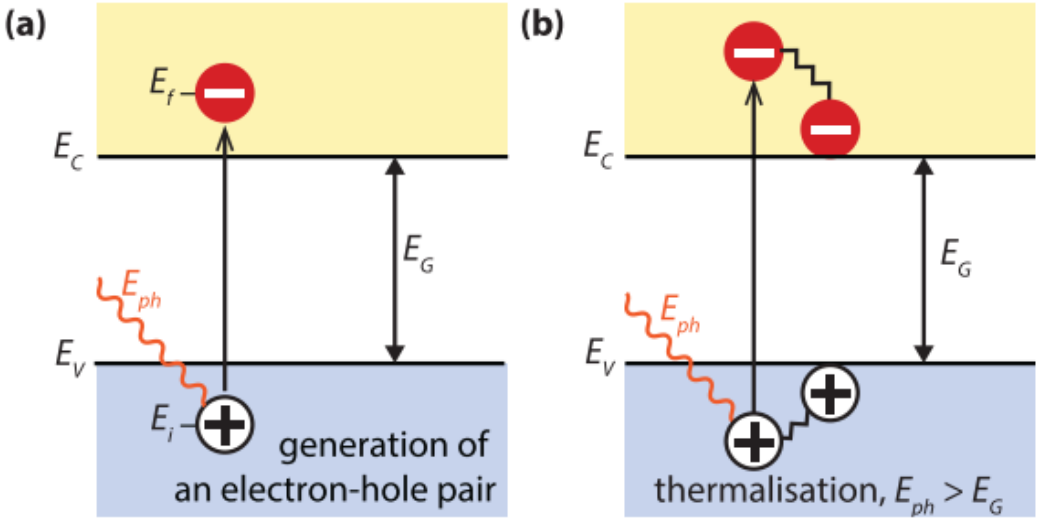

Figure 2.1 Illustration of the Absorption of Photons in a Semi-conductor Material with Bandgap Width E_g (Oliveti et al., 2014).

2.2.4 Evolution of Photovoltaic Cell Technology

The different stages of evolution of solar cells to date are referenced by the term "generation" (Singh *et al*., 2021). Currently, the PV market is still greatly dominated by "poly- and mono-crystalline silicon wafers" belonging to the first generation of photovoltaic technologies (ISE, 2014). Their continued market dominance is mainly attributed to the high output efficiencies under standard testing conditions (STC) compared to other factors such as material abundance and ease of manufacturing. High efficiencies imply that first-generation PVs will yield a higher electrical output in smaller spaces than other generation technologies. However, in cases where photovoltaics will be integrated, the authors outline other factors that influence the type of technology that will be selected. Some of these factors include; the orientation of the façade, the materials used on the façade, whether the transparency is a priority over opaqueness or whether the material is required to be flexible (Morini, 2021). The ensuing subsections will focus on the evolution of PV technologies. The focus will be on their evolution through their respective

generations. Furthermore, the different parameters that determine a certain PV technology's preference over another in the market are also considered.

2.2.5 Comparison of Market Share of PV Technologies

Different PV technology alternatives have emerged over the past decades. The table below summarises PV technologies based on their first reported years. The first generation could be summarised into two types, also considered the oldest PV technologies. The second, which mainly comprises thin-film s, has seen a continuous increase in the market share. Furthermore, the second-generation embraces a series of materials, production techniques, and application areas. The third-generation technologies evolved from the second-generation by exploring new materials and areas of application. Although still underdeveloped, the third-generation PV technology has a great potential to reach higher PCEs (Subtil Lacerda & Van Den Bergh, 2016).

Table 2.1 Various PV Technologies and the Year of the First Research Report. (Subtil Lacerda & Van Den Bergh, 2016).

PV solar generation	Technology alternatives	Year of first best research-cell efficiency reported
1st	Mono-crystalline	1954
	Multi-crystalline	1984
2nd	Amorphous silicon (a-Si)	1976
	Multi-junction thin silicon film (a-Si/μc-Si)	1976
	Cadmium telluride (CdTe)	1976
	Copper, indium, gallium, (di) selenide/(di)sulfide (CIGS)	1976
3rd*	Organic PV (OPV)	2001
	Dye-sensitized solar cell (DSCC)	1991

Subtil Lacerda & Van Den Bergh, (2016), argue that this diversity in the PV sector is one of the main reasons for the increasing developments in PV technologies. According to the authors, this diversity in energy resources plays a big role in ensuring energy security and energy accessibility over a wider geographical coverage.

The authors also suggest that there are mainly two driving factors behind the PV technological transformations; technological push and demand-pull. Under technological push, transformation mainly results from radical innovation. Demand-pull, on the other hand, evolves around market demand. To determine the direction and coverage of technology, "patents" are usually deployed. Between 2002 and 2010, 116 of the 422 clean energy-related patents registered in the U.S under the United States Patent and Trademark Office (PTO) were awarded to PV related technologies (Subtil Lacerda & Van Den Bergh, 2016). According to the authors, data from PTO is also used as an indicator of innovation. Of the 116 PV technology patents, 29% were first-generation, 41% second and 31% third generation. Since the statistics of distribution amongst the different technologies is not so variant, it indicates an almost balanced share of the market as well as an equal distribution of the efforts invested in developing the different technologies.

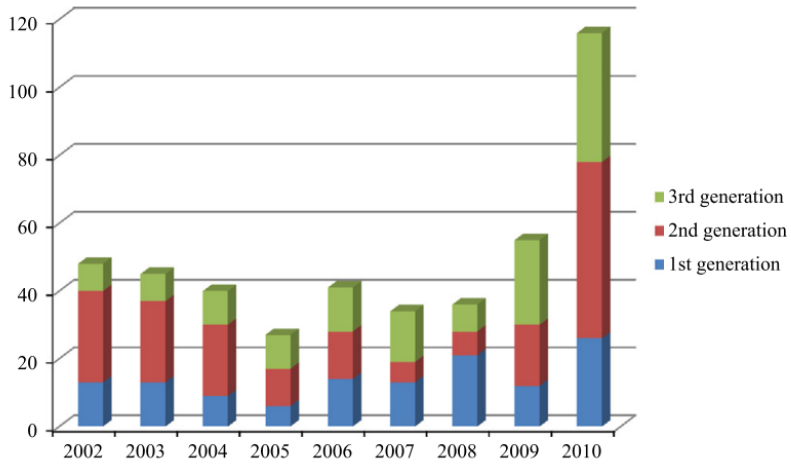

Figure 2.2 Number of Patents per PV Generation for 2002 and 2010. (Subtil Lacerda & Van Den Bergh, 2016).

2.2.6 Concept of the Solar Cell

Since the development of BIPVs follows those of conventional PV systems, it is important to explore the developments within the PV industry and technologies in general. The ensuing subsections of this thesis explore the different technologies based on their generations.

Generally, high-grade silicon that has been processed with negatively charged and positively charged semiconductor phosphorous and boron, respectively, is used to manufacture solar cells. Electrons are freed from the negatively charged phosphorous to the positively charged boron when the solar cell is exposed to the sun. The electric potential difference creates a current, which is then collected and transported by a metal grid on the cell.

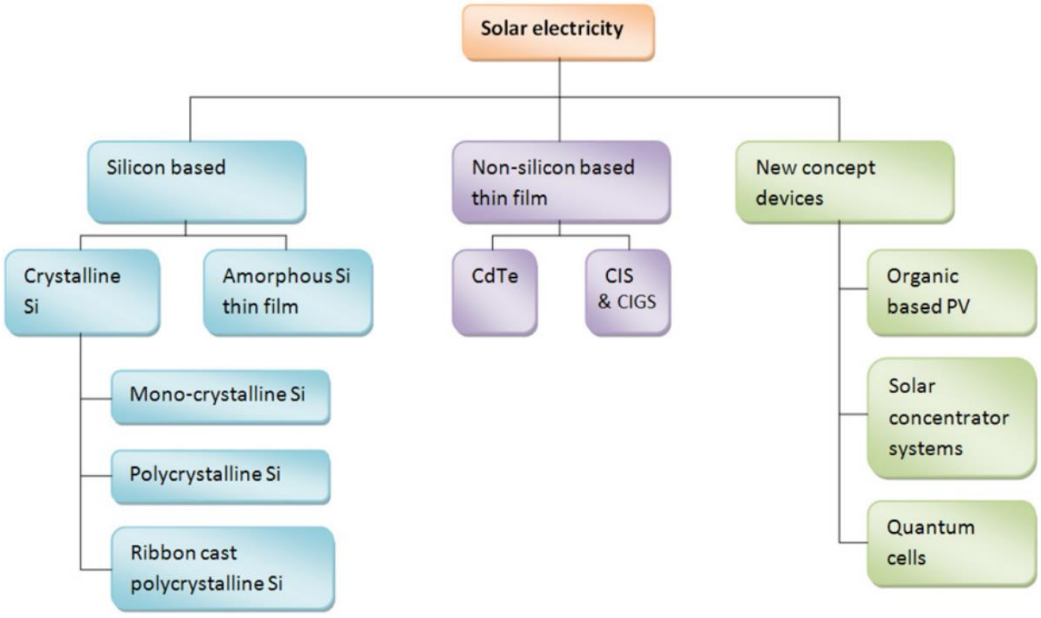

Figure 2.3 Graphic Illustration of the Different PV Technologies (Jelle *et al*., 2012).

2.2.6.1 Material Categorisation of Solar Cells

As previously mentioned, silicon is the most widely used material in the production of solar cells. In this subsection, both the silicon-based (in part a) and non-silicon-based PV solar cell technologies (in part b) will be explored. The following section will explore the characterisation of PV technologies based on their generations.

a. Silicon-Based Solar Cells

Silicon is the domineering solar cell technology material on the market currently. The domineering silicon cell technologies can be categorised into; monocrystalline, polycrystalline and amorphous silicon-based cells. Jelle *et al*., (2012) also identified a different type of solar cell; "ribbon cast polycrystalline cells." This particular one differs from the rest in its means of production as rather than cut wafers from silicon ingots; flat thin-film s are drawn from molten silicon, using ribbons. This reduction method reduces silicon waste as there is no shaping of wafers from ingots; however, the resulting cells tend to have lower efficiencies. Non-silicon-based materials include; gallium arsenide (GaAs), cadmium telluride (CdTe), copper indium diselenide (CIS) and copper indium gallium selenide (CIGS). The most expensive silicon-based cells are monocrystalline silicon, with higher PCE and a blackish-grey appearance. Polycrystalline silicon cells are those produced from multi-crystalline silicon ingots. The manufacturing of polycrystalline cells is usually less expensive; however, the resulting cells have lower efficiencies. Polycrystalline cells usually are characterised by a shiny blue colour resulting from the constituting crystals. These two types of cells *i.e.* monocrystalline and polycrystalline, form wafer-based technologies. These will be explored more in the following subsections.

On the other hand, amorphous silicon cells are characterised by a very thin layer of non-crystallised silicon that is deposited on a substrate layer. This creates thinner cells, also called "thin-film cells." Amorphous silicon cells are characterised by a brownish colour.

b. Non-silicon-Based Photovoltaic Cells

Similar to the aforementioned amorphous silicon cells, the non-silicon-based cells such as CdTe, CIS, and CIGS are thin-film cells. CdTe and CIGS have been identified as the most cost-efficient and economically promising solutions for decentralised electricity production. For the case of CdTe solar cells, a transparent substrate glass is used with fluorinated tin oxide (FTO) or TCO (transparent conducting oxide) layer as the front contact layer. The glass substrate is first coated with an n-type cadmium sulphide (CdS) layer and then the p-type CdTe absorber layer. According to (2012), CdTe is the cheapest of all thin-film solar cells to manufacture and has the greatest potential for wide-scale decentralised electricity production due to its high PCE. It is usually characterised by a dark green to black colour.

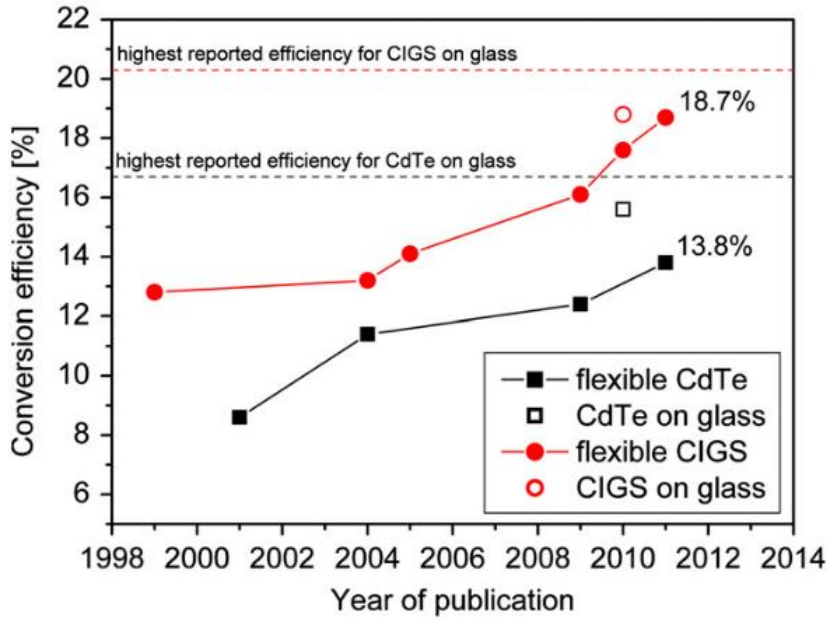

Figure 2.4 Conversion Efficiencies of Flexible CdTe and CIGS Solar Cells Fabricated by Low-temperature Processes (Jelle *et al*., 2012).

2.2.6.2 Generational Categorisation of Solar Cells

Solar cell technologies could also be categorised according to their different generations or eras of the invention. Overall, all presently used solar technologies can be placed under three different categories as described below;

2.2.6.2.1 First-generation Technologies

Photovoltaic cells belonging to the first-generation are generally crystalline silicon-based. Crystalline silicon is the most widely used material in PV module fabrication. The silicon wafers used in solar PV cells could be differentiated into two categories, namely, monocrystalline silicon and multi or polycrystalline silicon (Oliveti *et al*., 2014). This subsection elaborates on the different technical aspects of the monocrystalline and polycrystalline based solar PV technologies.

a. **Monocrystalline silicon (mc-Si);**

Monocrystalline silicon is also referred to as single crystalline silicon (Oliveti *et al*., 2014). According to the authors, mono-crystalline silicon is solid with a continuous unbroken crystal lattice. It's building particles (grains or crystals) do not have boundaries throughout the entire piece of silicon.

Monocrystalline silicon (mc-Si) solar cells have the highest electric conversion efficiencies and are made out of "high-purity silicon crystals." Under Standard Testing Conditions (STC), mc-Si cells have shown 16-24% efficiencies (Oliveti *et al*., 2014). The downside of mc-Si modules is they tend to cost more on the market. This is mainly due to their high-power conversion efficiencies and their more refined production process.

Figure 2.5 Mono-crystalline Cell Wafer.

Monocrystalline based solar panels tend to have a longer life span as compared to other solar technologies. According to Alba Energy (2018), m-Si-based solar panels could come with warranty periods of over 25 years, which greatly contributes to shortening the payback period in terms of energy and cost. In addition, m-Si-based solar panels have a better performance under low light conditions.

b. **Polycrystalline Silicon (p-Si);**

Polycrystalline Silicon, also referred to as polysilicon (p-Si), consists of numerous multi-oriented crystals with evident boundaries between the grains. The manufacturing process of p-Si wafers is much easier than the monocrystalline, thus being purchased at much lower costs though possessing lower Power Conversion Efficiencies (PCE). According to Morini, (2021), p-Si efficiencies under STC range from 14-18%.

Figure 2.6 Polycrystalline Cell Wafer

One of the vivid differences between the mono and polycrystalline cells is that monocrystalline wafers are mono-coloured. In contrast, the multi-crystals in a polycrystalline wafer are evidently visible based on the variation in colours of the grains. At the boundaries of the grains, there are usually “lattice mismatches”, which result in multiple defects at the grain boundaries (Oliveti *et al*., 2014). This makes polycrystalline cells incapable of carrying electric charge over long-life times than their monocrystalline counterparts.

Overall, polycrystalline silicon-based solar panels are more likely to cost less than the monocrystalline ones owing to their cheaper manufacturing process; however, they do have lower PCE, thus, requiring more installation area (Alba Energy, 2018).

Bergmann & Werner, (2002) illustrated the grain size effect on the charge carrying lifetime capability of wafer cells as shown in graph figure 2.7 below.

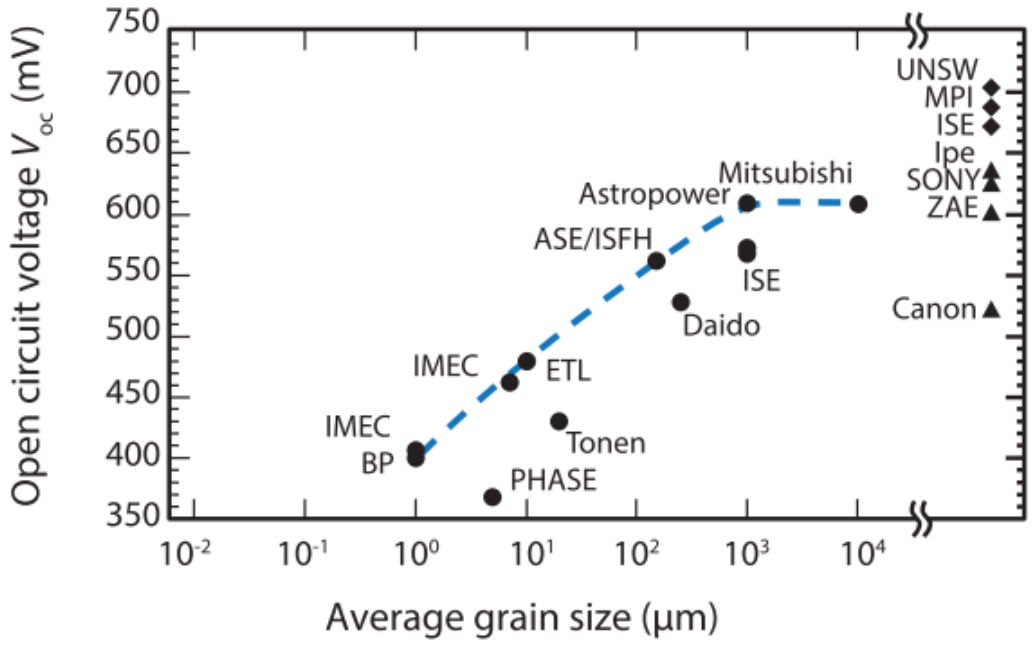

Figure 2.7 The Relationship Between the Open-circuit Voltage and the Average Grain Size (Bergmann & Werner, 2002).

The capacity of the wafers increases with the average size of the grains. This implies that in multi-crystalline wafers, the larger the grains, the larger the charge carrier lifetimes and the bandwidth width utilisation, implying a higher open-circuit voltage. The right side of the graph is open-circuit voltages of wafers based on monocrystalline silicon. However, since monocrystalline silicon wafers have no grain, they tend to yield higher voltages or possess higher capabilities of carrying charge (Oliveti *et al*., 2014).

Silicon-based PV technologies, especially monocrystalline-based technologies, have so far recorded the highest PCE values amongst all PV technologies. Thus, they have been found to generate more electricity per m^2 of installation area than other PV technologies. However, it's important to note that the efficiencies mentioned here are obtained under standard testing conditions (STC) with optimal orientation, direct irradiance and an optimal conversion temperature of about 25 ^{o}C, which will greatly differ in real-life outdoor conditions (Morini, 2021).

- **Downsides of First-generation Photovoltaic Technology**

Under real-life operating conditions, solar technologies generally will have lower electrical outputs than when tested under STC in a laboratory. This is mainly due to the many constraints the modules have to operate in. The module temperatures can rise as high as 70^{o}C under outdoor operating conditions, which greatly impacts the electrical output of the modules. In the case of silicon-based panels, it is expected that for every 1^{o}C rise in module temperature, there is an almost 0.45% drop in the module efficiency. This implies for module temperatures as high as 70-80^{o}C under real operating conditions, an even greater loss in module efficiency is experienced. It is also important to emphasize that the -0.45% reduction in conversion efficiency experienced in first-generation PVs is the highest compared to the second and third-generation PV module types. Second, the angle at which the modules are oriented as well as the "intensity" of the solar irradiation, also greatly affects their power conversion efficiencies. Furthermore, shading on silicon-based module top surfaces caused by dust or nearby objects could greatly impact how efficiently they operate.

However, with optimal exposure to solar radiation for first-generation silicon-based PV modules, for instance, when used on south-facing façades, first-generation modules have an outstanding performance compared to the other two alternatives.

- **The Crystalline Silicon-based PV Manufacturing Process**

The primary forming unit for first-generation PV modules is the "wafer." The production process of wafers from silicon is illustrated in figure 2.8 below.

Generally, the silicon used in wafer production comes from Quartzite ore, a rock formation consisting of "almost pure silicon dioxide." The silicon ore (quartzite) is heated and melted at around 1900^{o}C in a furnace with a sub-merged arc-shaped electrode. To "purify" the SO_2 carbon mixture of "coal, coke and wood chips" is added to the molten solution of SO_2 to produce Si and carbon monoxide (CO).

$$SO_2 + 2C \rightarrow Si + 2CO$$

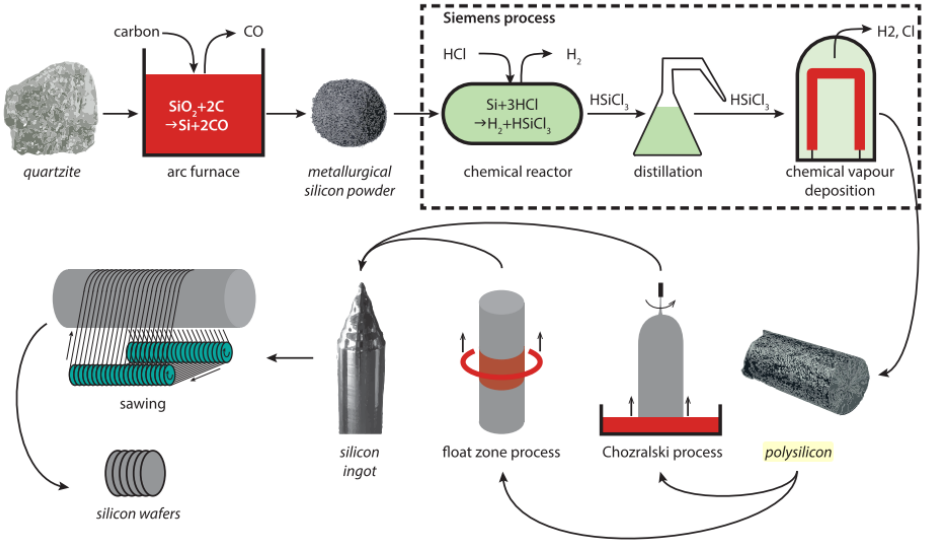

Figure 2.8 Manufacturing Process for Crystalline Silicon Wafers (Oliveti *et al*., 2014).

The resulting CO is released in gaseous form, and the residue silicon is drawn off the furnace. The third image in figure 2.8 above in the silicon wafer production process is off metallurgical silicon powder. According to Oliveti *et al*., (2014), only 1% of the metallurgical silicon powder from this process is used for electronic grade silicon production. 70% is used for aluminium-silicon alloy production and 30% for different chemical products.

Following metallurgical silicon in terms of purity is polysilicon, which is achieved by further processing the former in a process called *"Siemens."* During the Siemens process, hydrogen chloride is added to metallurgical silicon in a reactor in the presence of a catalyst to produce trichlorosilane, $HSiCl_3$ (Olivieri *et al*., 2014).

$$Si + HCI \rightarrow H_2 + HSiCl_3$$

Trichlorosilane (HSiCl3), by structure, contains "one silicon atom, three chlorine atoms and one hydrogen atoms" in gaseous form. The gas is then liquefied by cooling and purified by distillation, where all impurities that are contained and have boiling points lower or higher than Trichlorosilane are extracted. The trichlorosilane

is vaporised again in another reactor while hydrogen is added. In the reactor, Trichlorosilane is decomposed at high temperatures of 850°C to 1050°C on highly purified silicon rods. The rods attract the Silicon atoms, whereas the chlorine and hydrogen atoms are discharged from the surface of the rod back into the gaseous phase. Pure silicon is grown as a result of this process.

Further processing for the residue gas continues as it still contains chlorosilanes and hydrogen, processed and reused. Chlorosilane will then be liquefied, distilled and reused (Oliveti *et al*., 2014), whereas hydrogen is cleaned and sent back to the reactor for reuse. According to the authors, the Siemens process does consume a lot of energy. However, the pure silicon used in monocrystalline wafer cell production is obtained from this process.

- **Aesthetic and Physically Characteristics of Mono and Polycrystalline Wafers**

The shapes of monocrystalline wafers could vary from square or rounded corner squares; however, polycrystalline wafer cells are generally square-shaped. This difference in wafer shapes results from the shape of the “ingots” from which the wafers are cut. m-Si is usually produced from cylindrical shaped ingots, whereas p-Si is manufactured from square-shaped ingots (Morini, 2021).

Figure 2.9 Images of Monocrystalline Ingot (Left) and Polycrystalline ingots (Right).

One way of quickly distinguishing monocrystalline from polycrystalline is to compare and contrast the constituting cell colours. Monocrystalline cells will generally have a smooth black appearance, whereas polycrystalline cells have a scattered blueish appearance (Alba Energy, 2018). Figure 2.2.10 below clearly depicts the contrasting appearances of the monocrystalline (left) and polycrystalline solar cells (right).

Figure 2.10 Monocrystalline Cell with a Dark Smooth Appearance (Left); Polycrystalline Cell with a Scattered Blue Appearance (Right) (Alba Energy, 2018).

High-conductive metal contacts are printed to the top surface of both m-Si and p-Si to collect the electricity collected by the cells. Whereas these metal contacts could be used to achieve different aesthetic appearances of the modules, they also play a negative role in reducing the efficiency of the cells as they reduce the active area of the cell and contribute to shading portions of the cell in some cases.

By adjusting the thickness of the antireflective coating layer, it is possible to alter the characteristics of the crystalline silicon technologies such as colour or opaqueness; however, this will most likely lead to a drop in the cells' efficiencies. The alteration of the anti-reflective layer to achieve different coloured appearances despite giving the cells a special look does contribute to an increase in light reflection and about a 15 to 30% drop in their efficiencies (Dricus, n.d.).

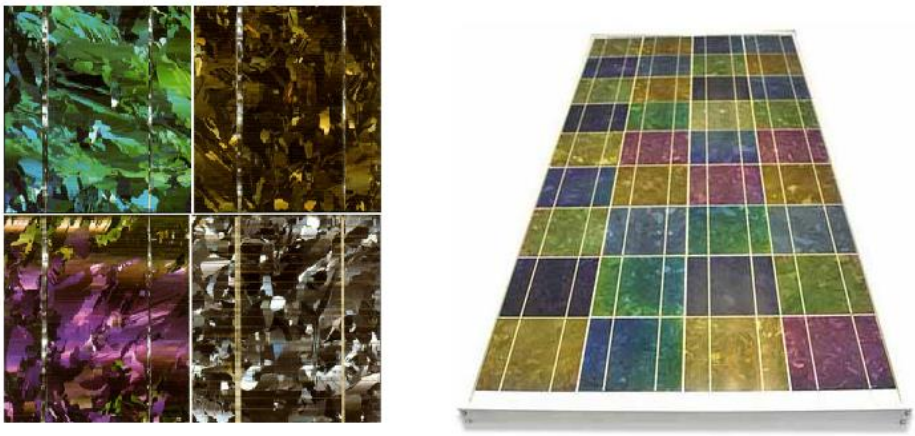

Figure 2.11 Left: Different tones of Coloured Cells (Left); A coloured Solar Module (Right)

Silicon-based solar panels usually are planar as different shapes are not easily achievable. However, through advanced “cold or hot processes”, it’s possible to create curved panels with very limited curvature (Morini, 2021).

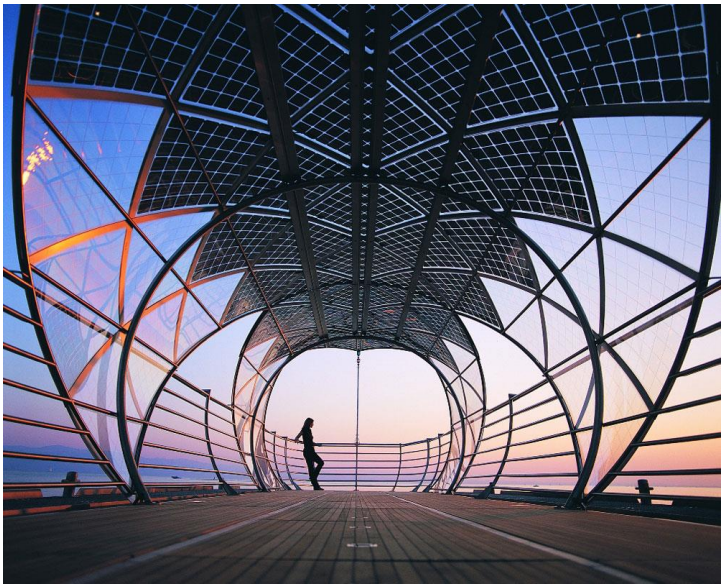

Figure 2.12 Silicon-based Solar Panels with Curvature Used on the RA 66 Shuttle Designed by Kopf Solar Design.

The alternative to archiving curvature with silicon-based solar panels in architecture is to use a structure with multiple subdivisions as was done at the Seine Musicale mixed-use music and cultural centre in Paris (Figure 2.13).

Figure 2.13 Structure with Multi Subdivisions Used to Achieve Façade Curvature with Silicon-based Solar Panels

It is also possible to alter the shapes, spacing, orientations, and alignments with silicon-based technologies. Due to the opaqueness of silicon-based technologies, transparency can only be achieved through the intermediate spacing between wafers or by boring holes through the wafers. For instance, it is possible to achieve transparency with good spacing between wafers, provided the substrate of the modules is transparent. This results in an interesting transparency configuration of the module, creating interesting lighting effects on the interior. The study on light trans-missive photovoltaics (LTPV) is an interesting one to look at by (Baum, 2017). The method of archiving transparency by wafer spacing or perforating holes through the wafers has the downside that it will reduce efficiency as well as module solar active area.

Furthermore, creating perforations on the PV module also increases manufacturing costs and production waste. However, further advancements in PV technology have seen the creation of even fully transparent cells as that created by researchers Vladimir Bulović and Richard Lunt at MIT (Nancy, 2013). The transparent technologies are the core focus of this thesis and will be discussed in later subsections of this chapter.

Figure 2.14 below shows the creative use of wafer spacing to achieve a light transmissive effect on the interior.

Figure 2.14 FKI Tower, Designed by Adrian Smith + Gordon, Seoul, South Korea

There has been a drop in the market price of first-generation PV technologies over the past few years. One of the main reasons behind this reduction in price is the massive flooding of the market with cheap Chinese manufactured PV panels.

2.2.6.2.2 Second-Generation Technologies

Second-generation PV systems are also referred to as thin-film photovoltaics. Second-generation PV cells are much thinner than the first-generation PV wafers' forming units. This implies that less material is used in their manufacturing than their first-generation counterparts, making them a more cost and material-efficient solution. Furthermore, thin-film PV systems; possess characteristics such as flexibility, lightness, transparency, and a homogenous appearance, making them a great solution for building integration. According to Janez & Marko, (2013) as reported in 2013, thin-film-based cells were already seeing an increase in the market share value with a total annual production of 3.2GW as early as 2010. These figures have increased exponentially since then.

Some of the advantages that second-generation based PV systems possess over their first-generation counterparts are; they experience lower operation temperatures, could easily be adopted to already established technologies such as glass and allow for the use of low-cost substrates. Thin-film technologies have generally been cost less, be more sustainable, and have high conversion efficiencies. However, despite all the advantages mentioned above over their first-class counterparts, thin-film PVs still struggle to catch up with first-generation technologies in terms of efficiency. In fact, whereas first-generation PVs have recorded efficiencies as high as 25%, thin-film s PVs have an average efficiency of only about 12%.

Second-generation PVs are generally manufactured from three different types of semiconductor materials of 1-2 micron thickness, applied on some substrate material such as plastic, metal or glass. The semi-conductor materials are generally one of the following three;

- Silicon, in amorphous (a-Si) and micro-morph (µm-Si) form,
- Copper Indium Gallium selenide (CIGS) or, without gallium, Copper Indium Selenide (CIS),
- Cadmium telluride (CdTe)

These three different semiconductor materials all have a direct band gap that enables their use with a very minimal thickness (Lee & Ebong, 2017).

In making thin-film solar cells, the semiconducting layer of CdTe, CIGS or a-Si, is placed between two layers of "transparent conductive oxide (TCO) and electric back contact." To limit the transmissive effect of thin-film s, a reflective layer is usually placed at the back of the cell. The TCO serves two purposes: to act as the contact at the front of the cell and direct the incident light radiation to the active layer. This implies that the TCO layers should be transparent and very conductive.

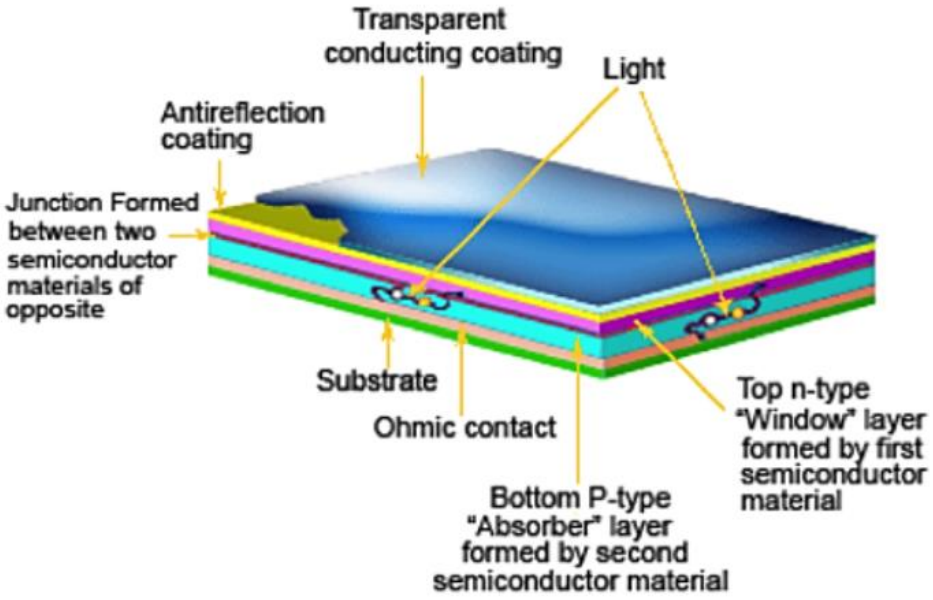

Figure 2.15 Structure of Thin-film Solar Cell (Barry, 2018).

Out of all the materials possible for TCO, Indium Tin Oxide offers the best transparency values with the best conductive properties. However, this is not suitable for large-scale application as one of the constituting elements *i.e.* indium is so rare in the earth's crust.

- **Advantages of Thin-film Photovoltaics;**

Thin-film solar cells are generally more lightweight than their first-generation counterparts, mainly due to their active layer's “micrometrical thickness”. Whereas the application of the active layers is mainly done over flexible sheets of metal or plastics, enabling the attainment of more flexible solutions for PVs, it is also possible to apply them over more rigid substrates.
Also, thin-film technologies tend to have a more homogenous appearance, making them standouts for the BIPV sector than the crystalline silicon ones.

In addition, besides having very low-temperature coefficients, their performance is minimally affected by the light intensity. This property makes them very suitable for incorporation into building-integrated photovoltaics.

Thin-film technologies also exhibit high performance under non-standard testing conditions, making them good contenders against the first-generation PVs whose high efficiencies under STC exponentially drop-in real-life application conditions.

a. Silicon-based thin-film modules: amorphous and micro-morph silicon PV

Amorphous and micro-morph silicon-based PV systems have profound advantages over their crystalline silicon counterparts. One of the most profound advantages is that the performance of both a-Si and µm-Si is less likely to be affected by high temperatures. Compared to first-generation crystalline silicon-based solar cells, these two thin-film alternatives have very low-temperature coefficients. Amorphous silicon, for instance, has a temperature coefficient that is less than half that of crystalline silicon, *i.e.*, 0.21%/°C. And although that micro-morph silicon is relatively higher, *i.e.* 0.25%/°C, it’s still more capable of maintaining high-performance under high-temperatures conditions than crystalline silicon-based PV systems.

Secondly, thin-film-based solar cell performance is less likely to be affected under low irradiation conditions such as partial shading or cloudy conditions. Thus, despite having lower PCE than the first-generation crystalline silicon-based cells, thin-film based solar cells could produce more electricity annually than c-Si-based PVs in cases where low irradiation conditions persist. This makes thin-film solutions better in building integration where solar cells face low irradiation resulting from orientation or shading by other building parts, nearby buildings, or vegetation.

Since the active layer of thin-film s is opaque to light, the only way transparency can be achieved through the reduction of the active layer thickness to let light through the glass encapsulating layers. However, through “a laser-scribing” process capable of micro perforating the cell, it is possible to obtain transparency of uniform homogeneity. Furthermore, the laser scribing process makes it possible to achieve different shapes, resulting in different transparency and illumination effects. However, it is important to note that the laser scribing process, which could help achieve different shapes, results in waste and reduction of the solar cell active layer.

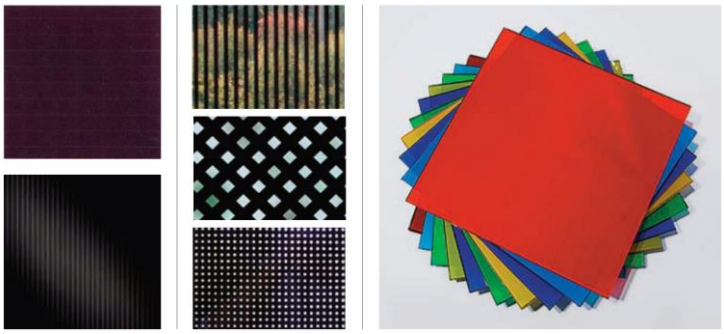

Figure 2.16 (left) Example of Typical Red-brown a-Si and Black µm-Si Module; (middle) Different Patterns for Different Transparency Levels, Defined in the PV Accept Project; (right)a-Si Modules in Different Colours, Provided by Onyx Solar (Morini, 2021).

In terms of colour appearance, a-Si film tends to have a uniform brownish colour, whereas µm-Si is generally black. However, in more transparent thin-film solutions,

it is possible to achieve various colours by varying the substrate colour. It is also important to note that the variation of the colours is done to the substrate and not the active cell layer. In figure 2.16 above, an example of different colour tones of the thin-film solution produced by Onyx Solar, a Spanish PV manufacturer specialising in BIPV. Furthermore, it should be considered that additional modifications to the appearance, such as variation of colour, directly affects the cell's efficiencies. This also goes as far as affecting the temperature co-efficiencies of the cell. Clear coloured cells will heat less than the coloured ones, which are more likely to absorb less light.

Figure 2.17 (Left) Exterior Appearance of Perforated Thin-film and its Interior Lighting Effect (Right) Manufactured by Onyx Solar and Installed on Balenciaga's New Storefront in Miami (Kelly, 2018).

The most profound downside of silicon-based thin films is that they require wider areas for installation owing to their very low efficiencies under STC. Morini (2021) reported that efficiencies for amorphous thins films range from 4-6% under STC, whereas micro morph silicon could reach up to 10%. The PCE value for these two thin-film alternatives is too low to contend against the first-generation PVs, which could reach as high as 25%.

Overall, the cost for a square meter for thin-film photovoltaics is generally much lower than that of first-generation crystalline silicon photovoltaics. In fact, according to Barry, (2018), thin-film s could cost as low as 1usd/watt. This could be mainly attributed to lesser semi conducting material being used to manufacture thin-film photovoltaics. Furthermore, thin-film s are made through deposition processes instead of the extremely energy-intensive process of cutting ingots in the making of first-generation PV systems. The different thin-film technologies and materials are explored below;

a. CIGS and CIS thin-film modules

CIS is used as an acronym for a group of semiconductor compounds that contain copper, indium or gallium, and sulphur or selenium, which naturally occur as mineral ore known as chalcopyrite (Soltecture, n.d.). The CIS thin-film s play a big role in reducing the amount of semiconductor material used. For instance, only 5 g/m^2 of silicon are used where normally 500 g/m^2 would be required in regular crystalline silicon cells. A shorter production process is achieved by reducing the amount of silicon used. Furthermore, only half of the energy normally used will be required to produce the thin film.

According to Morini, (2021), Copper Indium Gallium selenide based thin-films are a promising class of PV for integration in buildings. So far, the highest tested efficiency of CIGS solar cells is 20.7% in laboratory conditions (Fatemi Shariat Panahi *et al*., 2020). However, the efficiencies in real operating conditions for CIGS modules range between 11-15%. In addition, when used on more rigid substrates, PCE values of more than 15% are achievable. However, this is slightly lower when used on more flexible substrates. In fact, as of 2012, the highest recorded efficiencies on flexible substrates was 12.7% (Jelle *et al*., 2012).

Overall, CIGS based solar cells tend to have a better energy production than the first-generation crystalline silicon cell. This could be attributed to their "good and durable operating systems" and their much lower temperature co-efficiencies, *i.e.*, 0.35% /°C.

Generally, CIGS based cells tend to have a greyish to blackish colour, which could be modified to attain a more elegant shiny or mat appearance by applying the appropriate coating.

Figure 2.18 CIGS Based Modules; Modules Manufactured by Manz Used on Façade of House of the German Team at the 2009 Solar Decathlon (Left). CIGS Modules Manufactured by Sulfurcell Used on the Façade of Ferdinand-Braun-Institut für Höchstfrequenztechnik, Berlin.

b. CdTe thin-film modules Cadmium

Cadmium Telluride (CdTe) based photovoltaics have been recognised as the most widely successful thin-film PV for commercial application (Basol & McCandless, 2014). According to the authors, their first demonstration was done in the 1980s, where an efficiency of approximately 10% was reached. In 2014, another milestone was reached in the growth of CdTe cells when module efficiencies of 20% were recorded. In addition, a record efficiency of 22.1% under laboratory testing conditions and an efficiency of 18% under commercial use was achieved by First Solar, a CdTe specialist, at the end of 2020. Compared with other thin-film based technologies, CdTe thin-film s have the most competitive production costs (Jelle *et al*., 2012). Whereas there are a few notable issues of toxicity associated with CdTe PVs, the technology boasts of low carbon emission compared with its counterparts.

Furthermore, CdTe PV cells have short energy and greenhouse gas payback periods (EPBT & GPBT) mainly due to their cost and material-efficient production processes. CdTe-based cells' cost per watt was 0.5USD as early as 2013, making them a very competitive PV solution. In fact, according to the Office of Energy Efficiency & Renewable Energy, CdTe solar cells are regarded as the second most common PV technologies after crystalline silicon solar cells representing 5% on the solar market (Solar Energy Technology Office, 2019). Furthermore, CdTe based cells have temperature co-efficiencies ranging from -0.20 to -0.30 %/°C, which is very low compared to crystalline silicon PV systems.

CdTe-based solutions are made in two configurations: a superstrate or a substrate. In a superstrate configuration, a stack of a transparent conductive oxide (TCO) layer/ junction-partner/CdTe/back-contacts are applied over a transparent superstrate layer "through which light enters the cell." The superstrate configuration is more widely used for commercialised high-efficiency applications. However, in a substrate configuration, the stack is applied over a substrate, which could be opaque (Basol & McCandless, 2014).

Whereas the earliest manufactured cells were manufactured using film deposition techniques, deposition soon became evident, not producing highly efficient solutions. Initially, the hope was that it would be possible to obtain the highest-quality absorber and junction, thus manufacturing capitalised on film deposition techniques. It later becomes evident that other post-deposition steps would be needed for the already

deposited “CdS/CdTe film stacks” (Basol & McCandless, 2014).

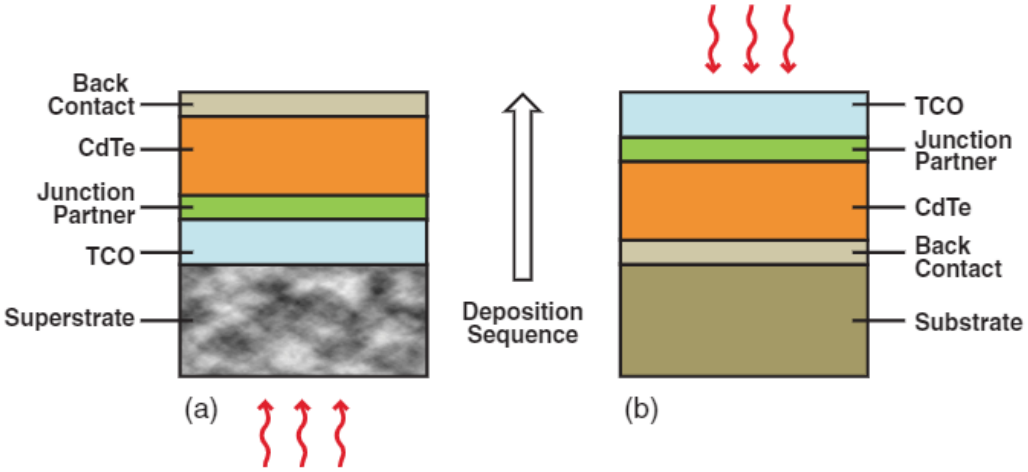

Figure 2.19 CdTe Solar Cell Configurations: (a) Superstrate and (b) Substrate (Basol & McCandless, 2014)

The toxicity of Cadmium and the limited abundance of tellurium as a natural material is the biggest limitation to the use of CdTe-based photovoltaics. Recycling CdTe cells at the end of their lives are considered one solution to the toxicity associated with the cadmium element.

CdTe based PV modules have a homogenous appearance of dark green or black coloured. It is also possible to have flexible solutions. However, transparent CdTe solutions are still not available on the market.

Figure 2.20 An Array of CdTe PV

2.2.6.2.3 Third-generation "Organic-based" PV Technologies

In the development of first and second-generation technologies, the main focus was on cost reduction; however, with the third-generation technologies, the focus is mainly on PCE improvement with a focus on overcoming the "Shockley-Queisser limit" (IEA, 2014; Subtil Lacerda & Van Den Bergh, 2016).

These technologies have been categorised in different ways following different aspects of their evolution. Mark *et al*., (2015) categorise third-generation photovoltaics into two categories based on; the increase in PCE, which covers technologies such as "hot carriers", multiple electron-hole pair creation, and thermophotonics. And cost reduction. Under cost reduction, the aim is usually to actualise mass production and reduce the required materials.

Also, according to the guidelines offered by the European Photovoltaic Industry Association, third-generation technologies that are already undergoing commercialisation could be further put under the following categories;

i. Advanced inorganic thin-film includes low-cost printed versions of existing inorganic thin-film technologies like spherical Copper Indium Selenide (CIS) and thin-film polycrystalline silicon solar cells.
ii. Organic solar cells; consist mainly of fully organic and hybrid dye-sensitized solar cells.
iii. Thermo-photovoltaic low band-gap cells; these particular ones are used in combining heat and power (CHP) systems.

Overall, third-generation PV technologies include the OPV Organic Photovoltaics, DSSC or DSC- Dye-Sensitized Solar Cells, quantum dot solar cells, and perovskite solar cells (J. Liu et al. Despite the PV market being dominated by the first two generations of PV systems, the third-generation of PV systems is drawing a lot of attention mainly due to the following reasons;

Their outstanding features include "lightness, flexibility, versatility, sustainability of materials, cost-effectiveness." These features make third-generation PV technologies the preferred option for Building Integration over other PV technologies.

The possibility of adopting production technologies from other printing sectors such as ink-jet, roll to roll printing, or flexible substrates plays a big role in cost reduction and product customisation. In addition, the use of borrowed printing technology allows for the adoption of third-generation PVs on other products such as textiles, auto-motives and portable devices.

Furthermore, with third-generation photovoltaics, it is possible to customise the cell colours to several options. This is an advantage over their 1st and 2nd generation counterparts, whose appearances vary only in opaque and dark colours.

However, despite all the advantages mentioned above of third-generation PV systems, there are still issues to enhance their durability, stability, and efficiency, which still have to be addressed (Morini, 2021). The different options within the third-generation of PV technologies are explored below;

a. Organic Photovoltaics (OPV)

Due to its low and persistently decreasing cost of production 0.50€/W, the OPV type is perhaps what will offer the third-generation technologies a chance at commercialisation (EPIA, 2014).

The semiconductor is sandwiched between a thin-film transparent conductive oxide coated substrate and a metal layer in OPV cells, which functions as a "counter electrode." The substrates used in OPV could be flexible such as Poly Ethylene Terephthalate, or PET or rigid such as glass. As per the test done by German company Heliatek, under laboratory testing conditions, opaque OPVs reached a record efficiency of 12%. In contrast, transparent ones reached an efficiency of 7.2%, which are relatively lower than those for the second and first-generation PV technologies. However, OPV displays a better performance under diffuse or angular solar irradiation than other generations of PV technologies. Furthermore, OPV cells have a positive temperature co-efficiency, enabling them to maintain good performance even under outdoor operating temperatures instead of other PV generations, which lose efficiency under outdoor operating temperatures that usually rise above 25^{o}C.

Figure 2.21 Organic Photovoltaic

Overall, compared with other PV technologies, Organic Photovoltaics standout, due to the following aspects:

The lightness of the cells is mainly due to the use of thinner active layers material. This also contributes greatly to reducing cost and the amount of material required. Great environmental performance due to their organic nature and low levels of embedded energy. Furthermore, it is possible to achieve a range of colours with OPV. This unique feature makes it particularly suitable for BIPV use. The colours widely used in OPV technologies include; grey, green, red on either opaque or transparent substrates. To achieve transparency, it is not required to subtract from the cell's active layer, but rather the cell itself is transparent.

The use of printing technology in production allows for different shapes and a great range of customisations. The possibility to customise designs with OPV cells was best displayed in the design of the German Pavilion Figure 2.22, left) at the 2015 Milan Expo, by Germany manufacture Belectric OPV.

Figure 2.22 OPVs Used on the German Pavilion, Milan Expo. (Left); Heliatek's HQ, Dresden (Right).

The manufacturing cost of OPV systems was estimated by Gambhir *et al*., (2016), to fall within the interquartile range of US$0.23–0.34/ Wp, with a median cost estimate of $0.28/Wp. Earlier Kalowekamo & Baker, (2009) had estimated the cost of purely organic solar cells to range from $50 to $140/$m^2$, which is an equivalent of $1.00 and

$2.83/Wp, assuming a 5% PCE and a 5-year life span. They used a very wide range to estimate, as the technology was still much younger. However, to contend the marketplace against other PV technologies, the lifetime will have to be increased to about 15 to 20 years, and the efficiency would be approximately 15%.

b. Dye-Sensitized Solar Cells (DSSC or DSC)

As is the case with OPV cells, Dye-sensitized Solar cells have also been drawing much attention recently due to their low costs, low toxicity, and easy cheap production process (Sharma *et al*., 2018). These particular types of solar cells have seen extensive research mainly over the past two decades. They have been regarded as a technical and economically viable alternative to the first-generation silicon types. Perhaps their initiation could be traced back to the 1960s when scientists realised that electricity could be generated by illuminating an organic dye in an electrochemical cell. However, the technology did not see many breakthroughs until the early 1990s when a DSSC could record relatively high efficiency of 7%, as noted by researchers O'Regan B and Gratzel M in 1991. The structure and operating principles of this technology are explored below.

- **Structure and Operating Mechanism of a DSC**

DSSC generally consist of a working electrode, sensitizer (dye), redox-mediator (electrolyte), and counter electrode.

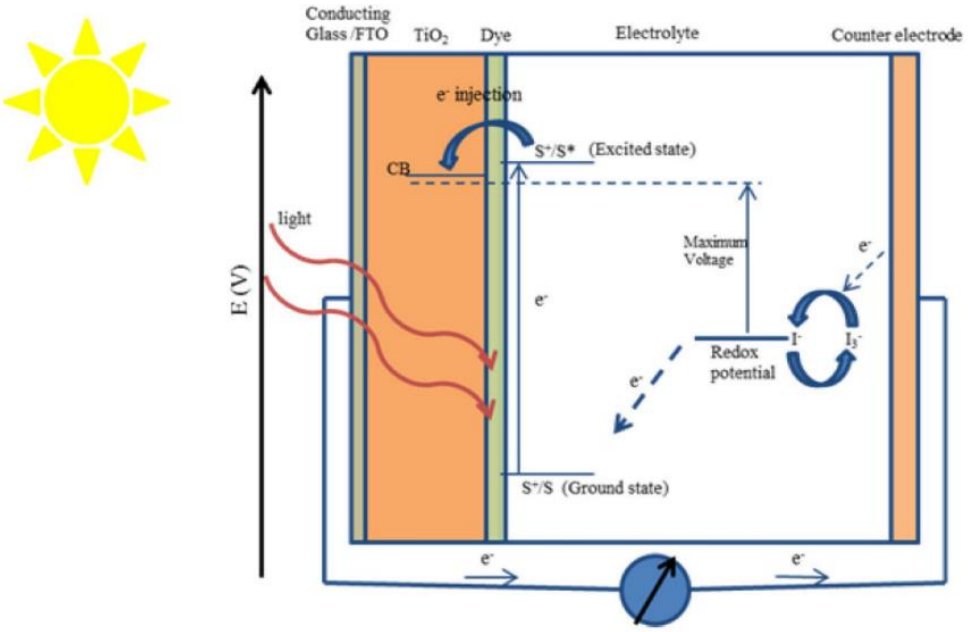

Figure 2.23 Construction of the Dye-sensitized Nanocrystal Line Solar Cells (Sharma *et al*., 2018).

Overall, a DSSC cell consists of two sheets of transparent conductive material, which act as the substrates for the deposition of semiconductor material and serve as a solar collector. The substrates need to have a transparency of about 80% to allow light transmission through to the active cell layer.

In addition, a Photosensitizer or Dye is applied to a DSSC to enable optimal light absorption. Generally, for a material to be usable as a Photosensitizer or Dye, it should be; luminescent, have an absorption spectrum that covers ultraviolet-visible (UV-vis) and near-infrared region (NIR) regions, have a HOMO which lies below the redox electrolytes, as well as have a hydrophobic periphery to enhance the cells longevity.

A DSSC also consists of an electrolyte with the following five components; “redox couple, solvent, additives, ionic liquids, and cations.”

Lastly, a DSSC cell should also have a Counter Electrode (CE), which is generally made of platinum (Pt) or carbon (C). Both working and counter electrodes are joined, and s syringe is used to fill the cell with an electrolyte solution (Sharma *et al*., 2018).

The process of electricity generation using a DSSC can be put under four main steps: light absorption, electron injection, carrier transportation, and current collection. First, when visible light strikes the cell, photons are absorbed by the photosensitizer material and used to excite the electrons from the ground state to the excited state. The excited electrons are transferred to the conduction band of a Nano-porous TiO_2 electrode lying below the excited state of the dye. The electrons are then moved to the back contact, and following an external circuit, the electrons reach the counter electrode. At the counter electrode, the excited electrons are regenerated back into the ground state through the reduction of I^-_3 to I^-.

As previously mentioned, one of the unique advantages of DSSC is its ability to maintain a good PCE under even diffuse lighting conditions. Perhaps even peculiar about its efficiency is its ability to maintain a good efficiency even under artificial lighting conditions. This outstanding feature of the DSC technology has been widely applied by tech companies such as Sony, which develop electric devices like calculators for use under indoor conditions. Furthermore, when DSC is applied to a transparent substrate, they allow for bifacial application, enabling exposure to light from both the exterior and interior of the building, thus adding to the time of exposure and the opportunity to take advantage of artificial lighting from the interior. On the exterior, bifacial configurations of solar cells could be utilised on vertical dividers such as parapets, noise barriers or bridges.

Furthermore, with a south-north orientation of DSC, it is possible to harness photons from the sun almost throughout the whole day. The cells will catch morning sun from the east and evening or afternoon sun from the west. Compared to other PV technologies, the temperature coefficients of Dye Sensitised Cells are approximately -0.005 %/°C, which is outstanding compared to -0.45%/^{o}C for c-Si or even 0.2 %/$^\circ$C

of a-Si (Heinstein *et al*., 2013). Implying that the operating temperature of the dye cell, which usually exceeds 25 degrees, do not deter the cell from operating with good efficiency; in fact, operating temperature could boost the efficiency of the cell (Morini, 2021).

The Dye sensitised solar cells' advantages above give the technology an upper hand over other technologies. In fact, it was discovered the DSC could potentially produce 10 to 15% more energy annually than other technologies that have higher efficiencies, such as the c-Si. For application in BIPV systems, the possibility of producing DSC in various colours, light transparencies, flexibility or opaqueness makes them the most suitable option.

- **Configuration of a DSSC**

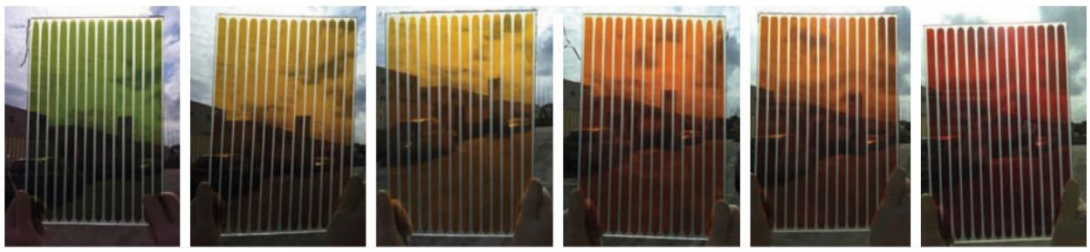

Figure 2.24 ye Sensitised Solar Cells of Different Colours (Morini, 2021)

DSSC comprises narrow rectangular solar active strips interconnected and very transparent gaps between the strips. An encapsulating material such as resin or glass is used to enclose the cells. The non-active spaces between the cells usually account for the bigger part of PCE loss. Different aesthetic configurations with different transparencies can be created by playing with the shape of the PV active portions of the DSSC. In fact, by varying the design of the active portions, transparencies of up to 40% have been achieved with a minimal drop in the cell PCE.

Power conversion efficiencies as high as 20.1% have been recorded with the DSSC technology. This was achieved using a thin layer of perovskite crystals with a solid hole conductor in place of a liquid electrolyte. As research and technology develop, speculation for further advancements have been made (Silvia *et al*., 2015).

By varying the dye compositions, DSSC could easily be varied from green, grey reddish, brown, orange, blue… colours. When a transparent substrate is used, such as glass, it is possible to achieve interesting shades of coloured light penetrating the interior of a building. Furthermore, the modules tend to have a homogenous appearance from a distance despite having a strip configuration of the active cell layers. Additionally, by altering the coloured layer thickness, it is possible to vary the tones of the same colour on a DSSC, enabling different designs such as those in image 2.2.25 below.

Figure 2.25 Designs on a DSSC Achieved by Varying Colour Layer Thickness

As of 2019, the DSSC global market size was evaluated at 90.5M USD (Market Analysis Report, 2020). The report predicted an annual growth rate of 12.4% between 2020 and 2027. Their exponential predicted growth can be traced down to

the low costs associated with the production of DSSC, its high-performance rates, and DSC's ability to maintain good efficiency under low light conditions. DSSC is bound to see an increased application in many different fields. These include; "outdoor advertising, portable charging, embedded electronics, BIPV/BAPV, and automotive (AIPV)", with the largest market being that of portable changing devices. Graph 2.26 below depicts the predicted application of DSSC.

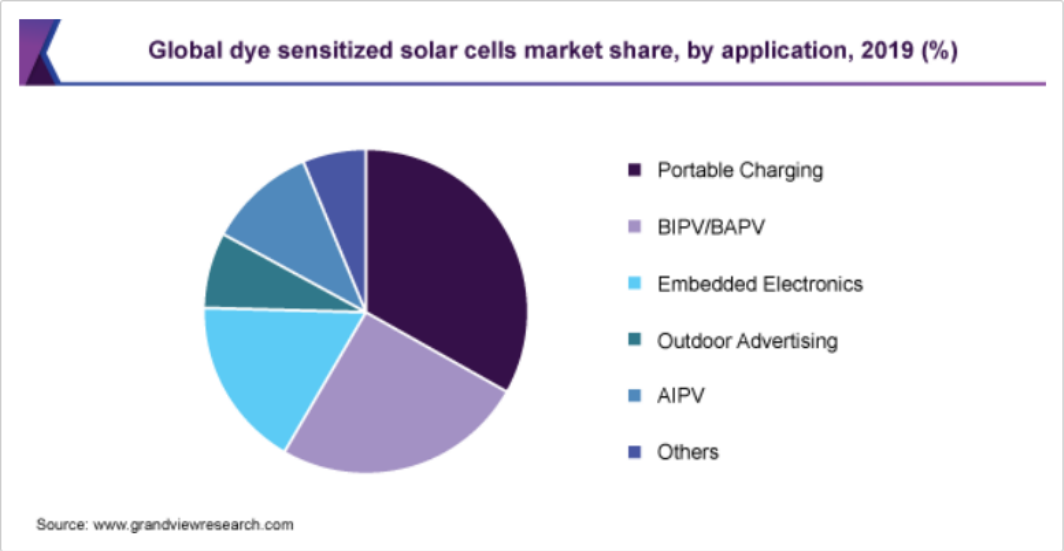

Figure 2.26 Expected Market Applications of DSSC (Market Analysis Report, 2020).

c. Perovskite Solar Cells

The Discovery of PSC technology was in 2009 when a team of Japanese scientists noticed the similarity between dyes and the organic metal halide perovskite. It was found that organic metal halide perovskite too can absorb sunlight.

Perovskites or perovskite structures are a mineral composed of "calcium, titanium and oxygen in the form CaTiO3 (Ossila, 2021)."

The Japanese scientists that made this discovery achieved a PCE of 3.8% when they applied a perovskite as a sensitizer in a liquid electrolyte-based dye sensitizer solar

cell (Kojima *et al*., 2009). Later, Kim *et al*., (2012) reported an all-solid-state PSC with a PCE of 9.7%. PSCs have attracted a lot of attention from researchers, and within a decade of their inception, a PCE of 22.1% has already been reached as of 2016. The comparison between the growths of PSC against its other thin-film counterparts is illustrated in the graph chat below by the National Renewable Energy Laboratory (NREL).

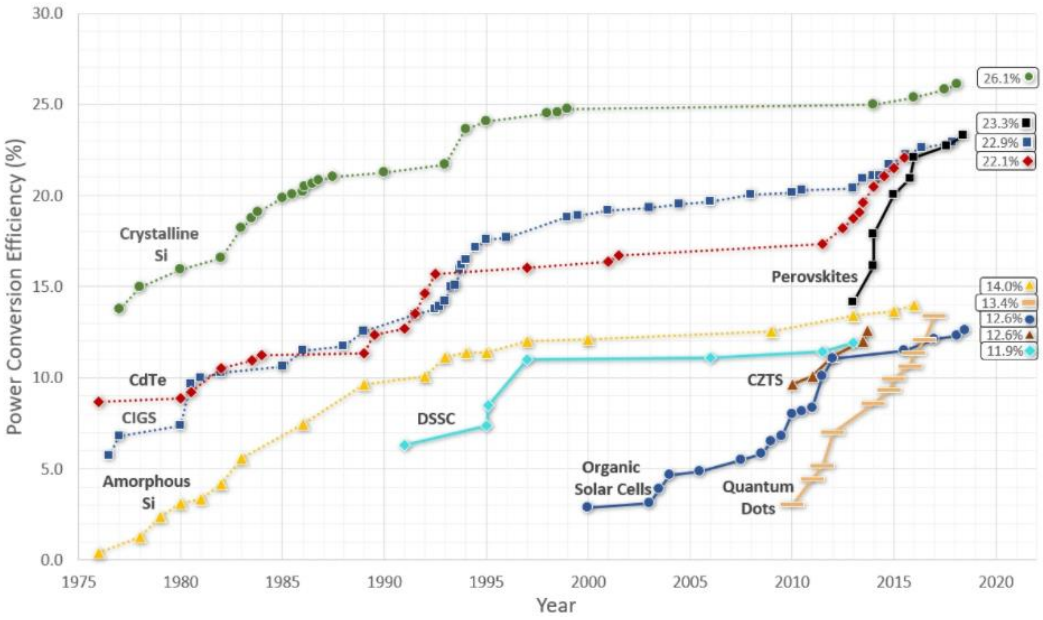

Figure 2.27 PSC (black) have Exponential Growth of the Perovskite Solar Cell's Power Conversion Efficiency Since its Inception Compared to other PV Technologies (Ossila, 2021).

Graph 2.27 above, developed by the NREL, illustrates a rapid increase achieved in the power conversion efficiencies of the PSC. In fact, within only four years from its inception, the PSC's power conversion efficiency had already surpassed that of the Cadmium Telluride (CdTe), whose research and development has been ongoing for over 40 years. Furthermore, by 2018, the PSC efficiency had surpassed all "non-concentrator thin-film technologies" such as Cadmium Telluride (CdTe) and Copper Indium Gallium Selenide (CIGS).

Another graph below compares the open-circuit voltage against the band gap. The graph depicts the number of photons lost when light energy is converted into direct current (DC). For organic solar cells such as the OPV, up to about 50% of the photon energy is lost during the conversion. However, the PSC utilises up to 70% and could even be increased. According to Ossila, (2021), PSC could eventually become cheaper than the c-Si technologies closest to the PSC in terms of efficiency and already 1000 times cheaper than the GaAs.

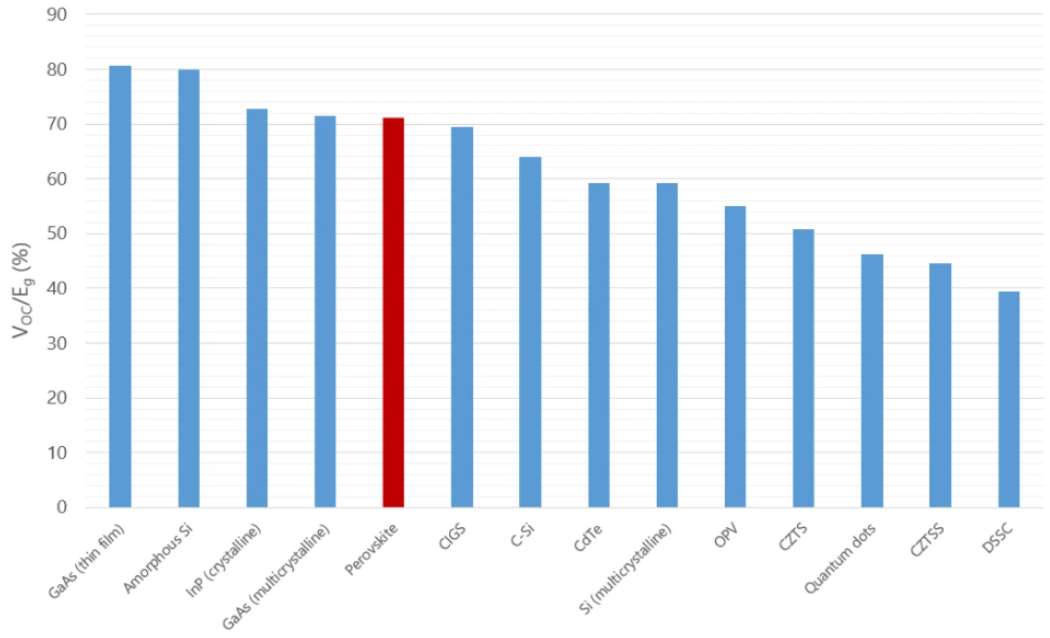

Figure 2.28 Maximum Photon Energy Utilisation is also referred to as the Open-circuit Voltage (Voc) divided by the Optical Band-Gap for Common Single-junction Cells.

- **Operation Principles of a Perovskite Solar Cell**

The PSC will absorb the photons when exposed to sunlight, resulting in the production of excitons (electron-hole pairs). The difference in the binding energy of the excitons within the perovskite material results in the creation of a current through the formation of free carries (electrons or holes) from the excitons or the recombination of carries into excitons. However, since the charge for recombination of the carriers is very low and the high mobility of the carriers, the lifespan and

diffusion distance is lengthened. The perovskite Solar Cell draws its superior performance over other PV technologies from these two aspects *i.e.* longer diffusion distance and longer carrier lifespans.

An ETM- Electron Transportation Material and HTM- Hole Transportation Material collect the free electrons and holes, respectively. The electrons are transferred from the perovskite material onto the ETM, which is usually made from TiO_2 and then collected by the FTO. Likewise, the holes are transferred to the Hole Transportation Material and later collected by the metal electrode. Finally, when the FTO is connected to the metal electrode, a photocurrent is generated and starts to flow in the outer circuit.

2.3 PART 3: Building Integrated Photovoltaics

Building-integrated photovoltaics (BIPV) allows for electricity production at the point of use within the built environment. Integrating photovoltaics into a building would imply adding an extra function to a would rather be a single or mono functional building component. The photovoltaic cells form the main components of any BIPV modules created by joining and encapsulating unit solar cells on various construction materials. The BIPV modules are then co-joined in strings to form an array. Like regular photovoltaic systems, exposure of the BIPV modules to direct or diffuse light will induce a photovoltaic effect within the solar cells of the BIPV materials. The induction of the PV effect results in the generation of direct current. The generated DC is run through an inverter, converting it into a useable alternating current. The electricity surplus generated from the BIPV array system could be stored in a battery system or fed into the electric grid. Like all construction materials, BIPV must meet certain physical and technical requirements stated in the Construction Products Regulation (CPR) 305/2011. BIPV modules are expected to serve as physical and technical components, and removing a piece of them would necessitate an immediate replacement with an equally functioning material. Also

being exposed defining elements on building façades, BIPV modules are also expected to meet certain aesthetic requirements. In the ensuing subsections, the potentiality of integrating photovoltaics into building envelop components will be explored while also making various definitions of Building Integrated Photovoltaics based on literature. Additionally, different design options that could enhance building aesthetics and building occupant comfort as relates to BIPVs will be discussed.

2.3.1 Definition of Building Integrated Photovoltaics

Building-integrated Photovoltaics are PV systems built into the building envelope to replace building parts (Jelle *et al*., 2012). According to the authors, this multi-functional purpose of BIPV helps reduce the cost of operating a building. BIPV systems can be placed under the following categories; photovoltaic foils, photovoltaic tiles, photovoltaic modules and solar cell glazing. Although non-silicon-based BIPVs are gradually becoming commonplace, the BIPV market remains predominantly silicon-based. The predominant silicon BIPV types are either silicon-based wafers or silicon-based thin-film s. BIPVs are mainly façade based or flat and sloped roof integrated. The main properties to be considered in BIPV evaluation are; open-circuit voltage, PCE, fill factor, short circuit current and maximum effect. Most important when evaluating BIPV are their impacts on the aesthetic appearance of buildings. This could come from different aspects of the BIPV, such as their colour. Additionally, it is important to consider how the selection of a certain BIPV component affects the comfort of the building occupants. The ensuing sections explore the different alterations that can be made to the configuration of BIPVs to enhance their adoptability within the building envelopes without affecting the aesthetics.

2.3.1.1 A Comparative Description of Conventional Photovoltaic and BIPV Module Configurations

The design of a PV module consists of a solar cell layer, two encapsulating layers which surround the solar cell and a rear and front cover. This configuration is referred to as a laminate (Kuhn *et al*., 2020). Additionally, a frame and junction box connected to the module enables mechanical and electrical connection of the module to the building. The frame is a part of the mounting system used to mount or attach the module to the building. The junction box contains the bypass diodes. The junction box is excluded from the module in a few unique cases. In such cases, as in streetlights, the module forms an integral part of a "complete system" and is usually used in device integrated PVs. The junction box is used for electrical connection through connectors or cables.

In some cases, the by-pass diodes are integrated into the laminate, which reduces the module size, in which case the junction box is only reduced to a connection box. One of the purposes of by-diodes is to eliminate the "hot-spot phenomena" that could potentially damage the photovoltaic cells (Solaredge, 2010). Eliminating hot spots in PV module circuits allows them to function reliably throughout their lifetime. Whereas bypass diodes play a critical role in bypassing modules in strings during shading periods, the authors argue that this could also be a great cause of loss in the functioning of the photovoltaic system.

In standard modules, the frame of the PV module will provide a point of anchoring to the rack. In BIPV modules, however, more complex mounting systems, which provide mechanical connection to the building and mechanical stability, are required. It is also important in the case of BIPVs to ensure that the mounting systems are visually concealed to avoid distorting the aesthetics of the building (Kuhn *et al*., 2020).

A few technical solutions involve rear covers that also serve as mounting systems; thus, the mounting systems; replace the rear cover in such cases, as is the case with AUTARQ solar designed modules.

In some technical applications, instead of using the two identical layers of the rear or front cover and encapsulates, it is possible to combine these into a single layer that serves as both the encapsulate and the rear or front cover. Ensuring the modules operate at optimal efficiency is key in PV systems. Thus, some have adopted cover materials of low reflective surfaces to enhance the efficiency of modules (Gochermann Solar Technology, n.d.).

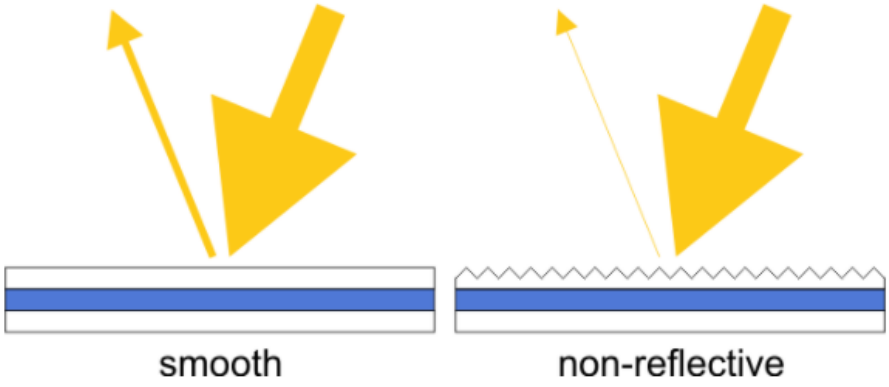

Figure 2.29 A Technical Solution to Reduce the Reflectiveness of Module Covers Using a Micro Structured Pyramidal-shaped Top layer (Gochermann Solar Technology, n.d.).

The high sensitivity of the embedding materials to humidity, moisture, and mechanical stress makes using separate layers for the encapsulate and rear or front covers more feasible and cost-effective than combining them.

2.3.1.2 Design Option for Building Integrated Photovoltaics

BIPV systems are expected to meet the aesthetic needs of the building and function efficiently enough as energy-generating components producing maximum power to subsidise energy costs incurred by the building owner (Mittag *et al*., 2018; PV &

Energy, 2018). The aesthetics of BIPV modules should be flexible in both design and appearance. Kuhn *et al*., (2020) suggest making variations in the aesthetic design of BIPV modules to increase energy efficiency or reduce their cost. The following subsections discuss the possible design alterations that can be implemented on BIPV modules to enhance their aesthetic appearance and electrical efficiency.

2.3.1.2.1 Design Option for the Front and Rear Covers

Kuhn *et al*., (2020) described the structures of the front and rear covers as consisting of the external surface, bulk material and internal surface. However, it is also suggested that the rear and front materials could be completely different. For example, it is possible to use glass material for the front cover and layered polymer films as the rear cover materials. Surfaces both on the outside and inside can be structured or coated. Additionally, additional layers can be used as finishing. It is also possible to combine both structuring and coating.

In some cases, the coating or structuring could be functional, but it could be merely aesthetical. Additive layers can be applied as a coating to the bulk material of the cover layer. Examples of coatings include sputtered coatings, enamel coatings or printed coatings. It is also possible to use vanishes and lacquer (Eder *et al*., 2019).

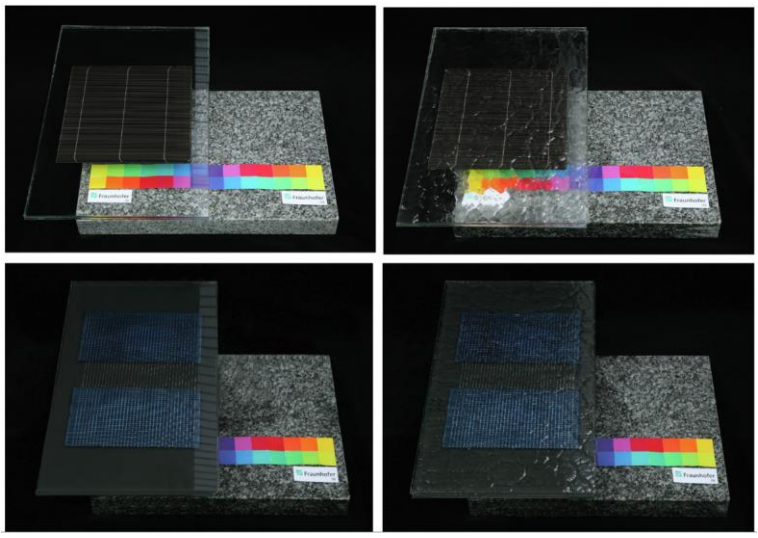

Figure 2.30 Different appearances of macroscopic surface textures.

The different images in figure 2.30 above compare the different appearances of macroscopic surface textures. The top row is more transparent, whereas the bottom row is opaque configurations.

- **Using Coating Materials to Enhance Module Appearance**

The coating on the module's structure will affect both appearance and reflection behaviour; thus, affecting the amount of glare from the module that results from the specular reflection of the sun. Classic flat antireflective surfaces such as *interference layers* or *nonporous structures* (k/4 layers) alone are not sufficient to eliminate the glare effect from the module. When such flat anti-reflective layers are used, the luminance of the sun can only be reduced by up to 99% (*i.e.* a factor of 10^{-2}). A 99% reduction factor, which is achieved, makes no difference to the glare that is perceived by the eye due to the logarithmic sensitivity of the eye and the sun's high luminance of 109 cd/m2. *Diffusing surface textures* could help resolve this issue by providing good anti-glare properties. Such diffusely reflecting surfaces have the potential to reduce the sun's glare by up to 10^{-5} through isotropic diffuse scattering enabling the achievement of good glare control. However, extra care must be taken in cases where diffusely scattering surfaces are used to ensure that the transmission

of the sun through the layers is not compromised, which could reduce the amount of electricity generated.

Figure 2.31 Figure of Spectrally Selective Morpho-Colour Structure Located on the Inside of the Front Cover (Kuhn *et al*., 2020).

The figure above shows matt coloured anti-reflective surfaces, which are examples of light-scattering, highly transmitting, anti-reflective surfaces.

The three coloured modules on the right are spectrally selective Morpho-Colour structures beneath the front cover. The upper left-hand figure illustrates the effect of using coloured green Morpho colours over a solar module placed on a white table. The lower left image is of the overall layer arrangement of the module with a Morpho-Colour layer (Kuhn *et al*., 2020).

Additional glazing layers could be added behind the back cover or used in its place instead. For example, in the figure below, the module is integrated into a double-glazing unit (DGU), which replaces the rare cover as a single polymer or glass pane with a complete glazing unit.

It’s also possible to add functional coating or structuring to either the internal or external surfaces. For instance, Anti-reflective (AR) coating is usually added to the external surfaces. An “adhesive strengthener” could be used on internal surfaces. In addition, due to the possible effects on the environment, applying the aesthetic coating is usually possible only on the internal surfaces.

The most commonly used bulk material is glass, which has many advantages for BIPVs. Its advantages over other bulk materials are high transparency, mechanical stability, low thermal expansion, non-combustibility, sustainability and recyclability.

2.3.1.2.2 Design Options for the PV Cell Layer and Electrical Module Layout

According to Kuhn et al., (2020), the cell layer of the PV module affects a number of the module's aspects which include; the appearance, amount of electricity yielded, and the lifespan of the solar module. Similar to conventional PV systems, BIPV technologies also use mainly two solar cell technologies, namely:

- The wafer-based technologies include crystalline silicon or the tandem solar cells that combine two layers of solar cells.
- Thin-film technologies.

An elaborate discussion of the above cell technologies is presented in section 2.2.6.2 of this thesis.

- **Types of BIPV Solar Cell Technologies;**

The solar cell technologies used in BIPV modules are similar to those used in conventional PV modules. Below, a recap is made of these solar cell technologies focusing on their efficiencies, market share, and adaptability for building integration as BIPV components. A more elaborated discussion of these technologies, materials, and production techniques can be found under section 2.2.6.2 of the thesis.

i. **Crystalline Silicon (c-Si) Solar Cells:** Crystalline silicon (c-Si) solar cells are the most widely used type of solar cell. Green *et al*., (2020) noted that the current efficiency of the c-Si cell stands at 26%. Various technologies have been developed with which different efficiencies can be reached. For instance, the PERC (passivated emitter and rear cell), which was first proposed in the 1980s by the UNSW (University of New South Wales), could

reach an efficiency of about 20.5% at the current stand of technological development.

It is possible to attain much higher efficiencies with later technologies such as the TopCon technology and heterojunction technology (HJT). For instance, Kuhn *et al*., (2020) noted efficiencies of 21% or 22% respectively for both technologies.

ii. **III-V Cells:** These have the highest efficiency recorded of all solar module configurations of about 29% for GaAs single-junction cells and 38.8 % multi-junction solar cells (Green *et al*., 2020; Kuhn *et al*., 2020). On the downside, the overall cost of an III-V solar cell is estimated to be about two times higher than the c-Si solar cell. This is mainly because rare materials are used in III-V cells and cost more overall. These multi-junction cell types have wide application in space technologies due to their high efficiencies and good resistance to radiation (J. Li *et al*., 2021). However, it is important to highlight the high cost of their manufacturing.

iii. **Perovskite on Si Tandem Cells**: When large size wafers are used for the perovskite solar cells, the overall efficiency of the cells could go up to 29. 1% in (N. Liu *et al*., 2020). So far, only an expected price range has been projected for these kinds of solar cells, as they have not yet reached the market. They are, on average, expected to cost more than the c-Si solar cells and the single junction concepts. However, they are expected to have a temperature and irradiation dependence similar to the c-Si solar cell. On the downside, the perovskite cells are more toxic as they contain lead.

iv. **Chalcogenide Thin-film Solar Cells (*i.e.* CIGS, CdTe):** According to Kuhn et al., (2020), this kind of solar technology is the second most relevant after the crystalline silicon solar cells in BIPVs. They have a homogenous appearance, which provides good aesthetics, making them suitable for building integration. The highest recorded efficiency reached with the Chalcogenide thin-film solar cells has been 22%.

According to Paire *et al*., (2014), CIGS can reach high efficiencies while only utilising fewer cells, making it a good alternative to crystalline silicon in BIPV applications. The good aesthetics of the thin-film also make it a good choice for building an integrated application on roofs or façades. Lightweight and flexible CIGS modules, which possess higher conversion efficiencies than silicon-based thin-film modules, make them suitable for application on industrial roofs.

As illustrated in figure 2.32 below, thin-film technologies based on amorphous and microcrystalline silicon, cadmium telluride, and CIGS are growing faster than wafer-based technologies.

The toxicity is not only a downside related to the perovskite cell, but rather all solar cell technologies contain a certain level of toxicity due to the amounts of lead used in their production.

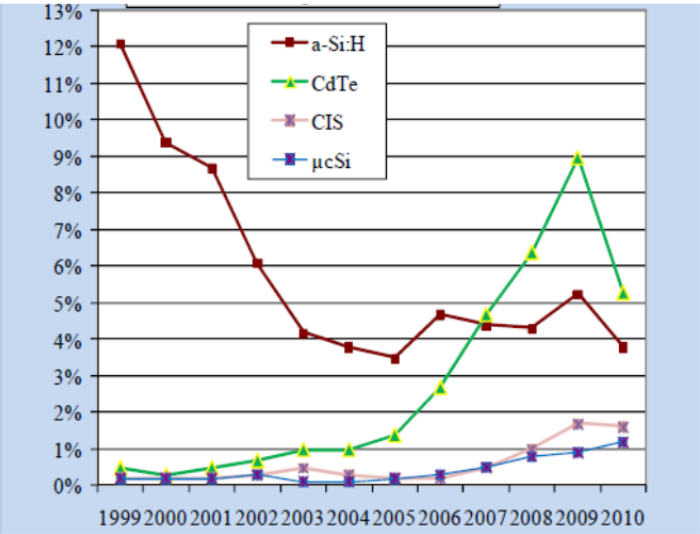

Figure 2.32 A comparison of Thin-Film-based Technologies' Market Share Growth (Paire *et al*., 2014).

v. Organic (OPV) Cells or Dye-sensitized Cells:

OPV cells have recorded a maximum efficiency of 17.4% and dye-sensitized cells 12.3%. Overall, their cost is expected to be less than other widely used technologies such as c-Si, but this advantage is not yet realised as there is still a limit on the number of producers of these kinds of cells on the market. Organic (OPV) cells or dye-sensitized cell technologies are also presumed to suffer more UV light degradation than other solar cell technologies. These cells, however, are also more bendable, making it possible to have curved modular fabrication.

vi. Perovskite Solar Cells:

Through perovskite solar technologies, higher efficiencies than those of Chalcogenide thin-film solar cells have been reached. Currently, the conversion efficiency of the perovskite cell is seen to be standing at 25.2 % (Green *et al*., 2020). These are projected to be quite affordable, but durability could be compromised by exposure to humidity. The use of perovskite in solar cells was first reported in 2009, and their advancement has seen fast growth (Huang *et al*., 2021). Tandem combinations of perovskite-perovskite have also been realised. When used in interiors under indoor lighting conditions of buildings, single-junction perovskite cells have yielded efficiencies of 35.2% (Dagar *et al*., 2018).

The above described solar cell technologies have been incorporated in BIPVs as well. These are illustrated in the figure below. The figure below also describes the different design options for the solar cell for the BIPV application. According to Kuhn *et al*., 2020, in wafer-based cell technologies, it's possible to alter different aspects of the cell, such as size, shape, and colour. However, the author notes that altering the size and shape would require extra processing as special cutting technologies are usually applied. By playing with the position and spacing of the modules, it's possible to achieve some transparency in the module. According to the author, altering the colour of the cell would result in reduced efficiencies.

The model of interconnection used in wafer-based technologies plays a major role in the overall appearance of the module. The general modes of interconnection in modules are shown in the figure below. Generally, four modes are used; the Z-busbars, wire interconnection, conducting foils and edge connectors for back contacted cells and the shingle technology.

When wafer-based technologies are applied, it is possible to alter different aspects of the cell, such as the cell size, cell shape (contour and perforation), cell position and spacing and colour. According to (Kuhn *et al*., 2020), altering the cell's colour could compromise efficiency. Furthermore, altering the cell size is relatively difficult, requiring special technologies to be incorporated into the production process. However, this has seen an easing due to the increase in the half-cell technology created using laser cutting technology.

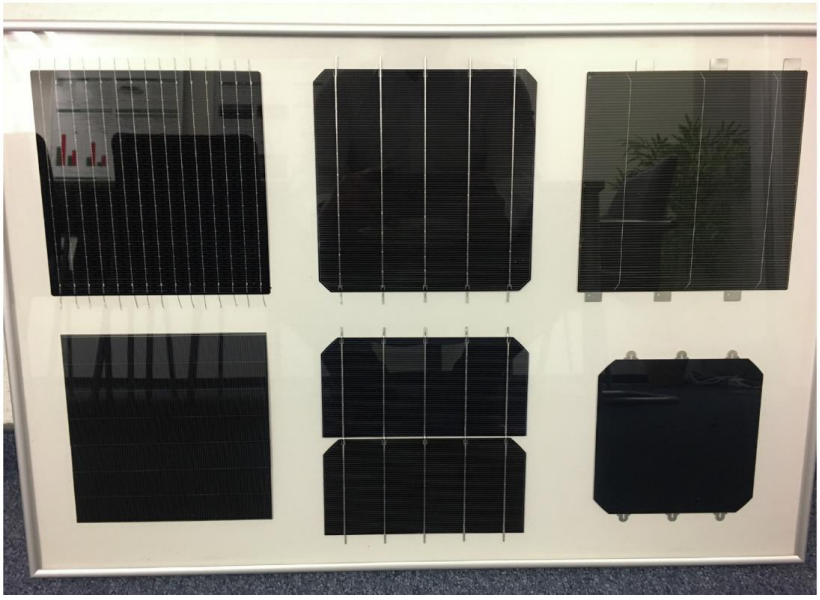

Figure 2.33 Comparison of the Different cell Interconnection Methods.

- **Linking Techniques Wafer-Based Cells**

The way wafer cells are interconnected in a module influences the module's general aesthetic. Generally, four different interconnection technologies are used in wafer-based cells. These are conventional Z-busbar method, wire-interconnection, Conducting foils and edge connectors for back-contacted cells and Shingle technology (Kuhn *et al*., 2020).

i. Standard Bus bar Method

Most commonly used are silver ribbon interconnections. These are placed on top of a dark coloured cell, which disturbs the overall aesthetics of the cell. And is less likely to be preferred by the architects. Several methods have been applied to conceal the silver ribbons on cells. These include:

a. Using a black sheet or tape to cover the cell after interconnection with silver ribbons.
b. "Aligning the ribbons behind a black print on the inside of the front cover."
c. Coat the ribbons with a somewhat dark colour before application.

The reflection of light by the brightly coloured ribbons greatly compromises the efficiency of the cells. Overall, the amount of light reflected by brightly coloured ribbons would otherwise be equivalent to 0.5% of the total electricity generated by the PV cell (Kuhn *et al*., 2020). When approaches 1 and 2 are used, there is likely to be considerable shading on the cell, which also compromises the efficiency of the cell.

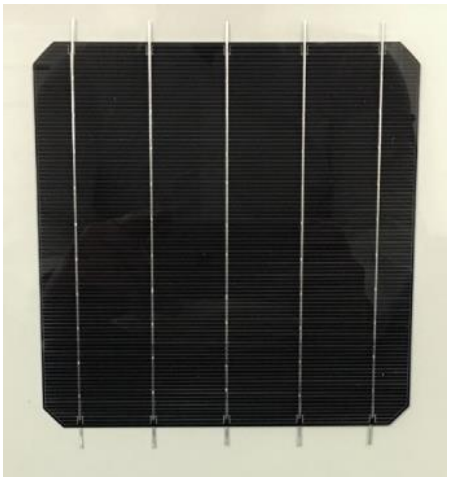

Figure 2.34 Standard Busbar Interconnection

ii. The Wire Interconnection Method

This method offers increased efficiency for standard modules. Usually, thin round wires are used to link the solar cells one to each other. The aesthetic benefit of using these is that their appearance is not as profound as silver ribbons used in the interconnected busbar cells.

iii. Back-contacted Solar Cells

This interconnection method is used to attain the highest electricity generation efficiency and the module's homogenous or black appearance. Kuhn *et al*., (2020) identified two different interconnection methods for the Back-Contacted Cells; one is the “IBC solar cell technology”, and the second is “emitter or metal wrap-through (EWT/MWT) solar cell technologies.”

The interconnection between the solar cells is placed at the back of the cells and is only visible in the small gaps between the cells. This makes it possible to have a completely homogenous black module appearance.

However, these solar cells cost more than cells utilising the busbar interconnection method.

iv. Shingled Interconnection Technology

According to Mondon *et al*., (2018), the shingled solar cell concept was first introduced in 1960 by D. C. Dickson. In a conventional module, the busbar interconnections are used at the front of the surface, increasing shading on the cell, thus reducing its efficiency. However, in a shingled setup, the busbars are placed at the edge of the cell and overlapping is done with the neighbouring cell. The active cell area replaces the inactive cell area by overlapping neighbouring cells, which increases the module's active area (Mondon *et al*., 2018).

Solar cells are cut into smaller strips, and contact between cells is made by overlapping the cells, such as in solar roofs. Conductive adhesive could be used to achieve contact between the cells. When smaller-sized cells are used, the conductive resistances are reduced, reducing the electric losses due to high magnitudes of resistance. Furthermore, a shingled setup is used to achieve a more homogenous appearance as no extra interconnectors are used. Furthermore, a shingled interconnection setup enables a “matrix interconnection configuration” when the cells are offset in a parallel direction. One cell interconnects with half of two other cells. See figure below:

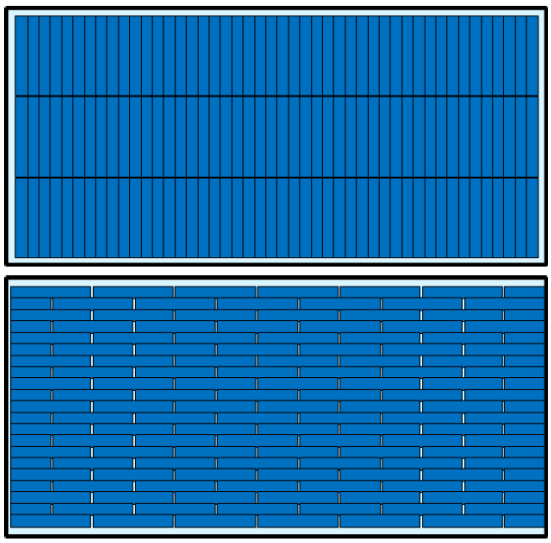

Figure 2.35 A Comparison of Two Module Cell Layouts.

The top configuration shows a parallel layout, while the bottom configuration displays a matrix layout (Mondon *et al*., 2018).

2.3.1.2.3 Design Options for the Electrical System

The main objective while designing the electrical system of any PV module is to achieve optimal power output at minimum cost. Specific to Building Integrated Photovoltaics is how the module will fit into the context of an already existing or newly constructed building. BIPVs, in particular, are prone to shading by nearby buildings or limitations in terms of flexibility of orientation of the unit. Thus, it isn't easy to have a BIPV module design that meets all technical, financial, and aesthetic requirements. The amount of current generated in an individual cell depends on the irradiance. Irradiance refers to the radiant flux (power) received by a surface per unit area. PV cells in a cell string are connected in series, implying that an “electrical mismatch” is bound to occur should the irradiance of a single cell be “inhomogeneous.” Thus, the current in the entire string of cells is limited when there is an overly shaded cell, resulting in big current losses. Implying that heavily loaded cells could be operated as “electrical loads (reverse bias)” in a string of cells, An outstanding amount of heating could occur in such cells. This section will evaluate the widely used options in the design of Building Integrated Voltaic Panels.

Below a breakdown of the technical structure of a BIPV module is presented. The evaluation is done in four different parts; first, the sub-structure level focusing on the inner structure of the individual module is assessed. Second, the individual module focuses on the external connections and other external electrical components such as the DC converter or micro-converter. Third, the entire BIPV system consists of several modules “electronic components like inverters (BIPV system level) and lastly, the whole building system level, including consumers, batteries, and grid connection.

i. Sub-Module Level;

This consists of components inside the PV module. The most important component is the PV cell itself. The type of semi-conductor such as crystalline silicon, amorphous silicon, CIGS, CdTe, organic; influences the efficiency of the solar cell by affecting related parameters such as temperature and the performance of the cell in low light conditions. Module configuration could vary along with the following parameters; the number of cells in the horizontal or vertical direction, adjacent distance between cells and the cells and edge of the module, cell orientation (parallel, perpendicular or rotated), and the interconnection technique. In cases where the module is prone to partial shading, it is often necessary to divide the module's cells into several electrical sub-systems. This ensures that every sub-section of the cell receives even illumination at each time of the day. In the façade of the Z3 building of Ed. Züblin AG in Stuttgart, Germany, the module's vertical wooden batten shade parts during the day. Thus, it was necessary to subdivide the module vertically into three parts to ensure each part is evenly shaded at each time. Implying that all the cells in the extreme left-hand side of the module are joined or connected in series, likewise, those in the central and right-hand columns.

In image 2.36 below, shading over some modules by the vertical wooden pieces is a likely problem in this particular façade. Thus, to prevent the panels' efficiency from being compromised due to the partial shading on one side of the panel at specific day hours, the panels were subdivided into three parts (left, middle and right). As a result, only one part of the panel is shade at a particular time, and the others can operate at full capacity without their performance being compromised.

By dividing the module into three sections vertically, consideration is taken for the recurring shading during different times that could vary from morning to evening. Implying that shading on one side of the module at a particular time of the day does not affect the total energy output of the whole module. All the cells in each of the columns (Left, middle and right) up-down the building are connected in series. This

considers the recurring shading on the panels in the evening and mornings. When one side (left or right) is shade in either the morning or evening, this does not affect the total output of the entire panel.

Figure 2.36 The Façade of the Z3 Building of Ed. Zublin in Germany.

ii. Module Level

Bypass diodes incorporated into junction boxes are mounted or attached to each module at the module level. Kuhn *et al*., (2020), identifies two types of junction boxes, namely, edge-mounted and those connected to the back of the module cover. The selection of the junction box mounting system could affect the aesthetic appearance of the module. Generally, passive by-pass diodes are used, which can "short-circuit the circuit of a sub-string and protect its cells against reverse voltage and hot spots." However, these are also associated with causing overheating in the module, current leakage and damage due to overvoltage. Thus, active bypass diodes can be used instead of passive bypass diodes. These use transistors, which reduce

losses due to conduction and “heat dissipation”, which results in increased efficiency and protection from active voltage.

Furthermore, an MPP is required for every system and the passive or active diodes connected to every string of cells. Central MPP tracking is usually applied in standard PV generators. However, in BIPV systems, panels general have varying orientations and geometric shapes; thus, decentralised MPP tracking could be necessary. This, according to the authors, could be done with DC/DC converters or micro-inverters at the module level. DC/DC converters are an interesting solution as they could be used to realise a local MPP while still connected to the central string inverter. Three different typologies are generally used on the system: buck, boost, and buck-boost converter. There is also a possibility of using micro inverters connected to the AC grid or obtaining local MPP tracking while in connection at the sub-string level.

iii. BIPV System Level

At the BIPV level, the design decisions are mainly centred around how the modules are interconnected. Generally, several modules are interconnected in series to strings. Furthermore, modules or strings could be connected in parallel. An inverter is connected to the modules to convert the *Direct Current into usable Alternating Current.* According to Kuhn *et al*., (2020), the inverter is the central component of the entire system which runs the whole system. Through Maximum Power Tracking (MPP), inverters determine the operating voltage of the entire system of modules. The authors, however, recommend that the type of inverter be selected carefully as some have to be equipped with a transformer to carry out the galvanic separation between DC and AC circuits or prevent Potential Induced Degradation (PID) effects. Presently, “transformer-less inverters”, which are smaller and more efficient, operate some PV modules in some cases. “Connecting strings of different orientations (e.g. east facade and west facade), which provide their maximum power at different times, to a single inverter can help to reduce the number and cost of inverters and to

increase self-consumption rates." Since most PV modules operate in low light or extremely hot conditions, selecting inverters with the right electrical parameters is important. Implying the start voltage has to be quite low and the rated powers. However, with future technological developments, it is hoped that a DC grid could be inverted, eliminating the need for having DC/AC inverted. It will be possible to connect the PV system directly to a DC house grid in such cases. With the inverter eliminated from the system, MPP will have to be done separately through a "charge controller" or "power optimizer."

iv. Design Options at Building Level

According to Kuhn *et al*., (2020), it becomes easy to balance the supply and demand of power at the building level when BIPV modules have different orientations. At the building level, choices can be made on whether to install a battery or not, including installation for EVs (Electrical Vehicles) or introducing large electrical loads such as heat pumps. Varying the orientation of the BIPV systems on different sides of the building could help match supply and demand.

2.3.1.3 A Brief Discussion on Half Cell Technology

According to (2015), improving the efficiency of solar cells is one of the main ways in which the cost of photovoltaics and, consequently, solar energy can be reduced. Different approaches such as the PERC cell have been seen to enable the conversion efficiency of solar cells to go beyond 20%.

Regarding the emergency of such new solar cell technologies, Kelly Pickerel of Solar Power World noted how they quickly became mainstream. The Passivated Emitter Rear Cells (PERC) that first came to the market in 2014 quickly grew to become mainstream by 2020.

Perhaps the next mainstream solar cell configuration after the PERC is the half-cell design (Pickerel, 2018). This cell design is predicted to see an over 35% growth on the market between its emergency in 2018 and 2040.

In a conventional cell configuration, panels are composed of 60 or 72 cells on the entire PV panel. However, in half cell setting, the panel will have the same size but consist of twice the number of cells. Thus, a panel with a half-cell module will have 130 or 144 cells. This creates more potential for the module to capture more sunlight sent into the converter.

Half-cell modules are composed of cells cut into half, implying a 60 and 72-cell module will have 120 and 144 cells, respectively. This helps improve the module's durability and performance.

The use of half-cells cuts the current into half, consequently lowering the resistive losses, implying the cells will produce "a little more energy." Furthermore, reducing cell sizes will also reduce the magnitude of the mechanical stress in the cells, which lowers the risk of the cells cracking. Overall, half-cell modules will have a higher output than conventional solar panels.

It has been predicted that half-cell technologies will exponentially grow over the coming year to overtake even the more commonly used c-Si technologies that are currently dominant on the market (see in figure 2.37).

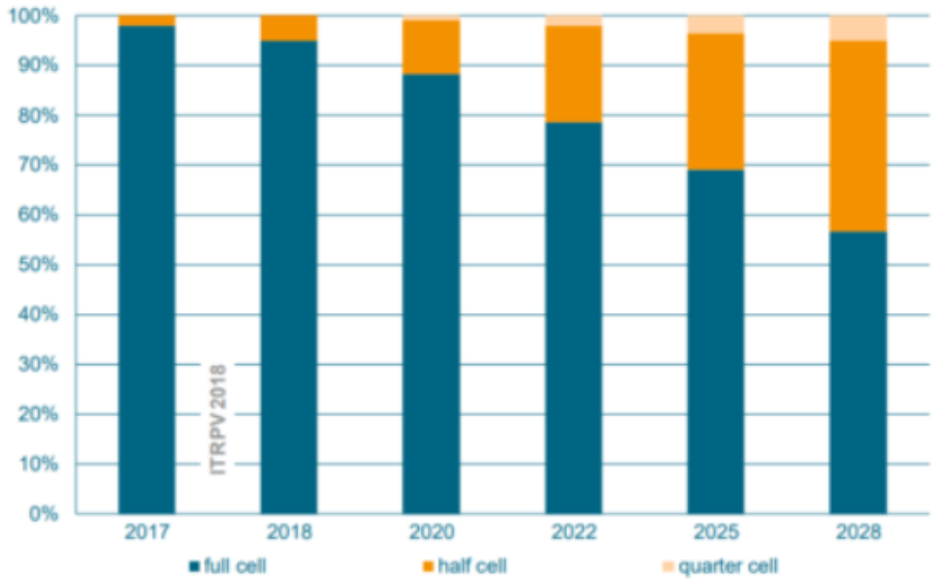

Figure 2.37 Predicted Growth of Cell Technologies (Pickerel, 2018).

2.4 PART 4: An Overview of Transparent Photovoltaics

This research aims to assess the benefits of adopting multi-functional PV components instead of mono-functional conventional building envelope components. The use of transparent solar systems has become one of the developing ways to utilise multi-functionality in buildings. Transparent solar systems are used in certain building parts, such as façades or skylights.

By definition, transparency is the material property that enables light transmission through an object (Pulli *et al*., 2020). The transparency of a material sorely depends upon the arrangement of atoms and electrons within the material.

Generally, conventional photovoltaic solar cells produce electricity from the light energy absorbed from the sun. However, transparent cells enable the passage of light (visible) without significantly affecting the efficiency of the cell.

Thus, when evaluating the possibility of TPV technology, the following two aspects or concepts are of uttermost importance;

a. Average Visible Light Transmittance (AVT):

According to Xue *et al*., (2018), is determined by selecting the average of the device transparency of the visible spectrum, *i.e.* 400-700nm, according to the spectral dependency response of the human eye.

b. Power Conversion Efficiency (PCE);

This is the ratio representing the energy output from the PV device to the photon energy input from the sun. Implying, it describes the amount of photon energy that is successfully converted to electrical power by a solar cell. This directly reflects the efficiency of a solar cell.

With regards to the above properties, transparent photovoltaic cells can be placed under two main categories;

a. **Wavelength-Selective Technologies:**

This type of TPV selectively absorbs Ultra-Violet (UV) and Near Infrared (NIR) light while allowing visible light to transit through them. According to Traverse *et al*., (2017), wavelength-selective TPVs have recorded an AVT of 50-90%.

b. **Non-wavelength-Selective Technologies:**

On the other hand, these technologies broadly absorb all radiant light; however, they enable transmittance by either segmenting the opaque photoactive layer or using very thin or low concentration photoactive materials.

2.4.1 Types of Transparent Photovoltaics

The two TPV mentioned above types could further be subdivided into the following subcategories based on the configuration or manufacturing;

- **Non-wavelength-Selective, Spatially Segmented PV**:
  Spatial segmentation involves spreading opaque solar cells units on the surface of the transparent substrate material. This will enable visible light to be transmitted through the gaps created between the solar cells. Widening the in-between gaps of the solar cells on the substrate could result in more visible transmission. However, this could result in the reduction of efficiency due to the reduced photoactive area. This method of archiving transparency could be adopted with any photoactive material. Some of the photoactive materials that have been used so far in the development of this technology include; silicon, copper indium gallium selenide and more recently, perovskite. SHARP has commercialised the Copper indium gallium selenide type of segmented TPV, particularly Solaria, Sphelar, and Sun partner Technologies (Traverse *et al*., 2017).

- **Non-wavelength-Selective Thin-film PV:** These, in particular, possess visible semi-conductors that are thin enough or of wide enough band gaps to enable the passage of visible light. These types of semiconductors are sometimes referred to as semi-transparent. Onyx Solar and Poly-solar (Traverse *et al*., 2017). According to the authors, recorded efficiencies with these Non-wavelength-selective thin-film PV range from 0.1% to 14% and the AVT could be up to 50%. However, as with spatially segmented TPV, increasing the PCE drops the AVT. The colourfulness of these types of TPV could greatly benefit the aesthetics.

- **Wavelength-Selective Thin-film PV:** These use "excitonic materials" capable of selectively absorbing UV and (or) NIR spectral light while enabling visible light to transit through. These technologies have been referred to as visibly transparent in some cases. These sort of excitonic materials include "small organic molecules, polymers, nanotubes, and salts." In organic and molecular semiconductors, the optical absorption of UV or

NIR occurs in different or unique molecular orbitals (S1, S2 … Sn) from the ground state (S0). This is illustrated in Fig. 2.4.1 below. The figure shows absorption intensity by overlapping nodes over the horizontal molecular orbital lines. The intensity of absorption is distinguished by line type, where; dotted means weak dashed is moderate and continuous lines depict strong absorption of spectral light.

Several studies, which yielded various breakthroughs regarding TPV, have been carried out. For instance, in 2012, a PCE of 4% and an AVT of 64% were obtained when polymer-based wavelength-selective TPV utilized poly benzo dithiophene-alt-5-dibutyloctyl and phenyl- C61 butyric acid methyl ester (PCBM) bulk heterojunction (BHJ) architectures were tested. The top electrode of the device consisted of a combination of Ag nanowires and ITO nanoparticles.

A similar study was conducted where polymer donors and small-molecule acceptors were used, resulting in 7.7% and 9.8% PCE and 26% and 32% AVT, respectively.

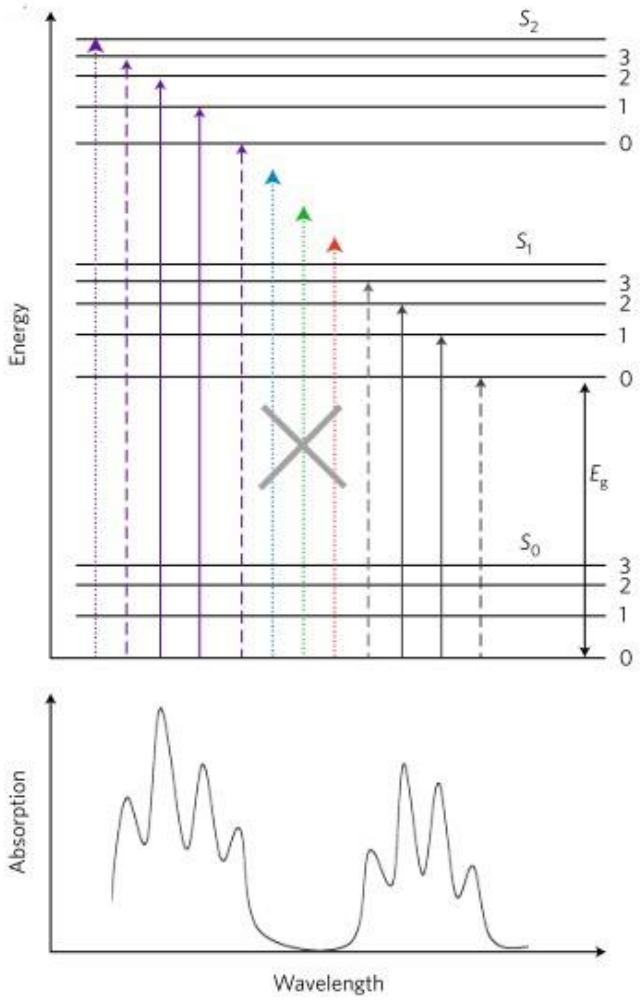

Figure 2.38 Figure of an Energy Diagram for the Ground State (So) and the Two Lowest Occupied Orbitals (S1, S2) for an Excitonic Material (Traverse *et al*., 2017).

2.4.2 Overview of Solar Concentrator Technology

In solar concentrators, incident radiation from the sun that is normal to the substrate surface is captured through dyes or the "scattering effect" and propagated towards the edges of the matrix to be collected by conventional photovoltaic cells attached to the edges. Like conventional photovoltaic cells, solar collectors are both wavelength selective and non-wave length selective. The main technology in this research focuses on the transparent form of solar collectors that transmit visible light through

their transparent substrates while also capturing light in the IR or NIR part of the spectrum for solar energy conversion. In the ensuing subsection, a comprehensive discussion on the different aspects and elements of transparent solar concentrators is carried out.

2.4.2.1 An Argument for the LSC Technology

By the end of 2017, the overall Worldwide PV installation capacity was estimated to be 400GW. This outstanding record capacity was further supported by the speculation made by GREEN *et al*., (2012), that the figure would further rise to exceed TW capacity within just a period of a few decades. Photovoltaic Technologies have been reported to help avert the greenhouse gas emissions that are currently overhead globally. Furthermore, recently, PV module efficiencies tend towards the Shockley–Queisser limit while the Levelized Cost of Electricity (LCOE) has dropped to as low as 2–4 cents/kWh in some regions (Moraitis *et al*., 2018). A combination of a series of factors such as; advancement in the technology, reduced manufacturing, installation and operation costs reached within the recent years with PVs have made it possible to recover the cost (payback period) of adopting PVs within less than a decade.

Overall, the dark blue conventional PV panels are still the most commonly used form of solar energy harvesters mainly due to their low manufacturing, installation cost, and high efficiencies.

However, conventional PV panels have limited use in urban areas despite the milestones mentioned above. This has mainly been due to the high cost of land in urban areas, irregularity of the city skylines that often results in shading, and limited roof top area for conventional PV module installation. Currently, it is estimated that to be able to harness 1kW of electricity using the conventional silicon-based crystalline photovoltaic systems; an approximate of $7m^2$ installation area is required. Though deemed efficient at household scales, this figure would be insufficient for a

huge city high-rise building. As mentioned above, the irregularity of the city skyline even further exaggerates the insufficiency of installation areas as rooftops of midrise buildings would be prone to shading by shadows cast by taller buildings.

According to Moraitis *et al*., (2018), in sustainable buildings, energy consumption has to be counterbalanced by on-site sources. This further highlights the need for innovative, 'economically viable solutions and do not compromise the quality of life of the building occupant and the building aesthetics. As a result, there has been an increase in the need for new creative means to increase the installation area for solar energy harvesting systems in urban areas. By transforming PV modules into a structural building component that can be integrated into the building envelope, façades of buildings can consequently be transformed into active energy surfaces. This has been achieved by using Building Integrated Photovoltaics (BIPVs).

An emerging BIPV technology that is gaining interest and could potentially foster PV integration in buildings is the Luminescent Solar Concentrators (LSC). Luminescent solar concentrators make it possible to transform glazing surfaces of urban buildings into solar energy harvesters while still letting in light (Moraitis *et al*., 2018).

Using LSC makes it possible to transform the energy passive vertical surfaces of high rise metropolitan area buildings into solar energy harvesters while maintaining the aesthetics and occupant confront (Debije, 2010). The idea of LSCs was first presented in the 1970s. The core aim behind their developments was to reduce the amount of silicon required to produce the conventional silicon-based PVs and drive down the manufacturing costs, which were rather high at the time. However, their purpose of application had since changed from when they were first invented. Adopting LSCs subdues the aesthetic inflexibility of the opaque and semi-transparent PV modules. Furthermore, LSC takes optimal advantage of their unique optical properties, making it possible to disguise their presence when integrated into the building fabric (Traverse *et al*., 2017).

2.4.2.2 Structure and Operation Principles of an LSC

The general structure consists of "plastic optical waveguide (e.g. glass or transparent polymer) doped with downshifting or up absorbing fluorophores. According to He et al., (2021), Downshifting (DS) fluorophores can transform higher-energy photons such as UV photons into lower-energy photons like NIR photons, up absorbing fluorophores, on the other hand, absorb low energy photons, which then are transformed into higher energy photons. In some cases, instead of doping glass with a fluorophore, a glass slab coated with active layers of emissive materials could be used. The main function of the embedded fluorophores is to absorb sunlight and release photons in longer wave lengths (G. Liu *et al*., 2019). The fluorophores absorb the directly and diffusely radiant light falling upon the LSC matrix at a shorter wavelength and re-emitting it at a longer wavelength. The strokes ' shift defines the difference between maxima in absorption and emission spectra related to the same transition.

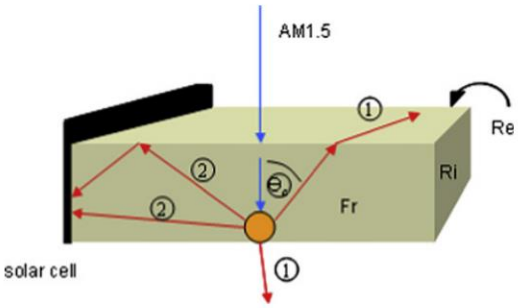

Figure 3. 1 Schematic 3D View of a Luminescent Concentrator.

Small PV units are attached to the edges of the polymer matrix. The emitter material absorbs radiant light and propagates it through total internal reflection (TIR) to the edge-mounted PV cells that convert it into electricity. LSC can increase the influx or "intensity" of radiation incident upon the "wave guide edges" since the LSC area exposed to the sun is much larger than the area occupied by the waveguide edge-

mounted PV units. This increases the photocurrent in the cell (Debije & Verbunt, 2012; Goetzberger & Greube, 1977). The ability to capture solar radiations using electrodeless semi-transparent waveguides allows applying LSC as PV windows. Since the edge-mounted PV cells receive indirect illumination from the light absorbed across the whole width of the wave-guide, efficiency losses and electrical stresses due to partial or total shadowing of a cell are minimized or eliminated. Such losses resulting from shadowing or shading are predominant in thin-film and bulk photovoltaic systems.

Bergren *et al*., (2018) argues that when the LSC device in use is of a sufficiently high PCE (> 6%) and its surface area is larger than the area of the edges; then its use could result in greater cost serving in terms of electricity generation compared to standard silicon-based photovoltaics.

Research has shown that by varying the semi-conductor material used in the edge-mounted PV units, achieving higher PCE of the entire LSC device is possible. For instance, with GaAs cells attached on all four sides of the LSC, the PCE as high as 7.1% can be achieved. In fact, with GaAs cells attached to only a single side of the LSC, the PCE was still as high as 4.6%.

Yang & Lunt, (2017), in their research, further describe the computation of other LSC related parameters such as; light-trapping efficiency, absorption efficiency, the PCE of the edge-mounted solar cells (η_{PV}), reabsorption probability, (η_{RAP}), and the maximum concentration ratio. According to the authors, the main limiting factor to the power production of an LSC device is the efficiency of the edge-mounted photovoltaic cells.

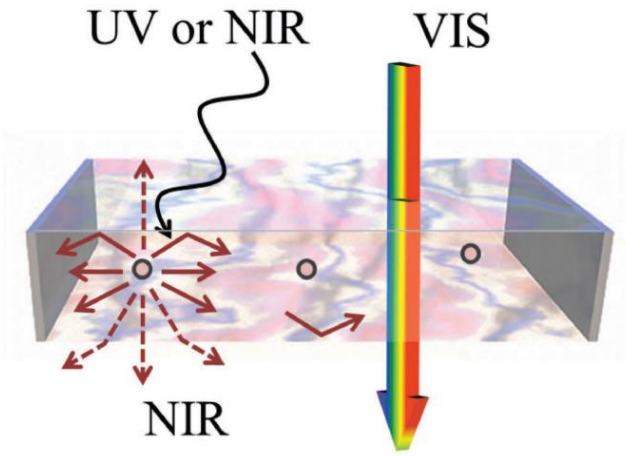

Figure 3. 2 Illustration of a Wave Selective LSC that Selectively Harvests UV and NIR Light while Passing Visible Light (Yang & Lunt, 2017).

2.4.2.3 Milestones in the LSC Technology Development

To date, the highest PCE recorded for LSCs is 7.1% (Slooff *et al*., 2008). The 50mm×50mm× 5 mm LSC matrix consisted of a poly-methyl methacrylate (PMMA) LSC sheet doped with a mixture of two organic dye luminophores and aligned four parallel-connected GaAs solar cells mounted to the edge.

The following year, Goldschmidt *et al*., (2009) reported another LSC of almost equal PCE. Their solution consisted of 2 smaller plates with a size of 20mm×20mm × 3mm using four gallium indium phosphide (GaInP) solar cells in a multi-dye stacked configuration. Their LSC had a PCE value of 6.7%.

Other closely high PCE reported range from 4.2% to 6.8% "with either single or stacked LSC configuration but without any of them exceeding 14 cm×14 cm in total surface area." In addition, in cases where back reflectors were added, up to 4% efficiencies were reported with sizes of up to 40 cm×40 cm. However, the many losses encountered in LSC operation still cause their PCEs much lower than other PV technologies (Moraitis *et al*., 2018).

2.4.2.4 Pro and Cons of LSC Technologies

Lack of suitable emitters has been the greatest hindrance to the advancement of LSC technology (Meinardi *et al*., 2017). The majority of emitters that have been tried to date have had different limitations. For instance, the organometallic chromophore emitters are limited in spectral coverage, whereas organic dyes and conventional core-only colloidal quantum dots incurred strong reabsorption of the guided luminescence. Since the radiation receiving surface area is greater than the side-mounted PV panels, this enables solar radiation concentration without requiring solar tracking (Slooff *et al*., 2008). Recent advancements in quantum dots design, which has made absorption possible over the entire visible spectrum, for instance, in colloidal quantum dots, make LSC technology for large-scale applications such as in PV windows possible. The aforementioned Colloidal quantum dots possess a wide absorption spectrum, tuned to harvest solar radiation across the visible spectrum and near-infrared (NIR). Furthermore, their luminesces could be tuned to match the peak response of the PV devices. Different material design alterations such as doping or hetero structuring can achieve decoupled absorption and emission functions, thus reducing the negative effects of reabsorption.

2.4.3 Energy Loss Mechanisms in LSCs

Krumer *et al*., (2017) identified four major energy loss mechanisms that are bound to occur in any LSC device leading to low efficiencies. According to the authors, the four major ways energy is lost are;

- The random dispassion of absorbed photon in different directions.
- Loss of initially absorbed light photons through the escape cone.
- The inability of the luminescent species to fully absorb “emittable” light photons or the part of the spectrum necessary for solar energy generation.

- Self-reabsorption where neighbouring luminescent species “reabsorb” emitted photons during the process of propagation towards the edges of the polymer matrix. This leads to photon recycling even of those photons already in wave-guiding mode before self-re-absorption occurred.

The main loss mechanisms within an LSC device are discussed below;

a. Reabsorption

Usually, a single emission event is assumed for every photon absorbed within a luminescent species in an LSC device. However, every absorbed photon undergoes a series of “reabsorption and reemission” events in the luminescent material before it reaches the LSC device's edges. Implying an overlap between the absorption and emission spectra is most likely to occur. While the “reabsorption and reemission” of a light photon within the luminescent material might not directly lead to loss of energy, the reoccurrence of this phenomenon several times in a row will most likely result in loss of energy.

In figure 2.4.2 below, the different ways in which radiated light energy from the sun is lost during the operation of an LSC are illustrated. Approximately 25.7% of the photons emitted will escape from either the top or the bottom of the LSC, as indicated by the blue colour of the plot. 5% (1−LQE) would undergo non-radiative recombination, resulting in the release of phonon instead of photons. By definition, a phonon is a mode of oscillation of a group of atoms where photons are a form of energy. Thus, the emission of a phonon in place of photons implies a direct loss of energy. Photons 500–600 nm region are subjected to 42% escape cone losses and 23.6% quantum yield losses. As a result, the larger the spectral overlap, the greater the LSC device's energy loss. One of the direct effects of the reabsorption loss effect is a drop in the luminescence intensity with increasing optical path length. This is regarded as the main cause of the dramatic drop in the PCE of LSCs. To counteract the decreased intensity of the luminescence due to the reabsorption losses, Goetzberger & Greube, (1977) suggested increasing the luminophore concentration.

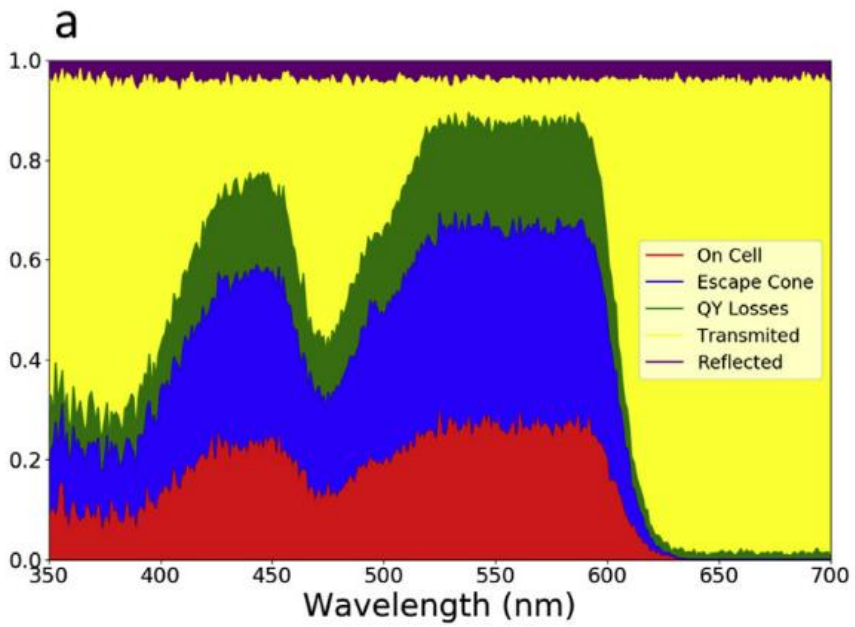

Figure 2.39 Modes of Energy Loss in a Lumogen F305 Dye-doped LSC Device. (Moraitis *et al*., 2018).

b. Surface Reflection

One other major cause of energy loss in the LSC device is the reflection of incident light at the surface of the concentrator device. According to Moraitis *et al*., (2018), an amount of light that is equivalent to $[(n-1)/(n+1)]^2$ where n is the refractive index of the surface material; is lost at the surface of the LSC as reflection before any light transits through the device. The formula used to determine the amount of surface reflected light above follows the Fresnel equations. Fresnel equations describe the reflection and transition of light through optical media. However, the losses due to surface reflections usually do not exceed 3.9% of the incident light. This is mainly because glass or plastic with a refractive index of 1.5 is used as the cover material in most LSC devices.

Similarly, according to Roncali & Garnier, (1984), the fraction L_r of light reflected from a surface S is determined by the refraction index n.

Implying under normal incident conditions;

$$L_r = [(n-1)/(n+1)]^2$$

Consequently, the fraction of incident light that the LSC would then collect would then be;

$$1 - L_r = 4n/(n+1)^2$$

c. Escape Cone Effect

Another loss mechanism that is most likely to occur during the operation of an LSC device is the loss of the initially absorbed fraction of light through the "escape cone" during the process of emission by the luminophore material. The escape cone, according to W. G. J. H. M. van Sark, (2013), is determined by the critical angle θ_c.

The critical angle, as previously described, can be determined as;

$$\theta_c = \sin^{-1}\left(\frac{1}{n}\right)$$

The rest of the absorbed light would then be guided to the edge-mounted photovoltaic cells through total internal reflection. It is hoped that there would not be any further loss of light within the angular range.

Of all the absorbed photons in the luminophore material, their sub-sequential absorption and emission to the edge-mounted PV cells depends on a certain mean optical path (l) taken within the polymer matrix. If the absorption coefficient of the polymer matrix equals $\epsilon_{m(\lambda e)}$. The partial yield η_{mat} would then be given by;

$$\eta_{mat} = 10^{\epsilon_{m(\lambda e)}{}^{l}}$$

The "escape cone" concept is illustrated in figure 3.4 under subsection 2.3.2.

d. Polymer Edge Reflections

The N emitted photons in the luminophore undergo a certain number of reflections at the mirrored edges, which depends on the type of polygons considered. This phenomenon also depends upon the geometries that are considered. According to Roncali & Garnier, (1984), for each type of polygon, a mean number of reflections *P* can be defined for these photons. If the coefficient of reflection of the reflecting edges is considered to be *r*, the "associated partial yield" would then be given by;

$$\eta_{lat} = r^P$$

e. Total Internal Reflections

Due to defective polymer surfaces, the process of total internal reflection may not occur perfectly. In other words, each reflection of the absorbed photons will not be "total."

$$\eta_{TIR} = R_i^{ni}$$

Where, n_i is the mean number of reflections and R_i the coefficient of internal reflection.

It's important to note that there is a strong correlation between the mean number of reflections n_i and the optical path as well as the LSC matrix thickness d and the mean angle of propagation $\bar{\theta}$ which varies between 0 and cos-1 (1/n), considering the critical cone. (See figure 2.4.3 below).

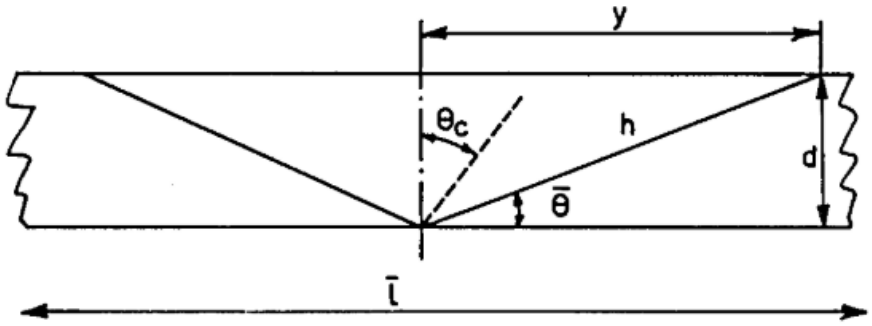

Figure 2.40 Illustrative diagram.

In figure 2.4.3 above, the mean propagation angle$\bar{\theta}$; d = LSC thickness; h = mean elementary step; y =h, projection in the LSC plane; and l = mean optical path.

2.4.4 Components of a Luminescent Solar Concentrator Device

The two main components of any Luminescent Solar Concentrator Device are the waveguide and the emitter materials. Any LSC device's other major forming part would be the edge-mounted photovoltaic cell that converts the concentrated light into electricity. Assessment of the edge-mounted PV cells is kept out of the scope of this work, as their principles are similar to the conventional PVs discussed in the earlier sections of this chapter. Therefore, these would better be discussed in detail independently. Thus, the ensuing subsections will sorely focus on a detailed description of former mentioned two components parts of any LSC device.

a. Hosts and Waveguides Materials

The host or wave-guide material refers to the two layers of embedding materials that are sandwiched or embedded within the emitter materials. The host materials are one of the significant parts of any LSC device as it directly affects the performance and electrical output of the device. The most commonly used materials in the building of LSC devices today are first poly (methyl methacrylate) (PMMA) followed by

polycarbonate (PC) based formulations and then glass (Debije & Verbunt, 2012). By virtue of their function in any LSC device, host materials must be highly transparent in the visible and NIR part of the spectrum. High transparency in the visible and NIR parts of the spectrum ensures the "unobscured flux of photons."

Besides just good transparency properties in the visible spectrum, there are many other properties that a good host material should possess to ensure its operation in an LSC device. One of these properties is the low reflectance of the exposed surface of the host material. This ensures minimal losses due to light reflection at the surface. Low reflectance implies that the reflective index n of the host material should be low as well. The downside of a polymer material with low reflectance is that such material's critical angles tend to be sharp. This is most likely to result in higher losses of photon energy through the escape cone. Generally, although a refractive index value of n=1.5 is acceptable, the optimal value should be n=2.0 (Ma *et al*., 2002).

In addition, high solubility to the luminescent species or emitter material is another required property of any good host material. High solubility aids with the achievement of maximum dissolution. It is important to note that the aggregation of materials could result in non-uniform distribution of the luminophore within the polymer matrix, resulting in the creation of "scattering centres."

Additionally, when integrating these transparent LSC devices into building fenestrations, it is required that wave-guide materials comply with certain environmental regulations lightness and exhibit good stability under different weather conditions.

For the case of glass as a wave-guiding material, high manufacturing temperatures of up to 1100 ^{o}C. According to Zettl *et al*., (2017), this is one of the glass's limitations as a host material as the high temperatures would prohibit using most of the luminescent or emitter materials which generally require only up to 300 ^{o}C at manufacturing.

One outstanding host material is the polymer plates. They particularly possess good visibility transparency in the NIR and visible part of the light spectrum and good solubility for the luminescent or emitter materials.

Generally, in most host materials, the surface such as in glass, quartz plates and different polymer plates; losses due to reflection would range from 7-11% of the incident light (Kastelijn *et al*., 2009). In addition, the authors concluded that quartz followed by PMMA exhibited the best optical properties. The downside of quartz would be that it is an extremely expensive material, making its application as a host material in LSC not feasible.

However, PMMA and PCCD (poly (1,4cyclohexylenedimethylene 1,4cyclohexanedicarboxylate)) materials were found to have the best performance in terms of optical efficiency.

b. Emitter Materials

Since emitter materials, also known as luminophores, play the critical role of light absorption and emission, they are generally regarded as the most important part of the LSC device. The most widely used emitter material categories include; semiconductor nanocrystals (or quantum dots), organic dyes and rare-earth ions. In general, the absorption bands of organic dyes are usually narrower than those of nanocrystals. This leads to limited absorption in the UV range of the solar spectrum when organic dye luminophores are used as emitters. Increasing the concentration of the organic dyes could help widen the absorption range in the UV region, as depicted by the "law of Beer-Lambert." According to the law of Beer-Lambert, increasing the concentration of the absorbing material results in an increased absorbance. Thus, the material concentration could be calculated by considering its absorbance (Edinburgh Instruments, n.d.). Increasing the absorbance of a luminophore material in the UV region will result in a higher absorbance of photons, resulting in an increased electrical output. The disadvantage of increasing dye concentration is that it will

cause the organic dye material to be more self-absorptive, which will lead to a drop in output.

Good emitter materials should possess the following properties; the ability to collect as many photons as possible, which requires the materials to have a wide absorption spectrum and high absorption efficiency. To subdue the quantum yield losses, luminophore materials should have an almost 100% Luminescent quantum Efficiency (LQE). By definition, the luminescence quantum efficiency (LQE) of the Luminophore is the ratio of the absorbed photons $N_{absorbed}$ and the number of emitted photons $N_{emitted..}$

Additionally, large stroke-shift values of luminophores could help regulate reabsorption occurrence in the luminescent material. In addition, good solubility of the luminophore solution is required as this would enable their use with polymeric host materials without negatively impacting their physical properties. Furthermore, photo-stability of the luminophore material over long periods (approximately 30 years) would help ensure their feasibility in building integration as this would ensure good long term solar power conversion capacity (Moraitis *et al*., 2018).

2.4.5 Categories of LSC Technologies

In this subsection, solar concentrator technologies are discussed under two main categories. The two main categories of focus are; luminescent solar concentrators and scattering concentrator technologies.

a. Non-wavelength-Selective and Colourful LSCs:

LCS could be a way of reducing the overall cost of PVs. This technology has been used in two ways: the colourful, *i.e.* non-wavelength selective devices and in plain windows (Wavelength selective).

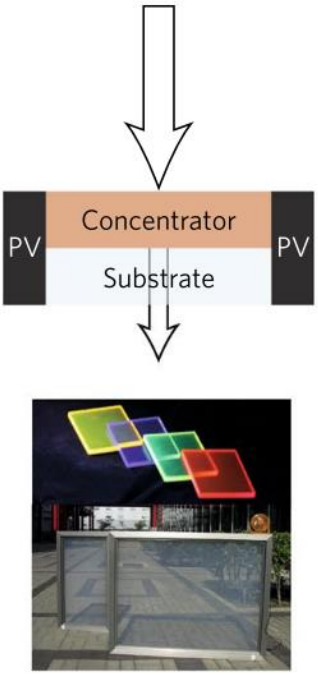

Figure 2.41 Illustration of a Non-wavelength-Selective Solar Concentrator, Coloured LSCs and a Scattering Concentrator. LSCs (Traverse *et al*., 2017).

LSC devices base their operations on a process known as "photoluminescence" to redirect light that is incident on an organic dye (or luminophore) coated substrate to its edges to be gathered by PV devices through a process called "*total internal reflection"* (Batchelder *et al*., 1979; Slooff *et al*., 2008). The light trapped by the concentrators is then redirected to the edge of the device, where PV devices convert the redirected light into electricity. When there is ideal light-trapping, the PCE of a non-wave length selective LSC is equivalent to that of a non-wavelength selective TPV (Yang & Lunt, 2017). In 2008, a PCE of 7.1% was obtained when LSC using GaAs cells was tested at European Laboratory Standards (Slooff *et al*., 2008). In fact, with even only one GaAs cell attached to one edge of the LSC, 4.6% PCE was recorded.

b. Non-wavelength-Selective Scattering Concentrators:

These consist of "light-scattering media deposited onto a clear wave guiding substrate." In this type of LSC, the wave with a length less than the "feature size" (nm) are scattered; this results in a visibly "hazy surface." Some of the scattered light is harvested by PV cells mounted on the glass edges. The downside of scattering concentrators is that the optical losses tend to be more significant in area scales above a few inches. This is mainly due to the multiple scattering events of the "wave guided photons." Despite limited use in cases where unobstructed views are required, these would come in handy in areas where high privacy is required.

c. Wavelength-Selective Transparent LSCs:

Wave length selective LSCs operate by either absorbing UV and emitting NIR light or absorbing NIR while emitting deeper NIR light.

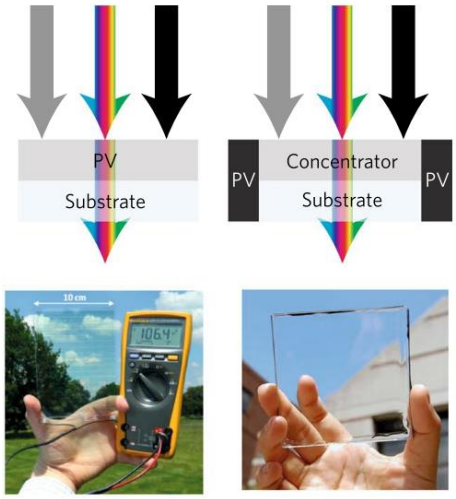

Figure 2.42 Display of a Wavelength Selective Luminescent Solar Concentrator Device.

The challenge with NIR absorbing LSC is that reabsorption is difficult to achieve when working with modules of larger sizes, *i.e.* square meters and above size

modules. However, these achieve similar high achieve similarly high AVT and CRI values to UV-absorbing LSCs.

2.4.6 Challenges Associated with Wave Length Selective TPV and LSCs:

The cell efficiencies of the edge-mounted PV units still possess one of the biggest limitations to adopt TPV (Yang & Lunt, 2017). In terms of performance challenges, both wave selective and non-wave length selective TPV and LSC face more or less similar challenges. This subsection discusses challenges associated with TPV and LSC in general.

a. High Conductive Resistance of Transparent Electrodes:

To date, the upscaling of TPV technologies is still hindered by scarcity of production materials from nature, the conductivity of the transparent electrodes, and the issue of defect tolerance and patterning. (Traverse *et al*., 2017). With these issues still prevalent, scaling TPV to large-scale applications such as PV windows or curtain wall façades would drop performance.

Transparent electrodes, which are generally used in TPVs and LSCs, generally are; transparent conductive oxides (TCOs) such as Indium Tin Oxide (ITO) based tend to have high conductive resistances as compared to the metallic electrodes. By definition, Transparent conducting oxides (TCOs) can conduct electricity but with very low light absorptive properties (Stadler, 2012). The high conductive resistivity of such materials results in a notable reduction of devices efficiencies when scaled up. Implying that scaling up the TPV technologies to almost window application sizes without compromising their PCE remains a big challenge. In addition, the deposition of metal oxides through sputtering processes led to the introduction of "shunting pathways" that could reduce the device's electric yields. In flexible devices such as laminated window coatings, polycrystalline ITO-based electrodes could greatly compromise their flexibility. Instead, the future advocates that "oxide-

based transparent electrodes" contain "amorphous, low-resistivity materials," which can easily be deposited.

However, the downside to flexible electrode use is that most contain Indium (In) which is in limited supply in the earth's crust. However, with the possibility of recycling indium, it will be possible to mitigate any future supply shorts.

b. Stokes Shift Efficiency for Wavelength-Selective LSCs

LSC technologies' predominant cause of power loss results from "reabsorption." Reabsorption occurs when luminescent dyes reabsorb emitted photons. The losses resulting from the reabsorption of the photons by luminescent dyes are directly affected by stroke shift and device length. The strokes shift is "the difference between the absorption and emission peaks of the luminophore."

Zhao *et al*., (2014), demonstrated the impact of stroke shift efficiency in scaling up TPV. In their study, the EQE (External Quantum Efficiency), *i.e.* (electrons generated per incident photon), decreased rapidly per increase in the photovoltaic cell plate sizes. This was directly related to reabsorption losses from strokes shift. According to Li *et al*., (2016), increasing the stroke shift to > 100 nm would increase the size of the LSC to more than 1 m^2. This would enable the use of LSC in almost all large-scale applications. Yang & Lunt, (2017) laid out solutions regarding materials and technical design that could help overcome the limitation in the scaling up of LSC. One of these was light trapping, yielding a PCE 35% fully transparent multi-panel device.

c. Angle Dependence:

When evaluating PV for building integration, it is important to consider the losses due to "oblique illumination" as some surfaces used for building integration may not have direct or optimal exposure for solar irradiation throughout the day. Generally, in buildings located in the northern hemisphere, south-facing façades will yield the highest power output and lowest Levelized Cost of Electricity (LCOE) owing to

harvesting the highest amount of solar influx from the southern direction. However, East-West facing windows can extend the useful power production throughout the day.

Regarding vertical solar power generation, ongoing research assesses the possibility of three-dimensional structures for solar power generation. It is possible to harness more sunlight using three-dimensional structures than solar tracking units. For instance, in the case of Boston, four sides of a building façade can harness 9.3 kWh per vertical m^2 per day compared to just 6.0kWh per horizontal m^2 per day collected from a solar tracking unit (Traverse *et al*., 2017).

Bernardi *et al*., (2012) studied issues related to three-dimensional solar collection computationally. They evaluated the possibility of combining absorbers and reflectors in the absence of sun-tracking to build three-dimensional photovoltaics that could potentially generate 2 to 0 times more energy than stationary flat PVs or 1.3–1.8 times more energy than flat panels with dual-axis sun tracking. According to the authors, three-dimensional photovoltaic (3DPVs) provide a more even source of solar generation from all latitudes. Compared to flat PV systems, when using 3DPVs, it is possible to double the number of peak hours and reduce the effects of season, latitude and weather variation. When using self-supporting 3DPV systems, creating "new schemes for PV installation is possible." Furthermore, due to the increased energy density, it is possible to adopt thin-film materials in cases of limited installation space. According to the authors, three-dimensional solar energy harvesting could pave the way for "Terawatt- scale generation."

By altering the thickness of layers on PV cells, it is possible to eliminate the parasitic reflections at oblique angles (Ball *et al*., 2015; Traverse *et al*., 2017). For instance, a wavelength selective Transparent Photovoltaic with an optimised active and top thickness of Indium Tin Oxide with an illumination angle of 80º could potentially retain 80% of the normally incident performance. As a result, under these conditions, the output of wave selective TPV could be increased by 15-40% annually for south-

facing windows, depending on the location. For the case of NIR selective TPV, designs that could potentially reduce losses due to variation in incident angles have been commercially demonstrated (Leem *et al*., 2014). For luminescent Solar Cells, their ability to reduce angle dependency lies in how they absorb light. Through their nature of light absorption intrinsically, LSC can reduce angle-dependent reflection to a single front side reflection, which allows for both direct and diffuse light-harvesting (Batchelder *et al*., 1979).

d. Lifetime;

Perhaps one of the most profound challenges for all PV technology systems, including the nanostructured ones, is the lifetime of the device (Traverse *et al*., 2017). One of the facts that could greatly put the live time of nanostructure PVs is the organic and Quantum Dot (QD) crystals' ability to react with moisture and oxygen. When used in different devices such as phones, their practical lifespan is less than ten years. However, it has been noted that in building applications, none of the PV technologies currently existent on the market could potentially last half of the building's life span. This brings into question the issue of replicability. For window-based TPV, it is possible to replace them as laminates on the window interior. Cost and energy payback times are the biggest determinates for the TPV replacement logistics. For the case of organic photovoltaic systems, the energy payback times are generally estimated to be within a few months or even weeks (Traverse *et al*., 2017). Comparing this payback period of months or weeks to the expected life times lying between 1-25years makes the application of organic PV (TPV inclusive) feasible for many applications, including building to and an extra function to components that would otherwise be only mono-functional.

Nanostructured materials have always been known to have the highest sensitivity levels in terms of sensitivity. However, due to technological advances, modules encapsulation techniques for the "commercialized organic light-emitting diodes (OLEDs) and quantum dot light-emitting diodes (QD-LEDs)" are beginning to

change this narrative. At$1{,}000\ cdm^{-2}$A lifetime of more than 1 million hours has been recorded for red fluorescent OLEDs. Furthermore, in an environment free of oxygen, Organic Photovoltaics (OPV) could last more than 25 years. As of 2017, non-life times had been reported for TPV; however, demonstrations done with OPV indicated the potential for lifetime applications.

e. Multi-junctions

Similar to conventional silicon-based PV technologies, multi-junctions could enhance the PCE of TPV. According to Traverse *et al*., (2017), multi-junction architectures comprise "current-matched complementary UV- and NIR-absorbing sub cells that are connected in series." So far, multi-junction technology has been tried on conventional PV technologies and non-wave length selective TPV. However, demonstrations of it with wavelength selective TPV and LSCs bearing maximum AVT are yet to be carried out. According to the authors, just as it is with single junctions, it is possible to optimise multi-junctions for "oblique illuminations." However, optimising at oblique angle illuminations could be challenging in cases where sub-cells have different angle dependencies.

2.5 PART 5: Brief Overview of Energy Storage Technologies

An energy storage system is a critical part of any energy generating system. Storing energy allows it to be used later than its generation period and allows for transportation to other locations (Alanne & Cao, 2019). Generally, high power charge solutions that could be integrated, transported, or scattered are preferred. Power storage options include; "battery energy storage (BES), superconducting magnetic energy storage (SMES), fly-wheel energy storage (FES), ultra (or super)-capacitor energy storage (UCES)." Other solutions include "various hybrid technologies, such as combined high-energy battery and high-power ultra-capacitor hybrid energy storage (Ren *et al*., 2015)."

Lamnatou *et al*., (2020), classified energy storage systems into three categories; 1) active, 2) passive, 3) hybrid. In general, energy storage is classified as either electrical, mechanical or thermal (Akbari *et al*., 2019). In particular, this thesis' focus will be on electrical storage systems. The authors listed four different electrical energy storage systems, namely;

a. Supercapacitors (electrochemical capacitors): This type of storage system could also be referred to as an "electric double-layer" capacitor, "Supercapacitor", or "Ultra-capacitor." The authors particularly used the terms "double-layer" for the "electric double-layer" capacitor to imply "ability to physically store electrical charge at a sur- face-electrolyte interface of high-surface-area carbon electrodes."
b. Electrochemical systems, such as batteries and flow cells

The purpose for which the generated electricity will be used will determine which storage system will be used. According to the authors, batteries can be used for AC and DC end-use purposes. However, in cases where the end-use of the electricity will be heating, it is necessary to convert the generated electricity into heat.

Electrical energy is converted into a storable form through a process known as *Electrical Energy Storage (EES).* This allows the stored electricity to be converted into a usable form when needed. According to the authors adding a storage system to a PV system helps maximise the capacity of the PV system *i.e.* the amount of usable electricity harnessed from the PV system. For example, using a battery system also enables the electricity generated from the PV system during the day to be stored up and used later at night. Thus, when a PV battery storage system is added to the PV system, this increase self-sufficiency by reducing the need to draw electricity from the grid (Weniger *et al*., 2014). Self-sufficiency fosters reduced grid dependency, thus reducing carbon emissions and reducing the building occupants' financial burdens.

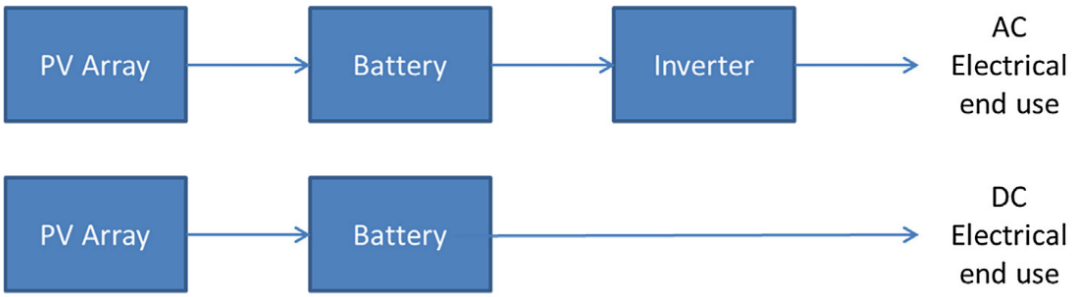

Figure 2.43 The Schematic Diagram above is of PV Electrical Storage and Usage System (Akbari *et al*., 2019).

- **Benefits of EES in a PV System;**

According to Akbari *et al*., (2019), the major role of an EES in a PV system is curbing the intermittency of the system. Before 2012 in Germany, PV systems were mainly installed to generate electricity fed back into the grid for remuneration. However, when the feed-in tariffs used as remuneration for PV generated electricity undercut the household retail electricity prices for PV systems below 10kWh, it found it more convenient to use PV generated electricity at a household level.

Using a battery storage system together with a PV system increases self-consumed electricity (Weniger *et al*., 2014). Generally, demand-side management is used to increase self-consumption in the residential sector to shift deferrable loads consumptions to times of PV surplus.

CHAPTER 3

THE FRAMEWORK

A Framework for Electrical Output Assessment of Transparent Solar Device

In a conventional sense, the electrical output of a photovoltaic device could simply be defined as the ratio of incident light energy to the output energy. However, the case of LSC differs from this, as its mode of electricity production does not follow the conventional way. As described in the "principle of operation of an LSC device" section 2.4.2.2, this particular device follows the mode of concentrating solar light received through a wide surface to a series of narrow attached PV cells at its edges through a process of total internal reflection (TIR). Thus, the computation of its electrical output would then differ from the conventional one by virtue of its operation process.

In this thesis, a framework that can be used to assess the electrical output of an LSC device is described and then applied to determine the electrical performance of a transparent façade of a selected reference building. The framework to be described in this section consists of eight major steps as described below;

Step 1; Determining the Solar Radiation on the Matrix Surface

Solar radiation is perhaps the most important element in the functioning of any solar harvesting device. Its abundance in a given locality is bound to increase solar energy yield. Whereas solar radiation is often measured using mainly physical solar radiation testing equipment such as pyranometers which measure global radiation, pyrheliometer, which measures direct radiation or sunshine recorder, accurate assessments could also be acquired through software simulation using cloud database systems.

Figure 3.1 Pyranometer *(Z. Li et al., 2021).*

Theoretically, it is known that 2.8×1023KW of energy leave the sun, and approximately s 1.5×1018KWH reach the earth's crust yearly. The loss in solar energy travelling from the sun is due to scattering where sunrays collide with atmospheric particles of matter, absorption due to water vapour, cloud cover, and reflection from high geographical terrains such as mountains.

Generally, the amount of solar energy radiant upon any surface is referred to as solar insolation measured in kW/m^2. When a surface is placed in direct orientation to the sun, the amount of insolation present on the surface of that object is approximately; 1.37 kW/m^2, which is also referred to as the solar constant. However, considering those mentioned above atmospheric and environmental players that could alter the amount of solar energy that reaches the earth's surface, it has been noted that on a clear day at noon, about only 1kW/m2 of energy will be reaching that surface. 1 kW/m2 is usually referred to as the PEAK SUN ("Insolation," 2011). Solar insolation is also denoted as 'I'.

On the other hand, solar Irradiance is the amount of solar energy received on a unit surface expressed in units of kWh/m^2. Irradiance adds a time factor to the aforementioned insolation characteristic of solar energy. Therefore, Solar Irradiance is always measured over a given period.

Besides physical measurements, other computer-based software cross-linked with certain databases could be used to simulate the amount of solar radiation on given surfaces. For instance, in this research, the Revit Architecture software coupled with the Insight plugin is used. Weather data of local geographic location was extracted from a cloud-based database using the coordinates specific to the location.

Solar radiation information can also be acquired from other online databases. The National Renewable Energy Laboratory (NREL) provides a list of databases for acquiring metrological data on different aspects, including solar. One of the most profound ones is the National Solar Radiation Database (NSRDB), which is closely linked to the NREL and provides hourly and half-hourly data on solar radiation following the three most common solar radiation units: global horizontal, direct normal and diffuse horizontal irradiance. Although this is still only widely used in the United States, it has spread its data collection to a few other international locations. Another outstanding database for radiation data is the Global Solar Atlas. This particular database was developed by the World Bank Group, a collaborative organisation comprising the World bank itself and the International Finance Corporation. It aims to provide quick access to solar power-related data for its clients.

Overall, solar radiation plays a critical role in decision making regarding the orientation of the solar photovoltaic system. Thus, determining solar radiation is critical and should be the initial step in any electrical analysis of a solar photovoltaic system.

Step 2; Determine the Luminescence of the Luminophore Material

The operating principle of a Luminescence solar device is that the light from the sun that falls on the surface of the matrix is absorbed by the luminophore material and reemitted at a longer wavelength. Through a process of Total Internal Reflection, the reemitted light is transferred to the edges of the matrix, where it is absorbed by the edge-mounted solar cell PVs and converted into electricity. Thus, photoluminescence, the absorber material's ability to absorb and reemit light, becomes an extremely critical aspect of LSC technologies. In fact, Spectra, (2021) suggests two types of photoluminescence; fluorescence and phosphorescence. Since the Luminophore material of the LSC plays such a critical role in its electricity production, determining its efficiency or luminescence also becomes essential to predicting the electrical output of the LSC device. To Determine the Luminescence of the emitter, the following steps can be followed;

a. Determine the Absorption Capacity of Luminophore

The photoluminescence process in any luminophore material starts by absorbing photon energy from the light source. According to Weber & John, (1976), the absorption capacity of a luminophore material can be derived from its absorption efficiency denoted as Q_A and could be derived as;

$$Q_A = \int_0^{\lambda c} \frac{d\lambda N(\lambda)\{1-\exp[-\alpha(\lambda)d]\}}{\int_0^{\lambda c} d\lambda N(\lambda)} \qquad (1)$$

Where N (λ) = flux of the photons in the solar spectrum. The value of N(λ) is approximately a 5500-K blackbody source; d is about twice the layer thickness for a double-pass system and the absorbing path length; and λc is the cut-off wavelength of the semiconductor (Weber & John, 1976).

Alternatively, the absorption efficiency of the luminophore materials (η_{ABS}) can be derived using the following formula;

$$\eta_{Abs} = \int_{300\ nm}^{E_G^{lum}} AM1.5(\lambda) * A(\lambda)d\lambda / \int_{300\ nm}^{\infty} AM1.5G(\lambda)d\lambda \quad (1a)$$

Where; is the absorption spectrum of the luminophore, G_E^{Lum} is the bandgap of the luminophore (in nm), and AM1.5G is the air mass 1.5 global solar photon flux spectrum (Yang & Lunt, 2017).

According to (1976), luminophores should have high absorption in the visible where the solar spectrum peak lies, a high luminescent efficiency, and high transmittance in the emission region. By the time of authoring, rare-earth-doped laser glasses and dyes used in dye laser were identified to possess the properties mentioned above of good absorber materials.

b. Determine the Amount of Absorbed Light

The amount of light absorbed by the luminophore is determined following "Lambert-Beer law" and depends on polymer thickness.

$$A = 1 - 10^{-\varepsilon cx} \quad (2)$$

where x is the optical length of the light through the LSC; ε denotes the molecular absorption coefficient of the luminophore. Value c denotes the concentration of the luminophores. The unabsorbed light travels through the waveguide material like any transparent material (Moraitis *et al*., 2018). Although increasing the sheet thickness would increase the light absorption, resulting in a decreased device concentration factor *C*.

c. Determine the Luminescence Quantum Efficiency LQE of the Device

By definition, the LQE is the ratio of "absorbed photons N*absorbed* and the number of emitted photons N*emitted*."

$$\text{LQE} = \frac{Nabsorbed}{Nemitted} \quad (3)$$

Determining the LQE becomes extremely critical as not every all absorbed light photons get emitted by luminophore; some of them recombine "non-radiatively" (Moraitis *et al*., 2018).

d. Determine the Light Trapping Efficiency of the Device;

The operating principle of a luminescent solar concentrator device is that the light absorbed by the luminophore material is trapped within the sandwiched matrix and gets transferred to the edges of the matrix through a process known as Total Internal Reflection (TIR). However, for the TIR process to efficiently take place, the polymer matrix should have good light-trapping efficiency. According to Yang & Lunt, (2017), the Light Trapping Efficiency η_{TRAP} of a Polymer matrix can be given by;

$$\eta_{TRAP} = \sqrt{(1-1/n_{sub}^2)} \qquad (4)$$

In the above equation, the value n_{sub} refers to the index of refraction of the waveguiding polymer matrix.

The process of Total Internal Reflection occurs following Snell's Law, which is a ratio that describes the angles of incidence and refraction when describing light bound between two isotropic materials.

e. Calculation of the Efficiency of Suppressing Reabsorption (ηRA)

To account for the successive events of photon reabsorption and emission, it becomes necessary to compute the efficiency for reabsorption suppression (η_{RA}). This is defined by:

$$\eta_{RA} = \frac{1-\eta_{RAP}}{1-\eta_{RAP}\,\eta_{PL}\,\eta_{TRAP}} \qquad (5)$$

The probability of reabsorption (η_{RAp}) combines all the angles of emission. The absorptive path length is corrected for each take of angle in a rectilinear system as;

$$\eta_{RAP} = \frac{\int_0^{\infty} d\lambda * \int_{\theta_{crit}}^{\pi/2} d\theta * \int_{-\pi/4}^{\pi/4} \sin(\theta) * PL(\lambda)\left(1-\exp\left[-\varepsilon(\lambda)C\frac{Lt}{2t_0 \sin(\theta)\cos(\theta)}\right]\right)}{\int_0^{\infty} d\lambda * \int_{\theta_{crit}}^{\pi/2} d\theta * \int_{-\pi/4}^{\pi/4} \sin(\theta)} \quad (6)$$

The critical angle (emission cone) is θcrit = sin− 1(1/nSub). ε denotes the molar absorptivity. C refers to the concentration of the emitter material (luminophore). L ≈ plate length. Θ denotes the azimuth angle relative to the normal of the LSC plane. t is the thickness of the film with the luminophore coated on the front surface of the waveguide. t_0 denotes the thickness of the waveguide. φ is the in-plane rotation angle. However, if the photon absorbing luminophore is directly embedded within the matrix, implying no other film is used, then $t = t_0$ (see Figure 3.2 below). The schematic in figure 3.2 below is of ultraviolet (UV) and near-infrared (NIR) light selectively harvesting transparent LSC device.

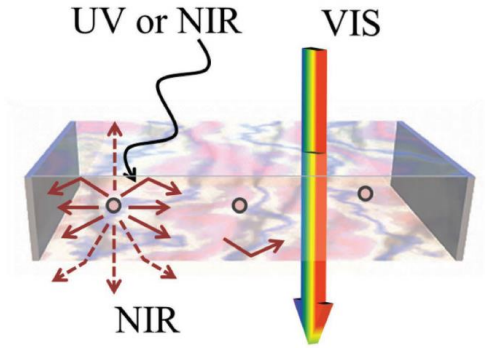

Figure 3.2; UV and NIR selectively harvesting LSC device (Yang & Lunt, 2017).

Step 3: Assess the Internal and External Losses

Within the LSC device, several “loss mechanisms” can be identified that could add up to the specific efficiency of the device (Moraitis *et al*., 2018). Such losses include; reabsorption and light escaping from the top of the LSC surfaces. A more comprehensive overview of internal losses in an LSC device is described in Chapter 2, subsection 2.3.6 of this thesis. The computations for the different internal and external losses that could add to the loss in efficiency within an LSC are described here.

a. Surface Reflection at Polymer (R)

Before even the radiant solar energy enters the device, some light is reflected at the surface. The amount of light that gets reflected at the surface of the matrix, according to Roncali & Garnier, (1984), equates to;

$$R = [(n-1)/(n+1)]^2 \quad (7)$$

Where *n* denotes the polymer's refractive index.

The computation of reflection losses in LSC devices follows after the Fresnel Equations. However, it is important to note the Fresnel losses in LSC do not usually exceed 3.9%. This is mainly because polymers of LSC devices are usually made of glass or plastic whose refractive indices do not exceed 1.5. For instance, for a polymethyl methacrylate (PMMA) polymer with an n value of 1.49, the Fresnel Reflection loss is equivalent to 0.0387. One way to reduce the loss effect through surface reflection would be to apply the anti-reflective coating. Otherwise, the amount of light that eventually gets absorbed depends on the specific emitting material. It is important to note that overall organic dyes will have narrower absorption bands than Quantum Dot (QD) emitters.

b. Escape Cone Surface Losses

Part of the light absorbed by the luminophore eventually falls within the Escape cone while getting emitted towards the device edges. The light that gets emitted in the escape cone escapes through the surface of the polymer matrix. The escape cone refers to the angle formed by the smallest angle of incidence for light to be successively trapped within the matrix. (Moraitis *et al*., 2018). The escape cone is highly dependent upon the critical angle θc. In the schematic figure below, path-1 depicts the light that falls within the escape cone defined by critical angle θc. Light type two is the light that successively transmits to the edge-mounted PV cells through TIR.

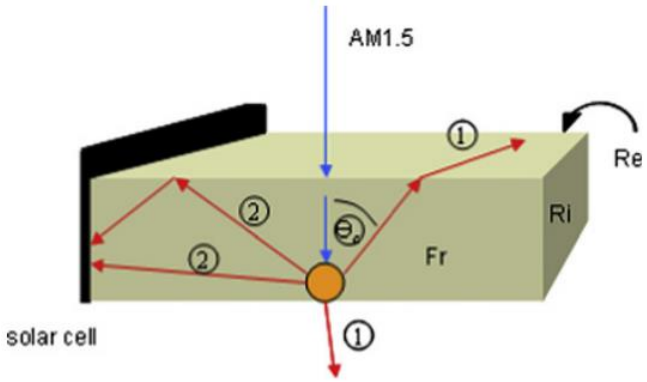

Figure 3.3; Schematic figure of LSC device showing different light parts (W. G. J. H. M. van Sark, 2013).

In the above schematic, light type (1) is the light that is lost through the escape cone, while light type (2) is the light that is trapped within the matrix.

In reference to the schematic figure 3.3 above, the critical angle of a polymer matrix can be computed as;

$$\theta_c = \sin^{-1}(\frac{1}{n}) \qquad (8)$$

Generally, the critical angle is θ = 41.970° (like in a PMMA/air interface). In addition, in materials that isotopically emit light, such as luminophore, the probability of successively transmitting the trapped light to the edges is 0.7435. The ray-trace simulation model *PVtrace* described by Daniel Achatten (Daniel, 2014) could compute the different efficiency losses in an LSC cell device. For instance, in the plot below, losses in a 5 cm x 5 cm x 0.3 cm LSC device were simulated by representing the photon destination when the device is exposed to light. The LQE of this LSC device was set to 95%, and in the device, Lumogen F305 dye was used as a dopant. The concentration of the Lumogen dopant was 184ppm.

The red coloured region represents the light lost on the cell's surface. The blue region represents the light lost through the escape cone. Green depicts the light that is lost due

to the Quantum Yield. The yellow region represents the light that is transmitted through the polymer matrix. The purple region represents the light, which is reflected.

The script for the *PVtrace* model by Daniel Achatten, is available at (https://doi.org/10.5281/zenodo.12820).

Figure 2.5.4 below shows how photons of light travel through an LSC device.

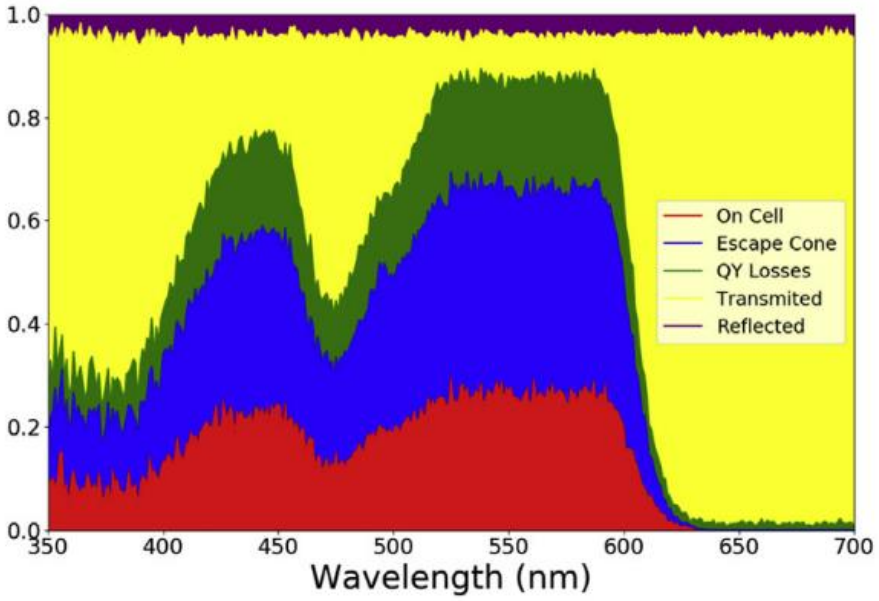

Figure 3.4 Possible losses of photons in an LSC device. (Moraitis *et al.*, 2018).

c. Determine Losses Due to Photon Reabsorption

When assessing loss mechanisms in an LSC device, it is usually assumed to be a single photon absorption and emission phenomenon. However, there is usually an overlap of the absorption and emission spectra in most luminophore materials. This overlap of the two spectra leads to a series of reabsorption and reemissions occurrences of photons in neighbouring luminophores. According to Moraitis *et al.*, (2018) this does not directly result in loss of energy; however, it's bound to occur numerous times as the photons get redirected towards the matrix edges. This repetitive absorption and emission will consequently lead to the photons' energy

losses. Losses due to reabsorption could also be calculated using the Daniel Achatten model described above. For instance, in the schematic figure depicting the losses according to the photon destination above, it was found that the 5% (1-LQE) of the emitted photons would undergo non-radiative recombination. However, the larger the spectral overlap between the absorption and emission spectrum, the greater efficiency reduction. This loss due to the spectral overlap can denote the reabsorption cross-section.

According to (Krumer *et al*., 2017), reabsorption cross-section σ_{SA} per centimetre of optical path taking into account absorption (Aλ) and emission (E λ) spectra, as follows;

$$\sigma_{SA} = \frac{\int A(\lambda)E(\lambda)d\lambda}{\int E(\lambda)} \qquad (9)$$

One of the most profound effects of the reabsorption occurrence is that the intensity of the luminescence is bound to reduce as the length of the path increases (Olson *et al*., 1981). This can also be linked to the dramatic efficiency reduction in large area LSC devices.

One way of compensating for the reabsorption losses is to increase the luminophore concentration. Overall, the loss in device efficiency due to reabsorption can be calculated according to the following formula;

$$\frac{\Phi_{LSC}}{\Phi_{in}} = \eta_{abs}(1-\eta_{int})^{(N_{SA})} \qquad (10)$$

Where ΦLSC is the edge emission power flux. Φ_{in} is the amount of power, which is incident on the top surface of the LSC device; N_{SA} is the average reabsorption.

However, it is important to note that the most effective way of deducing reabsorption losses is by considering the stroke shift, the distance occurring between the absorption and emission spectrums.

Step 4; Determine the Collection Efficiency (Qc)

Since the first-ever design Luminescent Solar Concentrators device was referred to as a "Luminescent Collector" consequently, the term Concentration Efficiency was used to describe the number of photons reaching the device's edges. The term concentration efficiency, as first used by Weber & John, (1976) was defined as the amount of light collected at the edges of the device matrix where the PV cells were mounted. According to the authors, the collection of light at the edges is made possible since the absorbed light is emitted at more "grazing angles to the surface" than the critical angle; thus, this makes total internal reflection possible. This allows the light to be trapped in the collector (waveguide), where it is then successively reflected the edges where it is then "coupled out." The authors listed the ability of the device to collect light (Q_c) as one of the principle quantifiers of the overall quantum efficiency of the collector device. The other two quantifying parameters are; the Absorption Efficiency (Q_A) and the Luminescent Quantum Efficiency (Ƞ). Thus, the Concentration Efficiency is then computed using the following formula;

$$Q_c = (2\pi L)^{-1} \int_0^L dy \int_0^{\frac{\pi}{2}} d\phi \int_{\theta_c}^{\frac{\pi}{2}} * \sin\theta d\theta \left\{ exp\left[-\alpha_e \frac{(L-y)}{\sin\theta \sin\phi}\right] + exp\left[-\alpha_e \frac{L+y}{\sin\theta \sin\phi}\right]\right\}\left\{2 - |r_s(\theta,\phi)|^2 - |r_p(\theta,\phi)|^2\right\} \quad (11)$$

In the formula above, θ and φ denote the usual spherical polar angles defining the emission direction. θ_c is the critical angle for total internal reflection. The attenuation coefficient at the emission wavelength is denoted as α_e . And $r_{s,p}(\theta,\phi)$ is the amplitude Fresnel reflection coefficient for *s* or ρ polarization at the boundary y = L (Weber & John, 1976).

In the schematic of the first-ever design LSC device below, perfectly reflecting mirrors where placed at the edge where y=0. On the other side of the device where y=L, photovoltaic cells were placed.

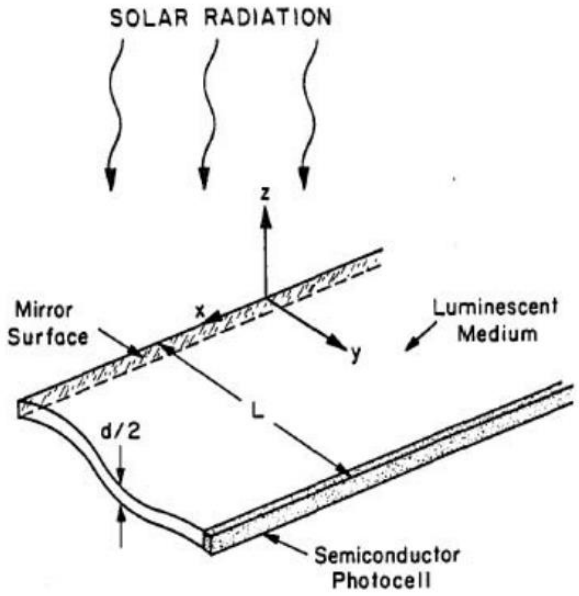

Figure 3.5 Diagram of an LSC Device (Weber & John, 1976).

In the schematic above, light rays are assumed to be normally incident upon the surface of the LSC device.

Step 5; Determine the Optical Efficiency of the LSC Device;

Whereas Yang & Lunt, (2017) suggests that the optical efficiency of an LSC η_{opt} can be reduced to; $\eta_{Opt} = \eta_{Abs}$, there have been numerous suggestions of how it could be computed.

In LSC devices, the optical efficiency is the number of photons reaching the side surfaces when divided by the number of photons that fall onto the front surface of the LSC (Tummeltshammer *et al.*, 2016). The authors suggest that the optical efficiency accounts for the surface reflection and the photons that do not get absorbed by the luminophore during its computation. Additionally, it is necessary to consider the "internal optical efficiency θ", which refers to the probability that an absorbed photon will reach the edge of the matrix to be converted into electricity by the edge-mounted PV cells.

Thus, according to the authors, simply multiplying the total internal optical efficiency with the probability or chance that a photon contained within an incident light beam gets absorbed by the luminophore yields the optical efficiency of the LSC (η_{Opt}).

$$\eta_{opt}(\lambda) = \theta\sigma(\lambda) \qquad (12)$$

where σλ( ) denotes the fraction of the light incoming that eventually is absorbed by the LSC at wavelength λ. The probability of absorption can be determined using an absorbance measurement of the LSC (Tummeltshammer *et al*., 2016).

Roncali & Garnier, (1984) defined the effective concentration ratio C of a device as its optical efficiency provided it's of a given geometric gain G. In other words, the optical efficiency could be defined as the ratio of the power output to that of the power input.

$$\eta_{opt} = \frac{Pout}{Pin} = \frac{C}{G} \qquad (13)$$

Where C is the Concertation ratio. G value denotes the Geometric gain.

With the optical efficiency expressed this way, the power output of the LSC device could be increased by simply increasing its geometric gain. According to the authors, this could be achieved by increasing the capitation area S or decreasing the collecting area by decreasing the thickness of the plates, or by only using one edge of the polygonal collect to collect the flux.

In similar terms, the optical efficiency has also been defined as the radiative power on the L_{edge} of the LSC to the radiative power incident on the surface L_{in}.

$$\eta_{opt} = \frac{L_{Edge}}{L_{in}} \qquad (12)$$

Step 6; Calculation of PV Normalised Cell Efficiency

This refers to the photovoltaic cells attached at the edges of the LSC device to convert collected light into electricity. According to Yang & Lunt, (2017), it's necessary to normalize the efficiency of the edge mount PV cells by its spectrum absorption efficiency and quantum efficiency at the luminophore wavelength to account for monochromatic conversion following the formula below;

$$\eta_{pv} = \left(\frac{\eta_{pv}\,(AM1.5G)}{\eta_{Abs}^{pv}(AM1.5G)}\right) * \frac{\int \eta_{EQE}(\lambda)PL(\lambda)d\lambda}{\int PL(\lambda)d\lambda} \qquad (13)$$

η_{EQE} denotes the external quantum efficiency of the PV as a function of wavelength. PL (λ) denotes the luminophore photoluminescence emission spectrum as a function of wavelength. $\eta\frac{pv}{Abs}$(AMG1.5) is the absorption efficiency of the PV material instead of the luminophore.

The schematics plots below are of the best performing PV cell efficiencies as a function of the bandgap (figure a) and the reflection and trapping efficiencies as a function of the index of refraction of the substrate (n_{Sub}) for a simple optical waveguide. It's important to note that the plotted PV cell efficiencies represented only account for the fill factor (FF) and the open-circuit voltage (V_{OC}).

In figure 2.5.6 (a) below, the black line shows the "theoretical efficiency", and the dashed line shows the "the highest recorded efficiency of the solar cell. The golden line shows the normalised values of η_{PV}/η_{Abs}(AM1.5G).

As aforementioned, this represents only the efficiencies of the PV cells while only considering the fill factor (FF) and open-circuit voltage (V_{OC}) losses.

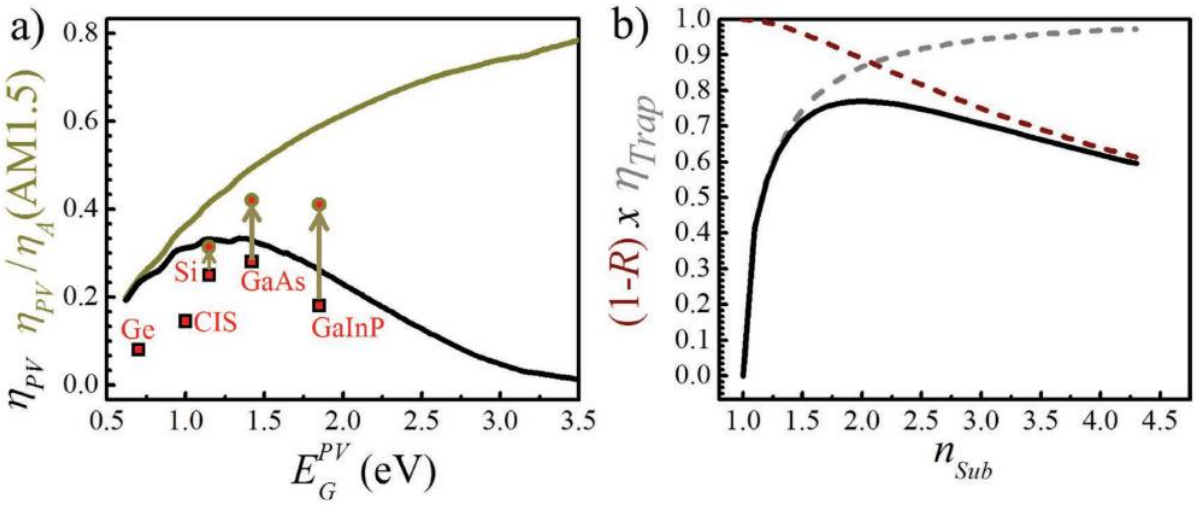

Figure 3.6 Comparisons of efficiencies for different edge-mounted PV cells.

Image (b) in dashed red line shows depicts the reflection. The grey line shows the efficiency of light trapping. Both factors are shown as functions of the index of refraction (n_{Sub}) plotted on the x-axis. The peak point for the product of both the reflection and trapping efficiencies happens when the refractive index: n_{sub} = 2.0 (Yang & Lunt, 2017).

Step 7; Determine the LSC Device's Overall Efficiency η_{LSC}

The overall LSC efficiency (ηLSC) would then be the product of the mounted PV cell efficiency and the Optical efficiency of the LSC device (Yang & Lunt, 2017).

$$\eta_{LSC} = \eta_{PV} \text{ x } \eta_{opt} \qquad (14)$$

where η_{Opt} denotes the optical efficiency.

Consequently,

$$\eta_{LSC} = \eta_{PV} * \eta_{opt} = (1\text{-R}) * \eta_{PVabs} * \eta_{PL} * \eta_{TRAP} * \eta_{RA} * \eta_{PV} \qquad (15)$$

Where, R is the reflections that occur at the front face of the LSC device.

η_{Abs} is the efficiency at which the absorbing material absorbs the sunlight. η_{PL} is the luminescence efficiency of the luminophore, η_{Trap} is the waveguiding efficiency of the LSC device. Finally, η_{RA} is the efficiency with which the reabsorption occurring in the emitter material gets suppressed.

Step 8; Calculate the Power out of the LSC

Finally, as is with other conventional photovoltaic devices, the overall efficiency is the dividend of the power out over the power input.

$$\eta_{LSC} = \frac{Pout}{Pin} x100 \qquad (16)$$

Where, η_{LSC} is the solar cell's overall efficiency, Pout is the power out of the device, Pin is the solar radiance received on the top surface of the polymer matrix (Moraitis *et al*., 2018).

Thus, the final power out of the transparent solar concentrator can be computed from the formula above.

CHAPTER 4

MATERIALS AND METHODS

In this chapter, the application of the proposed framework described in the previous chapter is demonstrated with computer-based software and plugins on a selected reference building in Istanbul, Turkey. In chapter 3, an 8-step framework for determining the electrical power output of a transparent solar luminescent concentrator device was proposed. This thesis chapter describes the methodology and materials used in its testing. The transparent solar harvesting system used in this study was adopted from a previous study by (Meinardi *et al*., 2017). This study selected and remodelled a reference building that best reflects the actual urban conditions in which a transparent solar harvesting system could be applied. The reference façade on the building chosen has a northern orientation, which helps simulate diffuse lighting conditions for most months of the year under which LSC technology is claimed to operate just as efficiently.

The subsequent subsections first describe the research materials used, *i.e.*, the reference building and façade, selected solar harvesting system, the simulation software, databases, and plugins used. Next, a detailed description of the testing methodology is made.

4.1 Research Materials

This subsection describes the materials used in the research, including a reference building and computer-based software. The process and the reason behind selecting the reference building are discussed in elaboration. First, a description of the reference building chosen for the study is made, followed by a description of the different software and databases used. Finally, a comprehensive description of the

Luminescent Solar Concentrator devices originally put forward by Meinardi *et al*., (2017) and adopted for this study is made.

4.1.1 Selection of the Reference Building

The building selected for this study is the recently completed (2017) cultural centre building for one of the largest Turkish banks: Yapi-Kredi. The building is also quite often referred to by its initials YKKS. The plot of land where it is located had initially been occupied by neoclassical apartments constructed in the early 20th century. These were later demolished in the mid-1950s and replaced with a rationalist office building for the bank. The plot on which the building sits is located midway on a 1.5km long busiest street of İstanbul, *i.e.* İstiklal Street. The street axis on which it sits was added to the city plan in the late 19th century. The original building that served as Yapi-Kredi's office building consisted of a rectilinear "concrete frame and featured a gridded travertine façade that opened with a portico at street level and was designed by a German architect; Paul Schmitthenner. Figure 4.1.1 below is of the old YKKS building constructed during the mid-1950s.

The new cultural centre building completed in 2017 was merely a result of a retrofit project by the architecture office TEGET. The decision to retrofit as opposed to demolition and reconstruction was because most city authorities were against the idea of demolition. The major transformation from old to new was the transformation of the north-facing façade from a perforated concrete wall into a *transparent glass façade,* as illustrated in figure 4.1.2 below.

Figure 4.1 Rectilinear Façade of the Old YKKS Building.

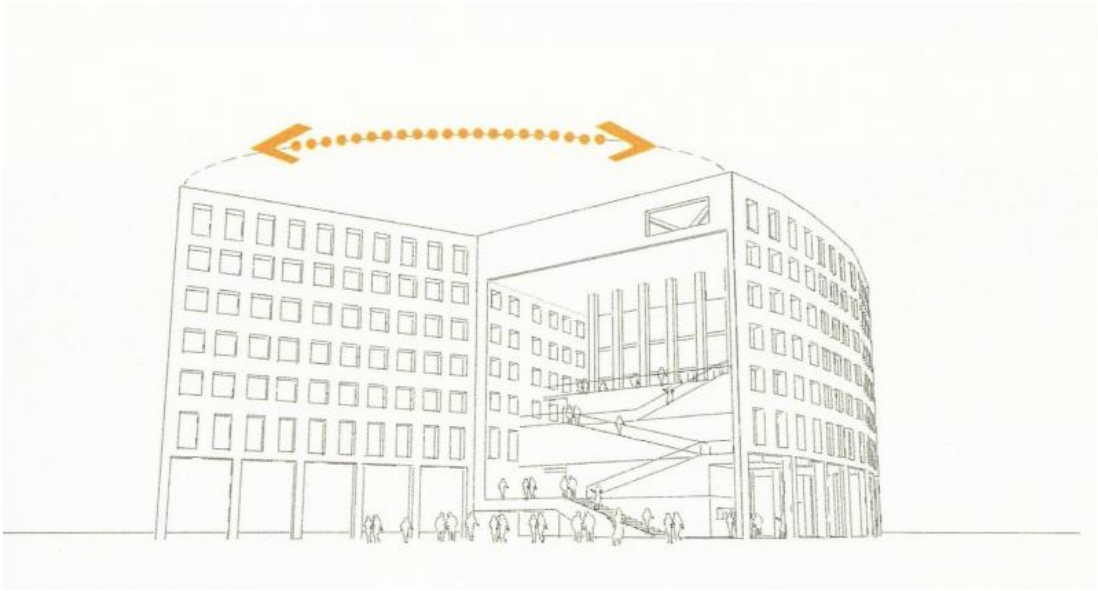

Figure 4.2 Transformation of the Concrete Perforate Wall Façade into a Transparent Facade by TEGET Architecture Office

This transformation resulted in a purely transparent façade with a two-vista opening to the interior galleries and the crowded Istiklal Street on the outside.

Figure 4.3 Views of the building completed in 2017. North Facing façade (Left); South facing façade (Right).

An argument for and Description of the selected reference façade

The reference transparent façade of the YKKS building that will focus on this study is a North facing façade. Conventionally, a south-facing façade would be preferred for solar energy harvesting due to direct exposure to solar radiation. However, only south-oriented façades would be insufficient to optimise solar harvesting areas in crowded urban areas. Implying that to sufficiently expand energy generation areas in urban centres, it is inevitable that some of the surfaces used for BIPV installation would be oriented away from the direction of direct solar radiation. Likewise, this obliquely oriented façade of the reference building was found suitable for the study because it would nearly imitate the actual urban conditions where most vertical surfaces would either be shadowed or oriented away from the sun in that only diffused sunlight would be available on these surfaces to be converted into electricity. The south-facing façade of the building that would have been preferred for solar panel installation also equally suffers from shading from nearby buildings

for the more significant part of the day. Implying shading is an inevitable issue to be addressed when adopting solar harvesting surfaces on buildings in urban areas. This also leaves the north-facing façade that barely experiences any shading as the best option for the study.

The reference façade is a curtain walling system consisting of 91 individual glass panels supported by an aluminium substructure. It is these 91 pieces that will be replaced and simulated as though they were actual energy-generating photovoltaic units.

4.1.2 Solar Energy Harvesting System

The solar harvesting system (LSC device) used in this study was developed and tested by Meinardi *et al*., (2017). Besides its high PCE compared to other LSC devices currently available, this particular solar concentrator device was chosen because of its potential environmental benefits. This particular device uses silicon quantum dots, where silicon is an earth-abundant material with limited toxicity. This makes this particular LSC device environmentally beneficial. In addition, besides the environmental benefits associated with the limited toxicity of the used Si-based QDs, the abundance of silicon on the earth's crust carries cost benefits that would make the manufacturing process cheaper due to the easy availability of materials. For instance, 8 million tons of silicon are produced yearly, of which only a small percentage is used for semi-conductor production in the PV sector. Most are applied in other sectors such as aluminium production. Also, this Si quantum dots based LSC device as designed by Meinardi *et al*., (2017) is reported to be the first realisation of an efficient large-area LSC based on indirect-bandgap colloidal nanostructures. One of the advantages of Si quantum dots is their suppressed reabsorption capability and their high compatibility with polymer matrices. This enables the achievement of an ideal LSC device that is free from reabsorption and scattering. Si QD-based LSC can also be scaled up to larger sizes without incurring any significant optical losses due

to reabsorption of the guided luminescence. This was verified using Monte Carlo numerical simulations. Furthermore, the possibility of flexible LSC with more complex curvatures will further foster the building integration of LSC devices.

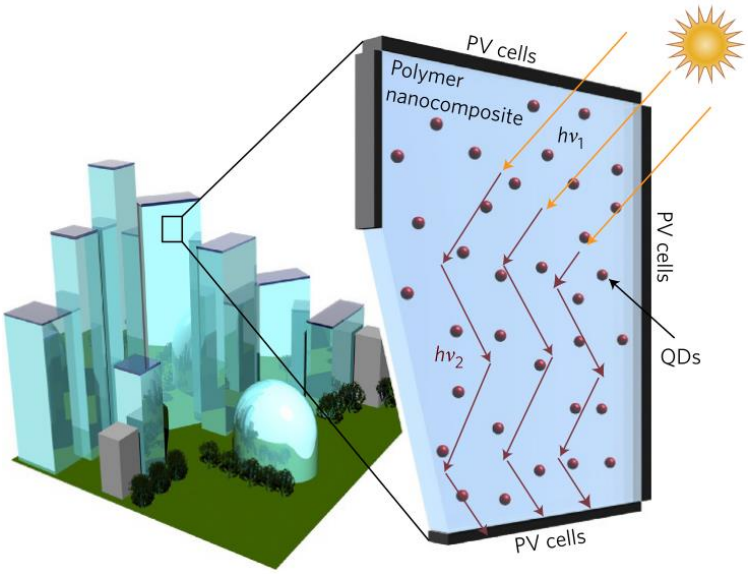

Figure 4.4 Illustration of LSC Window (Meinardi *et al*., 2017).

- **Technical Aspects of the LSC Device Used in this Study**

The LSC device adopted for this study was designed and a prototype manufactured by Meinardi *et al*., (2017), comprising PLMA cross-linked with ethylene glycol di methacrylate (EGDM). The size of the prototype device was dimensions of 12 cm× 12 cm× 0.26 cm containing 0.09% wt% quantum dots.

As previously mentioned, the structure of the LSC used in this study consists of Si quantum dots. The QDs used in this particular device have more than 800 nm emitting capacity. Furthermore, the QDs were synthesized in a non-thermal plasma reactor and then functionalized with 1-dodecane. Different ultraviolet light treatment was carried out to establish photo-stability of the covalently bonded surface species. The material of the wave-guide used was poly lauryl methacrylate (PLMA). The main advantage of this particular LSC is that it exhibits a “stroke shift” of zero due to

Si quantum dots' emission mechanism. The emission mechanism of Si QDs is a band edge transition based one.

On the left side of figure 4.5 below, the device's appearance when under illumination by UV light is shown. This also indicates the high optical quality of the LSC waveguide.

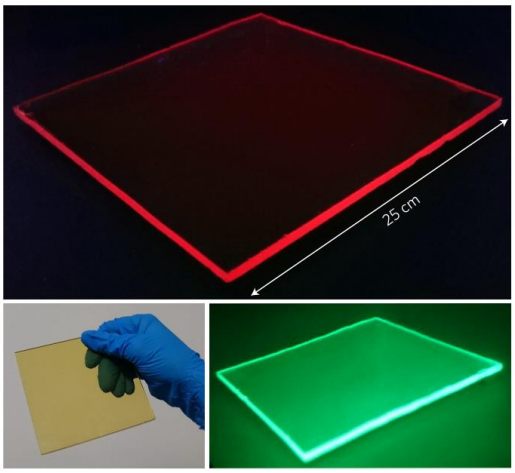

Figure 4.5 Image of the LSC Device Used Showing its Size and Effects of Different Spectral Lighting on the Matrix (Meinardi *et al*., 2017).

4.2 Research Aim & Methodology

This study in chapter 3 proposes a framework that can be used to determine the electrical output of a transparent luminescent solar concentrator. The proposed framework is applied and tested using computer-based software on a reference building using a selected luminescent solar concentrator device. The reference building consists of a wide transparent façade for which it was thought appropriate for testing. It provided a reasonably wide enough installation area for the transparent LSC system. Autodesk Revit software was used with the Insight plugin to determine the amount of solar radiation received on the reference façade of the building. Since the PCE of the selected solar harvesting system (LSC device) is already known from the study (Meinardi et al., 2017), steps 1 to 4 of the proposed framework are not

considered here. Rather the application of the framework pickups up from steps 5 through 8 to finally determine the electrical output of the device if were applied at the locality (section 4.2.2.2). The determined value of the electrical output is then fed into a computer software (PVsyst) that is used to simulate the solar energy performance of the solar system in actual life.

The following five subsections will first describe the assessment methods and data sources, then provide a breakdown of the research procedure followed for the study.

4.2.1 Assessment Methods and Data Sources

In this study, the computer program PVsyst is used to assess and simulate the performance of the selected transparent solar system on a reference building in the densely populated neighbourhood of Beyoğlu in İstanbul, Turkey. Determining the geographical location is the most essential and first step when assessing a solar system. Geographical coordinates are used to extract weather data for the simulation. First, following the described framework in chapter 3, the site coordinates were used to acquire solar radiation data using the Revit software and Insight plugin. Information on the solar radiation was then used to determine the electrical output of the LSC device as described 4.2.2.1 (d).

Similarly, while carrying out the electrical simulations in PVsyst software, weather data was imported from the Meteonorm 8 database using the site coordinates. Other data, especially regarding the reference building, was acquired from the architect of the building. This was used to estimate the size of the reference building and the building energy load used during the electrical simulations. Data related to the selected Luminescent Solar Concentrator device was acquired from the research paper (Meinardi *et al*., 2017) as described in subsection 4.1.2.

Section 4.2.2 describes the modelling procedure for determining the electrical performance of the transparent solar façade system under study in this research. The

simulation parameters, as well as the modelling and simulation procedure, are described.

4.2.2 System Performance Simulation

The ensuing two main sections, i.e. 4.2.2.1 & 4.2.2.2, describe the procedure used for carrying out the electrical performance simulation of the transparent solar façade system.

The first section will describe the procedures followed to determine the different input parameters used for the electrical simulation. PVsyst computes other input parameter-dependent variables during the electrical simulation, such as Global Horizontal Irradiation (GHI) the Effective global correction for IAM and shading (GlobEff), which are then presented in the Balances and main results (see table 5.1) at the end of the simulation. These variable parameters are summarised in the first column of Table 4.1 below and further described in Chapter 5 under the results and discussions.

Generally, the parameters considered during the electrical performance simulation of a solar harvesting system can be divided into two; (a) the System related parameters and (b) Environmental related parameters. System-related parameters are generally the constant or fixed parameters, whereas environmental-related parameters are usually variable and dependent upon fixed system parameters. Table 4.1 below provides a summary of all the simulation parameters.

Table 4.1 Summary of the Electrical Simulation Variables and Parameters

SUMMARY OF PROJECT PARAMETERS		
VARIABLE PARAMETERS	FIXED (PV SYSTEM & BUILDING-RELATED PARAMETERS	
ENVIRONMENTAL RELATED PARAMETERS	LSC (PV) RELATED	BUILDING RELATED

Solar radiation at the site	Reflective Index of LSC device (Equivalent to used PLMA matrix)	Electrical Load (Energy demand of building) = 300 LED (21.8 watts)
Convertible Solar radiation	PCE of LSC = 2.85% as stated by (Meinardi *et al.*, 2017)	Inverter Capacity
Global Horizontal Irradiation (GHI)	Luminophore of Earth Abundant Si QD material used	Battery type & capacity
Effective global correction for IAM and shading (GlobEff)	Temperature coefficient of the LSC device	
Available solar energy	PCE of edge-mounted GaAs PV cells = 29.1%	
Unused energy (Un convertible Solar radiation)	Electrical Resistance of PV array	

The variable parameters listed in the left-hand column of table 4.1 above under the variable parameters are calculated during the simulation process in PVsyst and presented in the 'Balance and main results' table 5.1. These parameters are also dependent upon the input parameters such as the geographical location (weather data), the electrical output of the solar harvesting system and the user's needs. The procedure for determining these three main input parameters is described below.

4.2.2.1 Procedure for Determining Electrical Simulation Parameters

This subsection describes the procedure for determining the input parameters used for the electrical simulation in PVsyst.

Assessing and determining the system's electrical output makes it possible to evaluate the feasibility in terms of the cost and environmental impacts of using an energy harvesting façade in place of a conventional one.

As previously mentioned, this study uses PVsyst software to simulate the energy performance of the transparent solar façade. The PVsyst software allows for several

different simulation alternatives to be carried out; for instance, a solar system could be simulated as grid-connected or a standalone system. In this research, the solar harvesting system was simulated as a SAPV. Irwan *et al*., (2015) described a standalone photovoltaic system (SAPV) that locally generates electricity independently and supplies it to the load without being connected to an electric grid. Although such systems still require electricity storage, any assessments and analyses on storage systems or other BOS components have been excluded in this work. The parts needed for the functioning of a SAPV system can be divided into two; the PV array and the Balance of System (BOS) component. Overall, a PV array combines PV modules for electrical power-boosting. Balance of System (BOS) components generally consist of all other parts besides the PV modules, such as; battery storage, MPPT charge controller, and wiring systems. These have been excluded from this research as they are beyond the scope of this work.

The electrical simulations in this study are performed using PVsyst version 7.2.0. PVsyst is a computer-based software package dedicated to assessing PV systems. During the simulation of the SAPV, PVsyst considers both the behavioural tendencies of the system and the system disturbances.

A Summary of Input Parameters

As input parameters, PVsyst requires the geographical location coordinates to be determined. This is mainly to acquire weather data from the PVsyst inbuilt database. Secondly, the solar harvesting system's electrical characteristics and the user's energy needs. The parameters used for this study are summarised in the table below and are further discussed in the subsequent subsections.

Table 4.2 Summary of Input Parameters

Input Parameter	value	source
Geographic Location	41.033051; 28.97665	Google Maps
Energy of Solar System	9.79 wh/m^2	Calculated under 4.2.2.2

User's Needs	300 LED laps, (21.8 W)	Manufacturer (ERCO)

The procedure for Determining the Parameters Mentioned above is Described in the Subsections Below.

a. Determine the Geographical Location

As discussed above, the modelling process in PVsyst first requires the definition of the geographical location for weather data acquisition. The reference building used for this study is located along the İstiklal Street in the Beyoğlu area of İstanbul, Turkey. The YKKS building lies at a latitude/altitude of 41.033051; 28.97665 on Google Maps. These coordinates were entered into PVsyst and used to retrieve the weather data of the locality at the reference building. PVsyst software is integrated with the Meteonorm 8 weather database software. Meteonorm 8 combines reliable data sources and sophisticated calculation tools and allows access to typical years and historical time series. It generates accurate and representative typical years for any place on Earth. The database consists of more than 8000 weather stations, five geostationary satellites and a globally calibrated aerosol climatology, which utilise sophisticated interpolation models based on more than 30 years of experience, providing results with high accuracy worldwide (Meteonorm, n.d.). Based on the site coordinate data fed into PVsyst software, it was revealed that the locality is Beyoğlu and belonged to time zone 3 with an altitude of 91 above sea level. The site was specifically chosen for its dynamic variations in solar radiation. It is expected that this will help determine the actual feasibility of adopting Building Integrated Photovoltaics in an urban area where energy-generating surfaces are prone to shading by traffic and nearby buildings.

Figure 4.6 Location of the Site along Istiklal Street

Furthermore, solar radiation studies revealed that the sun trajectory along the site is mainly from the east-west direction (see figure 4.2.2 below). This implies that the southern façade of the building receives most of the sunlight during the low grazing winter months of the year. Although the solar studies revealed that the sun would be mainly based on the southern side of the building, this was important and necessary for this study since the façade of interest is more northern oriented. The main reason for adopting BIPV is to expand solar active areas on buildings in urban areas. Some BIPV installations would inevitably be obliquely away from direct sunlight under real conditions. Thus, a northern-oriented façade would aid the simulation of actual urban conditions where some sites and surfaces used for solar generation would be obliquely oriented away from the sun's direction. In addition, it is important to note that one of the advantages of solar concentrating technologies over other solar harvesting technologies is their ability to work effectively under diffuse light *(Reinders et al., 2017)*; thus, their performance is not affected by the lack of direct sunlight, as is the case with conventional PV technologies. Therefore, it is assumed that the orientation of the reference façade used in this study should not significantly affect the system's effectiveness. This is also intended to help achieve results close to

actual outdoor conditions of any BIPV system in urban areas. It is expected that some building façades used for BIPV installation will be orientated away from direct sunlight.

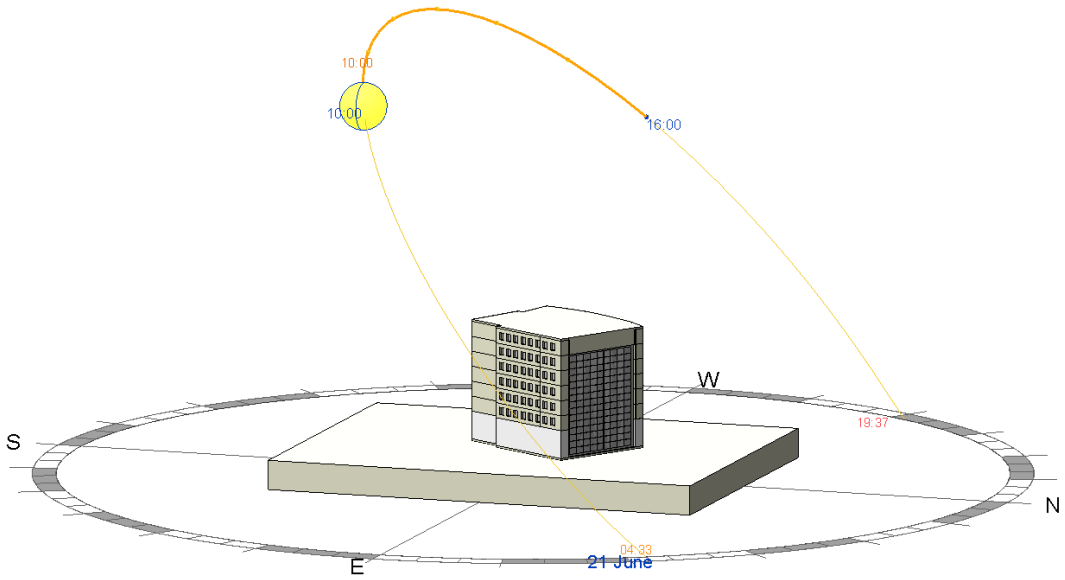

Figure 4.7 Sun Path along with the Reference-Building Site.

Solar Angular Assessment at Site Location

At the geographical location of the reference building, the grazing angle of the sun during the winter period between November 22nd through January 19th results in a higher solar exposure on the reference façade. This is mainly due to the northerly orientation of the reference façade. This balances the solar production from the reference façade even during the winter months at the location. The higher energy generation during the winter months is proof of the high solar exposure of the façade during these periods (see figure 5.2.1 Nominal Power Production). Figure 4.8 below shows the sun path angular movement along the reference façade. The highest sun angle at the site is on June 22nd. However, due to the orientation of the reference façade, the lowest grazing angles of the sun during the winter period from November 22nd to January 19th balance the solar exposure during these times, thus, the solar energy production at the site. Furthermore, the lower grazing angles of the sun result

in a higher solar exposure on the vertical solar façade, thus limiting the collection losses if the solar harvesting system were inclined. The higher collection capacity of the reference façade during angular grazing periods is also evidenced by the low collection losses, as shown in figure 5.2.1.

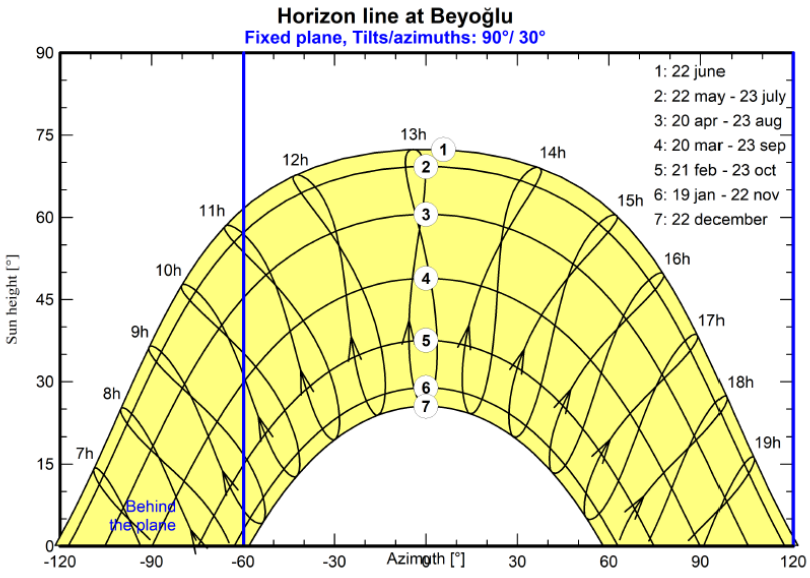

Figure 4.8 Sun Paths (Height / Azimuth diagram)

b. Assess the Solar Radiation at the Location

After determining the geographical location of the building, the amount of solar radiation at the locality was assessed following the framework described in chapter 3 of this study. For this purpose, Revit 2019 software coupled with the Insight plugin was used. The results of the solar radiation analysis showed that the North facing façade of the reference building receives on average 48 kWh or 0.10 kWh/m^2 of solar energy daily. The results of solar radiation assessment performed on the building are depicted in the visuals below;

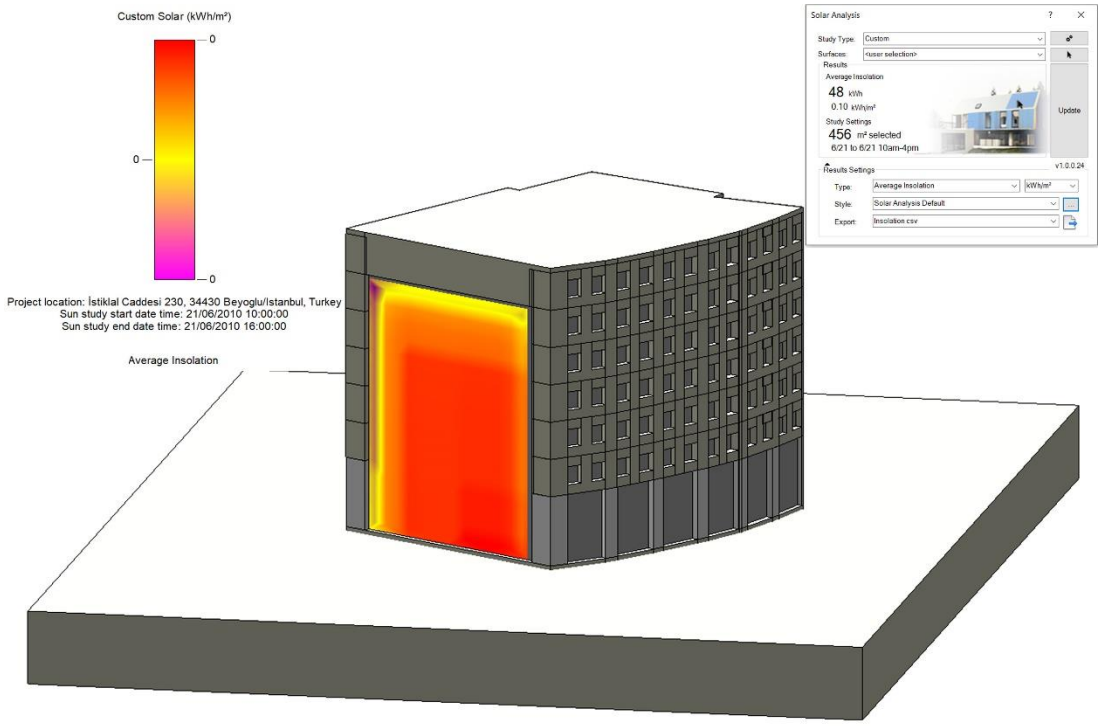

Figure 4.9 Solar Radiation Simulation on Building Reference Façade.

Weather data for the local geographical location was extracted using the geographical site coordinates; 41.033051; 28.97665. The single-day pre-settings of a summer solstice were used in Revit. The measurement was set to be PV energy in kWh/m^2. The overall surface area of the reference façade is 456m^2. However, the solar-active area (area useable for solar energy generation) would be less than the actual area due to resizing the façade glass panes to avoid potential shading at the corners.

c. Determine The Building Energy Demand

Though not an exclusive step within the energy assessment framework described in chapter 3 of this thesis as energy demand varies from building to building, determining the energy demand of the reference building is critical to assessing the fraction of the building energy that can be filled by the energy generated from the PV

system. Defining the building energy demand guides in the proper configuration and sizing of the system, i.e. Balance of System (BOS) components, which in actual conditions helps prevent system oversizing, resulting in increased system cost. The building energy demands of the reference building used in this study are estimated considering the energy-generating capacity of the solar harvesting system adopted. As will be further elaborated under subsection 4.2.2.3 (c), the generated solar energy from the PV system is assumed to only power the LED lighting in the exhibition area of the reference cultural building. Thus, the overall building load is considered to be 300 LED lights that consume 21.8 watts.

d. Determine the Optical Efficiency of a single LSC device

According to the energy assessment framework described under Chapter 3, the efficiency of the LSC device is the product of the edge-mounted PV cell efficiency and the optical efficiency (photons reaching the PV edge-mounted cells), which is given by;

$$\eta_{LSC} = \eta_{PV} \text{ x } \eta_{opt} \qquad (14)$$

According to Meinardi *et al*., (2017), the Power Conversion Efficiency (η_{LSC}) of the Luminscnet Solar Concetrator adopted for this study is;

$$\eta_{LSC} = 2.85\%$$

Also, as previously mentioned, this research uses GaAs-based solar cells as the edge-mounted PV cells. These have so far yielded the highest PCE when used with LSC devices, according to (Slooff *et al*., 2008). The power conversion efficiency of GaAs cells recorded today is 29.1%, according to (Yamaguchi, 2020).

Thus,

$$\eta_{PV} = 29.1\%$$

Implying, according to formula 14 of the framework, the optical efficiency of the LSC can be calculated as;

$$\eta_{LSC} = \eta_{PV} \text{ x } \eta_{opt} \quad (14)$$

$$2.85 = 29.1 \text{ x } \eta_{opt}$$

$$\text{Implying } \eta_{opt} = 0.0979 \text{ or } 9.79\%$$

Determine the Power Output of the LSC Device

The power output of the LSC is then derived following formula (16) from the assessment framework. With all possible losses considered for each LSC unit, the total photon energy reaching the PV cells mounted at each LSC can be derived from;

$$\eta_{opt} = \frac{Pout}{Pin} \quad (11)$$

According to framework formula 11, the power input is equivalent to the amount of solar energy received on the front surface of the LSC device. Based on the solar radiation simulation of the reference building power input $P_{in} = 0.1 kWh/m^2$.

Implying;

$$0.0979 = \frac{Pout}{0.1}$$

$$P_{out} = 0.00979\ kWh/m^2$$

The table below summarises all required simulation variables and input parameters. The geographical site coordinates used to extract local weather data from the cloud databases are 41.033051; 28.97665. The area of the reference façade is equal to the actual size of the façade of the building: 24mx20.42m (457m^2). However, the resulting solar active area was computed as 437m^2. The difference in the façade area and solar active area is due to the thickness of the dividing mullions on the façade as well as the automatic placement and resizing of the LSC modules during the modelling process in PVsyst software. Solar active area refers to the area that can be

used for the generation of solar energy, which also is the area covered by the LSC modules.

Table 4.3 Summary of Relevant Assessment Specifications and Parameters

FACTOR	VALUE	SOURCE
Geographical Site Coordinates	41.033051; 28.97665	Obtained from google maps
Available Solar Radiation	48 kWh or 0.10 kWh/m^2	As computed by Insight Plugin
Area of Ref. Façade	456 m^2	Actual Area of Ref Façade
Solar Active Area of Façade	437	As per PVSYST evaluation
Size of LSC Modules	1x1m	Resized to fit gap openings on Ref. Façade
Possible No. of Modules	437	23(vertical) & 19 (Horizontal)
PCE Solar harvesting system	2.89%	According to Meinardi *et al*., (2017)
Power Output of Single LSC Device	9.79 Wh/m^2	As per calculations under 4.2.2.2
Spacing Between LSC Modules	7cm	Matching façade mullion sizes

The solar harvesting system or LSC modules were resized to 1x1m to fit the gap opening on the façade. The resulting possible number of modules, 437 pieces computed using the Skelion plugin in Sketch-up, is also equivalent to the solar-active area computed in PVsyst. According to the proposed framework, the electrical power output of a single LSC module was calculated as 9.79 Wh/m^2 under subsection 4.2.2.2. The spacing between the modules was specified to match the actual mullion thickness of the reference façade.

4.2.2.2 Modelling Procedure for Electrical Simulation

After determining the power output of the LSC device, the values were then used to perform an electrical simulation in PVsyst software. First, the modelling was done in Sketch UP with the Skelion plugin, where the module layout on the façade and solar active area was determined. The modules were resized to be 1x1m. This was intended to match the measuring units (kWh/m^2) of available solar irradiation used to estimate the electrical output of the modules. Additionally, by resizing the modules to be 1x1m, they would match the realistic gaps on the aluminium façade structure. Both in Skelion and PVsyst, the power output of the modules was set to 9.79 Wh/m^2 as previously calculated. The overall surface area of the transparent façade was calculated to be 456m^2. However, some of this area was lost due to modules resizing, resulting in a final solar active area of 437m^2. Solar active area refers to the area on the reference façade that is fully covered by the 1x1m resized modules and excludes the area of the façade dividing mullions. In Skelion, a spacing of 7cm related to the thickness of the façade dividing mullions was used between the modules. The number of stacked modules was set to 23. The maximum number of possible panels was set to 450. The resulting layout of the modules in Skelion is shown in figure 4.2.4 below.

With the module layout done in Sketch UP using the Skelion plugin, the model was then exported to PVsyst for the energy simulation. Importation into PVsyst was done with the Near Shading 3D window in PVsyst. Since the reference façade is facing an open square, no shading pre-set was set in PVsyst. Other specifications had already been set out in sketch-up, such as the building orientation. Thus, no alterations to the angle of azimuth were made in PVsyst. Other data, such as the geographical data, were also imported directly from Sketch UP.

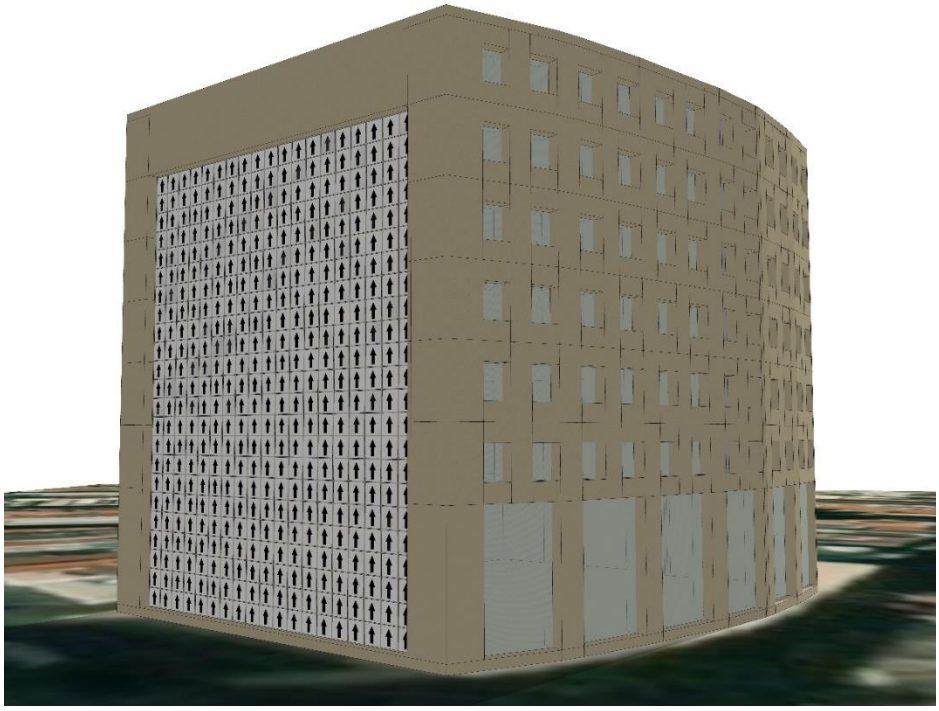

Figure 4.10 PV Module Layout on Façade

However, other parameters had to be remodelled before carrying out the energy simulations in PVsyst. The modelling process in PVsyst software requires different types of data categories. This is done following several steps, which need specific parameters to be set out and predefined. Mainly climate data of the local site area (metrological data), extracted from cloud weather databases inbuilt within PVsyst, electrical and mechanical specifications of the PV system, the PV system's peak power, and angular orientation details must be input into the software. Eventually, the overall electrical output of the system is determined from the set values entered for each parameter. This subsection gives a breakdown of the different modelling steps followed in PVsyst.

a) **General System Configurations**

From the PVsyst home window, the project was set as a Stand-Alone system (SAPV). A PV system design process in PVsyst follows several steps, starting with defining the project site location. The definition of the project site was done based on the location coordinates of the site. The coordinates used in PVsyst were initially explained in subsection 4.2.2.1 (a) above under the description of the geographical location. The coordinates stated for the particular area of the reference building were 41.033051; 28.97665 as determined from Google Maps. The meteorological weather data was then extracted from PVsyst's Meteonorm 8.0 weather database software and used for the study.

b) Location and System Orientation

After defining the site's geographical location and importing the weather data, it is then required to determine the orientation of the PV array and building. The vertical orientation of the modules was set to be 90 degrees to match the verticality of the building façade where the LSC panels are hung. The Azimuth angle within PVsyst was set to 30.2 degrees to match the approximate northward orientation of the reference building and façade along the south-north axis.

c) Building User's Needs

While setting out the "User's Needs," it was assumed that the power generated from the transparent solar façade would only be sufficient to support the general lighting of the building. Thus, the user's needs were only set to be 300 lamps installed in the building. It is assumed that the electricity would be generated during the day and stored in batteries to light the general areas within the galleries at night. The lamps used are Eclipse 48V manufactured by ERCO, running at 21.8 watts for 12 hours after working hours. The reset of the predetermined users' needs, such as electronic appliances, have been excluded from the study as the electricity generated by the façade panels is assumed insufficient to support their functioning.

d) PV System Definition

With the building orientation and electricity user load determined, the modelling process in PVsyst next requires the definition of the PV array and Balance of System (BOS) components. Under these, the modelling procedure in PVsyst requires that the storage system and PV array system be defined. A lithium-ion storage battery system was selected for the PV system, and the rest of the settings under this parameter were left as default. A new PV module was designed based on an already existing type in PVsyst. The already existing PV type selected was Gallium Arsenide-based (GaAs) cells. The peak power for the modules was then set to be the electrical power output of the LSC device as calculated in section 4.2.2.2. GaAs-based modules were selected for this study since they have recorded the highest power conversion efficiencies to date of any other PV cell (see figure 3.6). Additionally, a generic system controller with an MPPT controller mode was selected. The area covered by the LSC modules was resized to match the reference building's actual glazed area ($457m^2$); however, due to spacing between the modules, the resulting solar active area was $437m^2$.

An operating PV system can be divided into three main parts: the PV array, The BOS, and the User (load). These parts are depicted in the circuit system diagram shown in figure 4.2.5 below.

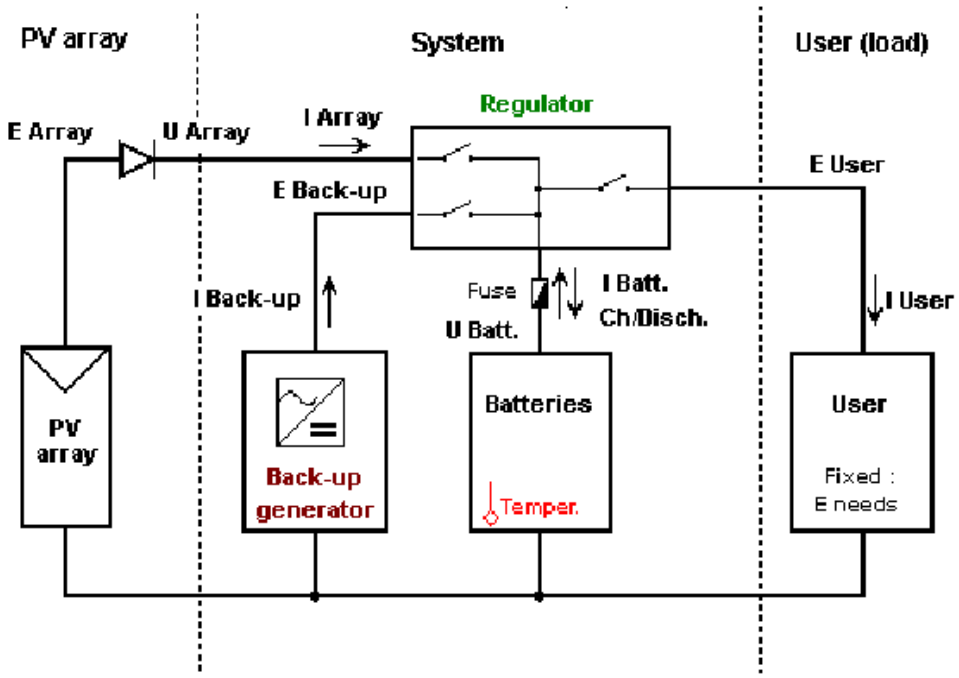

Figure 4.11 Typical Layout for a Stand-Alone PV System

e) System Losses

Definition of system losses is one of the required steps while modelling a PV system in PVSYST. However, the alterable parameters that have to be set under the system losses in PVsyst primarily relate to modules that have direct exposure to solar radiation, *i.e.* conventional PN junction based solid modules. It implies that most of the predetermined system losses within the software do not apply to LSC.

However, it is essential to note that electrical losses due to internal and external factors are among the biggest hindrances to higher power conversion efficiencies (PCE) in any solar harvesting system. For the case of LSC devices, overlaps between the absorption and emission spectra are the leading causes of lower device efficiencies. This phenomenon is referred to as “reabsorption.”

However, as previously mentioned in section 4.1.3, while describing the structure of the LSC adopted for this study, the real-stroke shift between the absorption and

luminescent spectra is zero for this particular LSC device. This is because the light photon emissions by Si quantum dots used in this specific device is due to a band-edge transition. Thus, the reabsorption losses are negligible.

Furthermore, other expected losses would occur within the edge-mounted solar PV cells. However, these are neglected as they are assumed to be already taken care of within the system model.

f) Environmental Disturbances

Environmental disturbances are occurrences that would alter or directly affect the system's electrical performance due to their proximity to the building façade. These are mainly losses resulting from shading by nearby objects or buildings. However, since the façade of interest on the reference building is positioned facing away from any possible shading objects, shading losses were also neglected. Thus, no alterations were made in the model to account for nearby shading.

CHAPTER 5

RESULTS AND DISCUSSION

With the solar system modelled and all different parameters specified, the electrical simulation of the system was carried out. The main outputs from the electrical simulation in PVsyst software are produced (normalised) energy (kWh/year), specific energy production (kWh/kWp/year), performance ratio and losses of the system. This chapter consists of two main sections. In the first section, the input parameter depends variables are described in detail, and their respective simulation results are presented and discussed. The second section of the chapter presented the simulation results for the electrical performance of the solar harvesting system.

5.1 Overall System Performance Variables and Simulation Parameters

Simulation of a solar harvesting system in PVsyst software involves several variables accumulated in monthly values. While specifying the input parameters in the initial modelling process of the PV system, PVsyst verifies the consistency of variables with the main input values. The major overall system variables used to simulate the performance of a PV system in PVsyst software are calculated and summarized in balances and the main results table (See Table 5.1 below). The balances and main results consist of several variables, namely; Global horizontal irradiation, Effective global correction for IAM and shading, Available solar energy, Unused energy, missing energy, Energy supplied to the user, energy needs for the user, and solar fraction. These simulation variables are described in detail, and their simulation results are discussed and presented in the subsections below;

a. Global Horizontal Irradiation (GHI)

The global horizontal irradiation values at the geographical site are listed in the first column of the balances and main results table. By definition, Global horizontal irradiation (GHI) refers to solar radiation that is incident on a horizontal surface. Global horizontal irradiation (GHI) is the summation of Direct Normal Irradiance (DNI), Diffuse Horizontal Irradiance, and ground-reflected radiation. The GHI value in flat plane PV systems is usually used to determine the electrical output. The highest GHI values at the locality occur during the peak summer months of June and July. Likewise, the lowest value of GHI is in the peak winter months of December and January.

b. Effective global correction for IAM and shading (GlobEff)

These are presented in the second column of the balances and main results table from the PVsyst software. By definition, GlobEff is irradiation in the collector plane after disposition that is affected by the optical losses like Far and Linear shadings, IAM, and soling losses. It is usually computed from the horizontal global and diffuse irradiance in hourly values. It is dependent upon the geographical coordinates as well as the solar geometry. At the geographical site of the reference building in this study, GlobEff values range from 50 to 100, with the highest recorded values being in the two months of August and September.

c. Available Solar Energy

Available solar energy is convertible solar energy that can be transformed into electricity. On an annual basis, 29,570 kWh of energy would be available from the solar harvesting system as per the computation from PVsyst. Most of this energy is generated during the summer months when peak solar radiation is at the geographic site. Over 600 kWh of electricity would be harvested from the solar system during these months. The lowest values for the available solar energy are during the winter periods of November through March. However, electricity production during these

months is boosted due to the low grazing angles of the sun over the reference facade that result in more normal incident angles, thus, higher solar energy production.

d. Unused Energy

By definition, this would refer to harvested solar energy that goes unconsumed on any activity, for instance, when the battery storage system is overcharged and full. Simulation results of the system reveal that all harvested energy gets consumed.

The table below presents the average figures obtained from the simulation software of all the discussed aspects.

Table 5.1 Balances and Main Results

	GlobHor	GlobEff	E_Avail	EUnused	E_Miss	E_User	E_Load	SolFrac
	kWh/m²	kWh/m²	kWh	kWh	kWh	kWh	kWh	ratio
January	50.2	64.4	2072	0.009	0.0	2456	2456	1.000
February	59.7	58.3	1803	0.007	193.7	2025	2218	0.913
March	103.3	86.1	2782	0.000	554.6	1901	2456	0.774
April	143.1	88.5	2646	0.000	0.0	2377	2377	1.000
May	193.4	93.7	2582	0.000	0.0	2456	2456	1.000
June	211.7	90.2	2321	0.000	0.0	2377	2377	1.000
July	213.5	95.6	2482	0.001	0.0	2456	2456	1.000
August	183.7	105.1	3037	0.001	0.0	2456	2456	1.000
September	133.8	102.2	3265	0.000	0.0	2377	2377	1.000
October	82.0	79.2	2454	0.001	0.0	2456	2456	1.000
November	51.9	68.1	2282	0.008	0.0	2377	2377	1.000
December	41.6	56.8	1845	0.006	27.4	2429	2456	0.989
Year	1468.0	988.3	29570	0.033	775.6	28141	28917	0.973

GlobHor	Global horizontal irradiation	E_Miss	Missing energy
GlobEff	Effective Global, corr. for IAM and shadings	E_User	Energy supplied to the user
E_Avail	Available Solar Energy	E_Load	Energy need of the user (Load)
EUnused	Unused energy (battery full)	SolFrac	Solar fraction (EUsed / ELoad)

e. Missing Energy

Missing energy is a computation of the non-converted and unconverted available solar radiation at the geographic site. The amount of missing energy is relative to the amount of solar radiation available at the site. In other words, if the power conversion efficiency of a system were to be calculated as 25%, the missing energy would account for the other 75%. At the locality, missing energy is equivalent to an average of 775.6 kWh of energy. Some of this could be due to module surface reflections, heat conversions or losses due to shading and system wiring. In simple terms, it's the energy that cannot be accounted for yet available at the locality by virtue of the amount of solar radiation at the geographic location. There is also a high correlation between the missing energy and the energy deficiency of the building. In the winter months of December, February and March, the highest values of missing energy were recorded. This implies that such months also had a high energy deficiency due to low solar radiation.

f. Energy Supplied to the User

This would equate to the amount of energy available for the daily operations of the building or building occupant activities such as electric lighting. Monthly, the amount of energy made available to the user strongly correlates with the amount of energy harvested (available solar energy). In other words, the more energy harvested, the higher the energy available to the user. Overall, more than 2000kWh of energy are supplied to the end-user in most months except in March, where the lower amount of solar energy is produced (1900kWh). Lower grazing sun angles over the reference façade during the winter months helps counterbalance the low solar radiation availability, thus, boosting energy production.

g. Energy Needs of the User (E_Loads)

This is a computation of the energy demand of the building users' activity. In the case of this study, the overall building load is assumed to be consisting of 300; 21.8

watts LED lamps that operate 12 hours daily for the lighting of the exhibition spaces of the building. An average of 28,917 kWh of energy would be needed to run the building load fully annually. This figure is 21,158 kWh more than the available solar energy. Implying the PV system would be insufficient to run the building's load entirely. Almost throughout the entire year, an alternative energy source would help meet the building's energy needs.

5.2 Evaluation of the Electrical Performance of the System

In this subsection, we discuss the overall electrical performance of the PV system. First, the generated amount of electricity results is presented and discussed. Second, a summary of the performance ratio and solar fraction is presented, followed by an analysis of the building energy demand. Finally, the results of the system losses will be presented and discussed.

a. Electrical Energy Output

The standardised parameter for PV electrical output assessment is Normalised electricity Production presented in kWh/kWp/day. As previously mentioned, for purposes of carrying out the electrical simulation, the module sizes were set to 1x1m single-celled LSC device modules. This yielded an overall solar active area of $437m^2$ on the reference façade of the building. Also, it was determined from the solar radiation study that, on average, 48 kWh ($0.1\ kWh/m^2$) of energy are received on the reference façade daily. No shading was specified since the reference façade used for the study faces an open square. The simulation results showed that, on average, the overall solar energy production by the transparent solar harvesting system is about 2 kWh/kWp daily. The grazing angular orientation of the sun, coupled with the verticality of the solar harvesting system, as well as the northerly orientation of the reference façade, resulted in high solar exposure of the façade during the winter months November to January. This results in almost optimal solar energy production during the winter months. The lowest solar energy production of

about 1.5kWh/kWp/day was recorded during March. The plot below shows the normalised daily electrical production of the system during the other months of the year.

Figure 5.2.1 below depicts the electrical performance results of the PV system. The Normalized System Production, yf (kWh/kWp/day) in maroon colour, depicts the maximum possible amount of electricity that will reach the building occupant. Overall, the PV system is expected to supply 1.95kWh/kWp of electricity daily.

The green colour represents the amount of electricity lost (Ls) within the system from the electrical resistance within the wiring and (or) changing the battery system. On average, approximately 0.24 kWh/kWp/day of current is lost within the system.

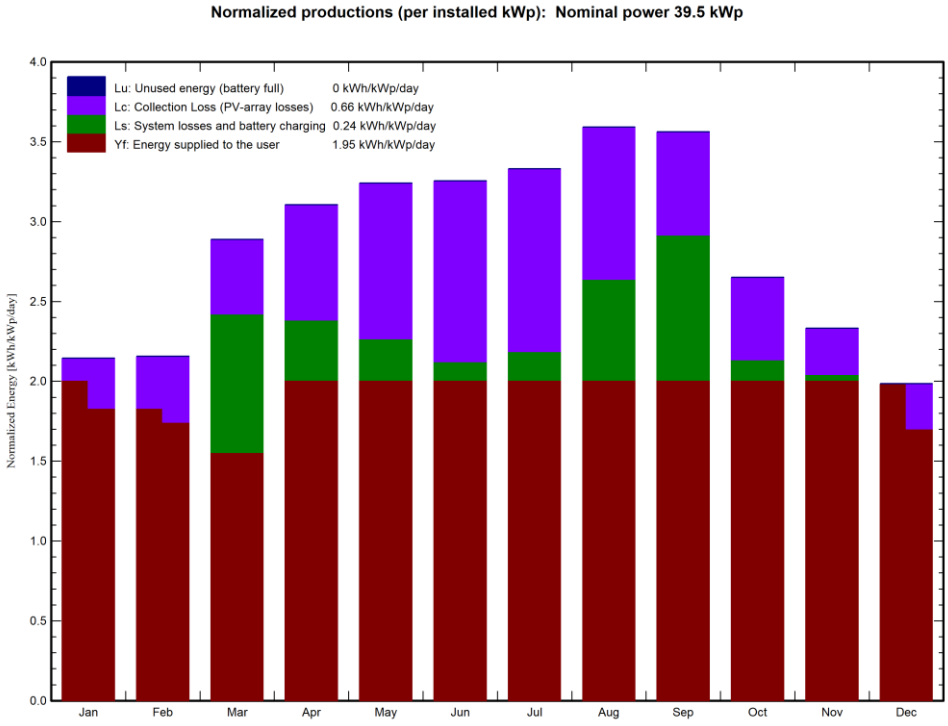

Figure 5.1; Normalised Electrical Production of the System

In addition, some solar energy from the sun is lost during the initial stages of solar energy collection due to occurrences such as surface reflection. Such losses are referred to as collection losses. The collection losses depicted in purple are lowest during the winter months of November to January, where the sun has a grazing angular projection over the reference façade. This is mainly because grazing angles of the sun yield a more normal or perpendicular angle of incidence of sunlight on the surface of modules, which fosters more light absorption and less surface reflection.

Similarly, the collection losses over the vertically oriented façade are highest during the summer. This results from less perpendicular incidence angles leading to more surface fall off of sunlight. Also, due to high collection losses resulting from a surface falloff of inclined sunlight, the electrical power production during these months is relatively similar to the rest of the year despite the higher level of solar radiation received.

Lastly, some other energy is expected to be lost when the battery system is fully charged. This is a very unexpected occurrence in the used system mainly due to the low PCE of the transparent LSC modules; thus, 0kWh of electricity is lost.

b. Performance Ratio

The performance ratio is a comparative quantity that compares the electrical output of the PV system (Effective energy supplied to the end-user) to that of an ideal PV system as measured at Standard Testing Conditions (STC). It's a unitless factor and is measured in percentages. The computations for the PR value consider all losses associated with the PV system. PR can be calculated by the formula below;

$$PR = \frac{E\_User}{GII\ x\ PnormPV}$$

E_User is electricity supplied to the end-user or building occupant (kWh/year), GII is the Global Irradiance Illumination value(kWh/m^2/year), and PnormPV stands for the solar systems installed DC capacity (kWp).

For the reference façade system studied in this research, an average performance ratio of 68.6% was computed. Figure 5.2.2 below depicts the system performance ratio for the entire year. Overall, the performance ratio for most months of the year ranges from 0.6 to 0.9, implying that high performance was registered during even the peak winter months. This is due to the low grazing angular projection of the sun on the reference façade resulting in a higher solar intake due to normal angles of incidence during these months. The lowest recorded performance ratio was in March (approximately 0.5). The predominately high-performance ratio values of the PV system recorded signify a tendency towards ideal behaviour measured under STC.

The performance ratio values in PVsyst are presented along with the solar fraction values, representing the ratio of the energy provided by the solar harvesting system to the energy demands of the end-user. In other words, solar fraction defines the amount of building energy demand covered by harvested solar energy from the PV system in a building.

$$\text{Solar Fraction (SF)} = \frac{Solar\ Energy\ Generated(E_{Sol})}{Energy\ Demands(E_{User})}$$

On average, the solar harvesting system has an SF of 0.973 throughout the year, with the lowest value recorded in March.

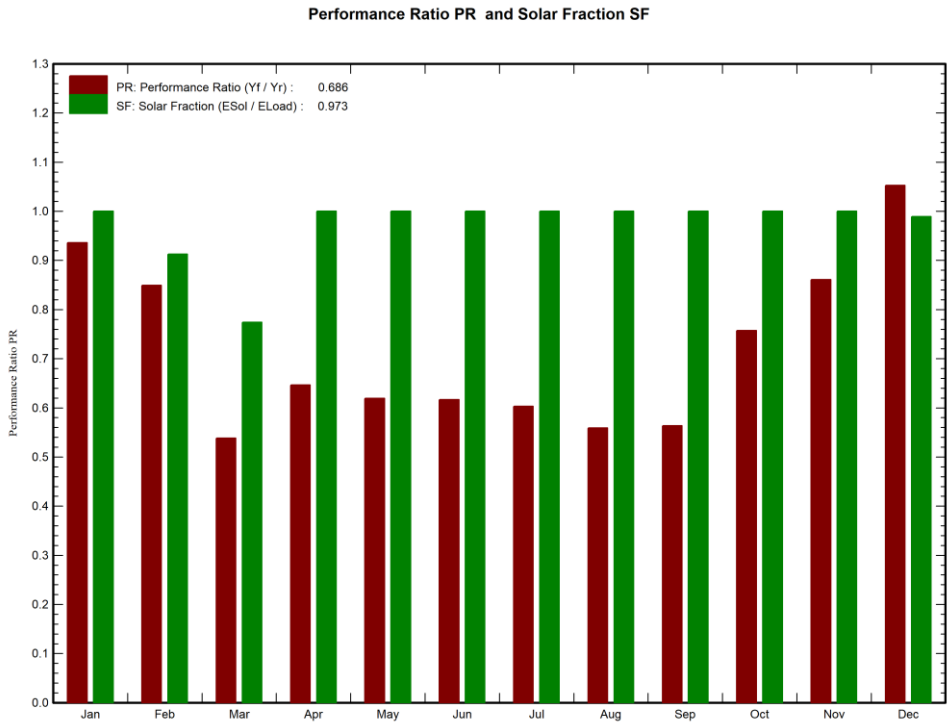

Figure 5.2 System Performance Ratio and Solar Fraction Measurements

The SF fraction average of the PV system across the different months of the year was computed to be 97.76%. Months where a slight variation in the performance ratio value (PR) was recorded also witnessed a significant variation in the solar fraction (SF), for instance, in March. This signifies a close correlation between the two parameters. A higher SF ratio value recorded during most of the months throughout the year indicates that a larger portion of the building energy demands could be met by a solar harvesting system, thus, less need for a backup supply of electricity. Likewise, lower SF values in March signified that a lesser portion of the building energy demands could be satisfied by the energy supplied from the solar harvesting system. Thus, a backup supply from a standby generator or grid would be required to meet the energy demands of that month. As depicted in figure 5.2.2 above, the average solar fraction and performance ratio fraction values during the year are 0.973 and 0.679, respectively. Also, table 5.2 below summarises the system performance values as discussed above.

Table 5.2 Summary of System Performance Values

System Production	29.6 MWh/year
Specific Production	749 kWh/kWp/yr
Performance Ratio	0.687
Solar Fraction	0.987

c. Building Energy Demand

During the design of the SAPV system, the energy demands of the building should be defined. This is intended to avoid oversizing the electrical system. For the case of this study, the power output of the transparent solar façade is presumed to be used for powering the exhibition area lighting system. Overall, 300 Eclipse 48V manufactured by ERCO, which run at 21.8 watts of power, were used for the simulation. The time of operation for the lamps was set to be 12 hours daily. The table below summarises the overall energy demand of the building. Overall, the building energy consumption is equivalent to 78,480 Watt-hours daily.

Table 5.3 Building Energy Demand

	Number	**Power**	**Use**	**Energy**
Units		Watts (W)	Hours/day	Wh/day
Lamps	300	21.8 W/Lamp	12.0	78,480 Wh/day
Daily Needs				78,480 Wh/day

The lamps were assumed to be operating at full capacity to light the exhibition area of the building throughout the day. Thus, the assumed energy usage of the building is spread across the 12 working hours of the day. The hourly energy distribution of the system is also shown in the graph below.

e. System Losses

In the PVsyst software, default values for the different loss mechanisms in a PV system are already set. The losses considered in PVsyst are internal, environmental, and losses in the specified Balance of System (BOS) components such as the inverters and battery storage systems. These losses include; efficiency drops due to temperature, module quality loss, mismatch loss, modules and strings, losses due to irradiance level etc. Overall, as depicted in figure 5.4 below, most solar energy is lost to external factors such as surface reflection and collision before photon absorption occurs. Table 5.4 below summarises the loss factors as measured against the input parameter-dependent variables.

Table 5.4 Summary of the Loss Mechanisms in the PV System

Input Parameter dependent variable		**Loss Factor & Value**		**Resulting Parameter & Value**	
Variable	**Value**	**Factor**	**Value**	**Parameter**	**Value**
Global horizontal irradiation	1468kWh/m^2	Global incident in coll. plane	-29.18%	Effective irradiation on collectors	988 kWh/m²
		IAM factor on global	-4.94%		
Array nominal energy (at STC effic.)	53757 kWh	PV loss due to irradiance level	-33.13%	Effective energy at the output of the array	30994 kWh
		PV loss due to temperature	-5.52%		
		Module quality loss	-3.00%		
		Mismatch loss, modules and strings	-2.10%		
		Ohmic wiring loss	-3.60%		
		Unused energy (battery full)	0.00%		
Effective energy at the output of the array	30994 kWh	Converter Loss during operation (efficiency)	-5.91%	Converter Output Energy/Battery Storage	29013 kWh
		Converter Loss over nominal conv. power	-0.65%		

		Converter Loss due to power threshold	-0.19%		
		Converter Loss over nominal conv. voltage	0.00%		
		Converter Loss due to voltage threshold	0.00%		
Battery Storage	29013 kWh	Battery Stored Energy balance	-0.05%	Energy supplied to the user	27499 kWh
		Battery efficiency loss	-0.98%		
		Charge/Disch. Current Efficiency Loss	-3.51%		
		Battery Self-discharge Current	-4.46%		
Energy need of the user (Load)				28917 kWh	
Balance Energy				4.90% (1418.0 kWh)	

5.3 Summary, Final Thoughts and Recommendations

Overall, despite the low power conversion efficiencies of transparent LSC technologies currently, the technology, when applied over a wide solar active area, can produce enough electricity to sufficiently subsidize the energy demands of a building. Furthermore, the vertical mounting of LSC modules on building facades could help optimise solar energy harvesting during the winter months when incident angles are grazing low. This is also seen to help balance out solar energy production during these months, thus reducing the fluctuation of solar energy production usually recorded with conventional PV technologies during winter months. However, it is recommended to apply an anti-reflective coating over the surfaces of the LSC modules. This would reduce the fall off of light from the surface, especially during

summer months when the sun is incident mainly at overhead angles, thus, increasing light absorption. However, with the current state of LSC technology, it's recommended to keep a full-time backup energy source at the building to meet the users' needs during low energy production periods. This can be done through a standby backup generator or connection to the public electricity grid.

Regarding research, a notable lack of good tools to study the different potentials of the technology was witnessed. For instance, for the assessment of the solar harvesting system in this study, PVsyst software was used to assess the performance of the solar harvesting system regardless of not providing direct ways of simulating vertically oriented transparent solar harvesting systems. Thus, its recommended that future efforts be directed at building more tools that can be used to assess the performance of transparent solar harvesting building integrated systems under actual conditions.

CHAPTER 6

CONCLUSION

Over the last two decades, an exponential change in energy demographics has been witnessed. It has also been revealed that a significant amount of resources are being invested in finding alternative energy sources while mainly capitalising on renewable forms of energy. The amount of efforts being invested in the advancement of renewables, especially solar energy, has been evidenced by the rapid increase in the installation capacity recorded over a period of just a few years. As earlier noted, by the year 2017, over 400GW of solar energy had been installed. Speculations further reported that this figure would surpass terawatt capacity in just a matter of decades from 2012. Perhaps one could argue that the increase in solar electrical output results from the increased efficiencies of the solar power harvesting technologies. However, it should be noted that increased efficiencies alone could not account for such high electricity production figures as, very evidently, the speed of advancement of the technology itself does not match the speculated electricity output. Furthermore, the increase in the photovoltaic equipment efficiencies should also prove the increased effort going into solar research.

It has been seen that photovoltaic technologies could play a significant role in helping avert greenhouse gases, as the mode of electricity production does not involve the burning of fossil fuels. Perhaps this advantage of photovoltaics over other energy modes is only getting more and more realised as the technology efficiencies tend towards the Shockley–Queisser limit. This only implies that less land is required for their installation, and consequently, lesser quantities of materials are used per unit amount of electricity produced. Additionally, an outstandingly low Levelized Cost of Electricity (LCOE) of only 2–4 cents/kWh was reported in 2018. This low cost of solar energy is one of the aspects that increases its attractiveness.

The growth of other technologies in the solar fraternity that use lesser materials, such as the luminescent solar concentrator technologies explored in this research, will further increase the benefits of solar technologies to the environment. Other solar technologies that have been noted to have great potential for environmental impact reduction are thin-film transparent and semi-transparent. By requiring less material, these carry a lessened environmental burden. Furthermore, these have the advantage of multi-functionality over their conventional counterparts, which further reduces the material needed in construction and the cost. Moreover, the possibility of using advanced manufacturing techniques for such light material PVs such as laser printing further increases their attractiveness.

The focus of this thesis has been to present a formula-based framework that can be used to determine the electrical output of a transparent luminescent solar concentrator system. The proposed framework was then tested on a reference building façade. PVsyst software was further used to simulate the operation of the solar system in actual scenarios. Although the harvested energy from the transparent solar concentrator device was found to be insufficient for the running of the different assigned building loads, it should be noted that the produced energy was sufficient to cover almost a third of it. The tested transparent solar façade system could produce over 7700 kWh of energy annually. Comparatively speaking, the amount of energy produced from the system could potentially cover an even bigger load at the household level.

Overall, this thesis has explored the different emerging and prevailing photovoltaic technologies, with an emphasis on transparent photovoltaics. It has been noted most of the research efforts were mainly focused on advancing conventional wafer-based technologies. This is evidenced by the power conversion efficiencies tending towards the Shockley–Queisser limit for these conventional PV systems.

It is quite evident that there is a need for even more research efforts to be turned towards the advancement of transparent photovoltaics to expedite their development

and integration in buildings. For instance, one of the most outstanding issues related to transparent photovoltaics that was also experienced during this study is the lack of good modelling tools specific to assessing this technology. Evident insufficiency in such a critical aspect of any technology could delay its acceptance and adoption, therefore, revealing the need for more research efforts to be invested. Thus, endeavours that will make the technology more acceptable in the construction sector especially will play a major role in expediting its adoption. The development of assessment tools for transparent solar technologies that can be integrated with existing building construction software could be a good starting point as these would make assessing the feasibility of adopting the technology easy for practitioners such as building designers, thus making this infant technology more acceptable within the industry.

REFERENCES

Abolhosseini, S., Heshmati, A., & Altmann, J. (2014). *A Review of Renewable Energy Supply and Energy Efficiency Technologies*. *8145*.

Akbari, H., Browne, M. C., Ortega, A., Huang, M. J., Hewitt, N. J., Norton, B., & McCormack, S. J. (2019). Efficient energy storage technologies for photovoltaic systems. *Solar Energy*, *192*(November 2017), 144–168. https://doi.org/10.1016/j.solener.2018.03.052

Alanne, K., & Cao, S. (2019). An overview of the concept and technology of ubiquitous energy. *Applied Energy*, *238*(June 2018), 284–302. https://doi.org/10.1016/j.apenergy.2019.01.100

Alba Energy. (2018). *Colors Of Solar Panels – What Are the Differences | Alba Solar Energy*. https://albaenergy.com/colors-of-solar-panels-what-are-the-differences/

Ball, J. M., Stranks, S. D., Hörantner, M. T., Hüttner, S., Zhang, W., Crossland, E. J. W., Ramirez, I., Riede, M., Johnston, M. B., Friend, R. H., & Snaith, H. J. (2015). Optical properties and limiting photocurrent of thin-film perovskite solar cells. *Energy and Environmental Science*, *8*(2), 602–609. https://doi.org/10.1039/c4ee03224a

Barry, T. (2018). *Thin Film Solar Panels For Cost Effective Solar Energy Production*. https://www.sunpowersource.com/thin-film-solar-panels/

Basol, B. M., & McCandless, B. (2014). Brief review of cadmium telluride-based photovoltaic technologies. *Journal of Photonics for Energy*, *4*(1), 040996. https://doi.org/10.1117/1.jpe.4.040996

Batchelder, J. S., Zewail, A. H., & Cole, T. (1979). Luminescent solar concentrators. 1: Theory of operation and techniques for performance evaluation. *Applied Optics*, *18*(18), 3090–3110. http://eutils.ncbi.nlm.nih.gov/entrez/eutils/elink.fcgi?dbfrom=pubmed&id=2021

2810&retmode=ref&cmd=prlinks%0Apapers2://publication/uuid/A360C702-E14B-447B-A22D-4A8EB60A9A7A

Baum, R. (2017). *LIGHT-TRANSMISSIVE PHOTOVOLTAIC (LTPV). March*.

Benedek, J., Sebestyén, T. T., & Bartók, B. (2018). Evaluation of renewable energy sources in peripheral areas and renewable energy-based rural development. *Renewable and Sustainable Energy Reviews*, *90*(October 2016), 516–535. https://doi.org/10.1016/j.rser.2018.03.020

Bergmann, R. B., & Werner, J. H. (2002). The future of crystalline silicon films on foreign substrates. *Thin Solid Films*, *403–404*, 162–169. https://doi.org/10.1016/S0040-6090(01)01556-5

Bergren, M. R., Makarov, N. S., Ramasamy, K., Jackson, A., Guglielmetti, R., & McDaniel, H. (2018). High-Performance CuInS2 Quantum Dot Laminated Glass Luminescent Solar Concentrators for Windows. *ACS Energy Letters*, *3*(3), 520–525. https://doi.org/10.1021/acsenergylett.7b01346

Bernardi, M., Ferralis, N., Wan, J. H., Villalon, R., & Grossman, J. C. (2012). Solar energy generation in three dimensions. *Energy and Environmental Science*, *5*(5), 6880–6884. https://doi.org/10.1039/c2ee21170j

Business Wire. (2020, January 30). *Ubiquitous Energy Installs First Transparent Solar Window Façade | Business Wire*. https://www.businesswire.com/news/home/20200130005187/en/Ubiquitous-Energy-Installs-First-Transparent-Solar-Window-Façade

Cole, L. (2021, January 30). *Solar entry: Aussie shopping centre starts world-first power trial*. https://www.smh.com.au/business/the-economy/solar-entry-aussie-shopping-centre-starts-world-first-power-trial-20190130-p50uii.html

Cook, A. G., Billman, L., & Adcock, R. (n.d.). *Acknowledgements*.

Corrado, C., Leow, S. W., Osborn, M., & I. Carbone, K. Hellier, M. Short, G. Alers,

S. A. C. (2014). Power generation study of Luminescent Solar Concentrator greenhouse. *Paper Knowledge . Toward a Media History of Documents*, *5*(2), 40–51.

Dagar, J., Castro-Hermosa, S., Lucarelli, G., Cacialli, F., & Brown, T. M. (2018). Highly efficient perovskite solar cells for light harvesting under indoor illumination via solution processed SnO2/MgO composite electron transport layers. *Nano Energy*, *49*(April), 290–299. https://doi.org/10.1016/j.nanoen.2018.04.027

Daniel, A. (2014). *pvtrace: Release to enable DOI integration | Zenodo*. Pvtrace: Release to Enable DOI Integration. https://zenodo.org/record/12820#.YcSGQmhBxPZ

Debije, M. G. (2010). Solar energy collectors with tunable transmission. *Advanced Functional Materials*, *20*(9), 1498–1502. https://doi.org/10.1002/adfm.200902403

Debije, M. G., & Verbunt, P. P. C. (2012). Thirty years of luminescent solar concentrator research: Solar energy for the built environment. *Advanced Energy Materials*, *2*(1), 12–35. https://doi.org/10.1002/aenm.201100554

Dricus, D. R. (n.d.). *Colored Solar Cells: specialities and limitations*. Retrieved May 16, 2021, from https://sinovoltaics.com/learning-center/solar-cells/colored-solar-cells-specialities-and-limitations/

Eder, G., Peharz, G., Trattnig, R., Bonomo, P., Saretta, E., Frontini, F., Polo Lopez, C. S., Rose Wilson, H., Eisenlohr, J., Martín Chivelet, N., Karlsson, S., Jakica, N., & Zanelli, A. (2019). *COLOURED BIPV Market, research and development IEA PVPS Task 15, Report IEA-PVPS T15-07: 2019*. http://iea-pvps.org/index.php?id=task15

Edinburgh Instruments. (n.d.). *Beer Lambert Law | Transmittance & Absorbance | Edinburgh Instruments*. Retrieved November 17, 2021, from

https://www.edinst.com/blog/the-beer-lambert-law/

EIA. (2021). *Preliminary Monthly Electric Generator Inventory (based on Form EIA-860M as a supplement to Form EIA-860) - U.S. Energy Information Administration (EIA)*. ELECTRICITY. https://www.eia.gov/electricity/data/eia860m/

EPIA. (2014). Global Market Outlook For Photovoltaics 2014-2018. *Encyclopedia of Governance*. https://doi.org/10.4135/9781412952613.n215

Eric Wesoff. (2020, April 9). *Ubiquitous Energy's clear solar windows harvest UV and IR light — an update – pv magazine USA*. https://pv-magazine-usa.com/2020/04/09/ubiquitous-energys-clear-windows-harvest-uv-and-ir-light-an-update/

Fatemi Shariat Panahi, S. R., Abbasi, A., Ghods, V., & Amirahmadi, M. (2020). Analysis and improvement of CIGS solar cell efficiency using multiple absorber substances simultaneously. *Journal of Materials Science: Materials in Electronics*, *31*(14), 11527–11537. https://doi.org/10.1007/s10854-020-03700-4

Gambhir, A., Sandwell, P., & Nelson, J. (2016). The future costs of OPV – A bottom-up model of material and manufacturing costs with uncertainty analysis. *Solar Energy Materials and Solar Cells*, *156*, 49–58. https://doi.org/10.1016/j.solmat.2016.05.056

Gochermann Solar Technology. (n.d.). *Non-reflective Module Surface – Gochermann Solar Technology*. Retrieved February 7, 2021, from https://www.gochermann.com/non-reflective-module-surface/

Goetzberger, A., & Greube, W. (1977). Solar energy conversion with fluorescent collectors. *Applied Physics*, *14*(2), 123–139. https://doi.org/10.1007/BF00883080

Goldschmidt, J. C., Peters, M., Bösch, A., Helmers, H., Dimroth, F., Glunz, S. W., & Willeke, G. (2009). Increasing the efficiency of fluorescent concentrator

systems. *Solar Energy Materials and Solar Cells*, *93*(2), 176–182. https://doi.org/10.1016/j.solmat.2008.09.048

Green, M. A. (2015). The Passivated Emitter and Rear Cell (PERC): From conception to mass production. *Solar Energy Materials and Solar Cells*, *143*, 190–197. https://doi.org/10.1016/j.solmat.2015.06.055

Green, M. A., Dunlop, E. D., Hohl-Ebinger, J., Yoshita, M., Kopidakis, N., & Ho-Baillie, A. W. Y. (2020). Solar cell efficiency tables (Version 55). *Progress in Photovoltaics: Research and Applications*, *28*(1), 3–15. https://doi.org/10.1002/pip.3228

GREEN, M., EMERY, K., HISHIKAWA, Y., WARTA, W., DUNLOP, E., BARKHOUSE, D., GUNAWAN, O., GOKMEN, T., TODOROV, T., & MITZI, D. (2012). Solar cell efficiency tables (version 40). *Ieee Trans Fuzzy Syst*, *20*(6), 1114–1129. https://doi.org/10.1002/pip

He, Y., Liu, J., Sung, S. J., & Chang, C. hung. (2021). Downshifting and antireflective thin films for solar module power enhancement. *Materials & Design*, *201*, 109454. https://doi.org/10.1016/J.MATDES.2021.109454

Heinstein, P., Ballif, C., & Perret-Aebi, L. E. (2013). Building integrated photovoltaics (BIPV): Review, potentials, barriers and myths. *Green*, *3*(2), 125–156. https://doi.org/10.1515/green-2013-0020

Huang, Y. T., Kavanagh, S. R., Scanlon, D. O., Walsh, A., & Hoye, R. L. Z. (2021). Perovskite-inspired materials for photovoltaics and beyond-from design to devices. *Nanotechnology*, *32*(13). https://doi.org/10.1088/1361-6528/abcf6d

IEA, I. E. A. (2014). *IEA Technology Roadmap*.

Insolation. (2011). *Encyclopedia of Earth Sciences Series*, *Part 4*, 393. https://doi.org/10.2307/40127766

Irwan, Y. M., Amelia, A. R., Irwanto, M., Fareq, M., Leow, W. Z., Gomesh, N., &

Safwati, I. (2015). Stand-Alone Photovoltaic (SAPV) System Assessment using PVSYST Software. In *Energy Procedia* (Vol. 79). Elsevier B.V. https://doi.org/10.1016/j.egypro.2015.11.539

ISE, F. I. F. O. S. Ener. S. (2014). *Fraunhofer ISE, 2014/15*.

Janez, K., & Marko, T. (2013). *Optical Modeling and Simulation of Thin-Film Photovoltaic Devices - Janez Krc, Marko Topic - Google Books*. https://books.google.com.tr/books?id=QjHNBQAAQBAJ&printsec=frontcover&source=gbs_ge_summary_r&cad=0#v=onepage&q&f=false

Jelle, B. P., Breivik, C., & Drolsum Røkenes, H. (2012). Building integrated photovoltaic products: A state-of-the-art review and future research opportunities. *Solar Energy Materials and Solar Cells*, *100*(7465), 69–96. https://doi.org/10.1016/j.solmat.2011.12.016

Kalowekamo, J., & Baker, E. (2009). Estimating the manufacturing cost of purely organic solar cells. *Solar Energy*, *83*(8), 1224–1231. https://doi.org/10.1016/j.solener.2009.02.003

Kastelijn, M. J., Bastiaansen, C. W. M., & Debije, M. G. (2009). Influence of waveguide material on light emission in luminescent solar concentrators. *Optical Materials*, *31*(11), 1720–1722. https://doi.org/10.1016/j.optmat.2009.05.003

Kelly, P. (2018). *Onyx Solar PV glass installed in Balenciaga's new storefront in Miami*. https://www.solarpowerworldonline.com/2018/04/onyx-solar-pv-glass-installed-in-balenciagas-new-storefront-in-miami/

Kim, H. S., Lee, C. R., Im, J. H., Lee, K. B., Moehl, T., Marchioro, A., Moon, S. J., Humphry-Baker, R., Yum, J. H., Moser, J. E., Grätzel, M., & Park, N. G. (2012). Lead iodide perovskite sensitized all-solid-state submicron thin film mesoscopic solar cell with efficiency exceeding 9%. *Scientific Reports*, *2*, 1–7. https://doi.org/10.1038/srep00591

Kojima, A., Teshima, K., Shirai, Y., & Miyasaka, T. (2009). Organometal halide perovskites as visible-light sensitizers for photovoltaic cells. *Journal of the American Chemical Society*, *131*(17), 6050–6051. https://doi.org/10.1021/ja809598r

Krumer, Z., van Sark, W. G. J. H. M., Schropp, R. E. I., & de Mello Donegá, C. (2017). Compensation of self-absorption losses in luminescent solar concentrators by increasing luminophore concentration. *Solar Energy Materials and Solar Cells*, *167*(April), 133–139. https://doi.org/10.1016/j.solmat.2017.04.010

Kuhn, T. E., Erban, C., Heinrich, M., Eisenlohr, J., Ensslen, F., & Neuhaus, D. H. (2020). Review of technological design options for building integrated photovoltaics (BIPV). *Energy and Buildings*, *231*, 110381. https://doi.org/10.1016/j.enbuild.2020.110381

Lamnatou, C., Notton, G., Chemisana, D., & Cristofari, C. (2020). Storage systems for building-integrated photovoltaic (BIPV) and building-integrated photovoltaic/thermal (BIPVT) installations: Environmental profile and other aspects. *Science of the Total Environment*, *699*, 134269. https://doi.org/10.1016/j.scitotenv.2019.134269

Lee, T. D., & Ebong, A. U. (2017). A review of thin film solar cell technologies and challenges. *Renewable and Sustainable Energy Reviews*, *70*(November 2016), 1286–1297. https://doi.org/10.1016/j.rser.2016.12.028

Leem, J. W., Guan, X.-Y., & Yu, J. S. (2014). Tunable distributed Bragg reflectors with wide-angle and broadband high-reflectivity using nanoporous/dense titanium dioxide film stacks for visible wavelength applications. *Optics Express*, *22*(15), 18519. https://doi.org/10.1364/oe.22.018519

Li, H., Wu, K., Lim, J., Song, H. J., & Klimov, V. I. (2016). Doctor-blade deposition of quantum dots onto standard window glass for low-loss large-area

luminescent solar concentrators. *Nature Energy*, *1*(12). https://doi.org/10.1038/nenergy.2016.157

Li, J., Aierken, A., Liu, Y., Zhuang, Y., Yang, X., Mo, J. H., Fan, R. K., Chen, Q. Y., Zhang, S. Y., Huang, Y. M., & Zhang, Q. (2021). A Brief Review of High Efficiency III-V Solar Cells for Space Application. *Frontiers in Physics*, *8*(February), 1–15. https://doi.org/10.3389/fphy.2020.631925

Li, Z., Zhang, W., Xie, L., Wang, W., Tian, H., Chen, M., & Li, J. (2021). Life cycle assessment of semi-transparent photovoltaic window applied on building. *Journal of Cleaner Production*, *295*, 126403. https://doi.org/10.1016/j.jclepro.2021.126403

Liu, G., Mazzaro, R., Wang, Y., Zhao, H., & Vomiero, A. (2019). High efficiency sandwich structure luminescent solar concentrators based on colloidal quantum dots. *Nano Energy*, *60*(March), 119–126. https://doi.org/10.1016/j.nanoen.2019.03.038

Liu, J., Yao, M., & Shen, L. (2019). Third generation photovoltaic cells based on photonic crystals. *Journal of Materials Chemistry C*, *7*(11), 3121–3145. https://doi.org/10.1039/c8tc05461d

Liu, N., Wang, L., Xu, F., Wu, J., Song, T., & Chen, Q. (2020). Recent Progress in Developing Monolithic Perovskite/Si Tandem Solar Cells. *Frontiers in Chemistry*, *8*(December), 1–22. https://doi.org/10.3389/fchem.2020.603375

Ma, H., Jen, A. K. Y., & Dalton, L. R. (2002). Polymer-based optical waveguides: Materials, processing, and devices. *Advanced Materials*, *14*(19), 1339–1365. https://doi.org/10.1002/1521-4095(20021002)14:19<1339::AID-ADMA1339>3.0.CO;2-O

Mark, B., Samantha, W., & Jarett, Z. (2015). Is $50/MWh solar for real? Falling project prices and rising capacity factors drive utility-scale PV toward economic competitiveness. *Progress in Photovoltaics*, *20*(6), 1114–1129.

https://doi.org/10.1002/pip

Market Analysis Report. (2020, September). *Dye Sensitized Solar Cell Market Growth Report, 2020-2027*. https://www.grandviewresearch.com/industry-analysis/dye-sensitized-solar-cell-market

Meinardi, F., Ehrenberg, S., Dhamo, L., Carulli, F., Mauri, M., Bruni, F., Simonutti, R., Kortshagen, U., & Brovelli, S. (2017). Highly efficient luminescent solar concentrators based on earth-Abundant indirect-bandgap silicon quantum dots. *Nature Photonics*, *11*(3), 177–185. https://doi.org/10.1038/nphoton.2017.5

Meteonorm. (n.d.). *Meteonorm Software - Meteonorm (en)*. Retrieved February 23, 2022, from https://meteonorm.com/en/product/meteonorm-software

Michael, B. (2021). *ClearVue Solar Glass Greenhouse Officially Opened - Solar Quotes Blog*. https://www.solarquotes.com.au/blog/clearvue-solar-greenhouse-mb1962/

Mittag, M., Reise, C., Wöhrle, N., Eberle, R., Schubert, M., & Heinrich, M. (2018). Approach for a Holistic Optimization from Wafer to PV System. *2018 IEEE 7th World Conference on Photovoltaic Energy Conversion, WCPEC 2018 - A Joint Conference of 45th IEEE PVSC, 28th PVSEC and 34th EU PVSEC*, 3194–3199. https://doi.org/10.1109/PVSC.2018.8547350

Mondon, A., Klasen, N., Fokuhl, E., Mittag, M., Heinrich, M., & Wirth, H. (2018). *Comparison of Layouts for Shingled Bifacial PV modules in Terms of Power Output, Cell-to-Module Ratio and Bifaciality*. 24–28.

Moraitis, P., Schropp, R. E. I., & van Sark, W. G. J. H. M. (2018). Nanoparticles for Luminescent Solar Concentrators - A review. *Optical Materials*, *84*(July), 636–645. https://doi.org/10.1016/j.optmat.2018.07.034

Morini, M. (2021). *ARCHITECTURE AND PHOTOVOLTAICS: Strategies, technologies and novel components for the building envelope*.

Nancy, S. (2013). Transparent, near-infrared organic photovoltaic solar cells for window and energy-scavenging applications. *MIT Energy Initiative*, *98*(11). https://doi.org/10.1063/1.3567516

NS Energy. (2021). *Top five countries with the largest installed solar power capacity*. NS Energy. https://www.nsenergybusiness.com/features/solar-power-countries-installed-capacity/

OECD. (2012). *CITE AS Linking Renewable Energy to Rural Development*. http://dx.doi.org/10.1787/9789264180444-en

Oliveti, G., Marletta, L., Arcuri, N., De Simone, M., Bruno, R., & Evola, G. (2014). Solar energy. *Green Energy and Technology*, *0*(9783319030739), 159–214. https://doi.org/10.1007/978-3-319-03074-6_4

Olivieri, L., Caamaño-Martín, E., Moralejo-Vázquez, F. J., Martín-Chivelet, N., Olivieri, F., & Neila-Gonzalez, F. J. (2014). Energy saving potential of semi-transparent photovoltaic elements for building integration. *Energy*, *76*, 572–583. https://doi.org/10.1016/j.energy.2014.08.054

Olson, R. W., Loring, R. F., & Fayer, M. D. (1981). Luminescent solar concentrators and the reabsorption problem. *Applied Optics*, *20*(17), 2934. https://doi.org/10.1364/ao.20.002934

Ossila. (2021). *Perovskites Solar Cell Structure, Efficiency & More | Ossila*. https://www.ossila.com/pages/perovskites-and-perovskite-solar-cells-an-introduction

Paire, M., Delbos, S., Vidal, J., Naghavi, N., & Guillemoles, J. F. (2014). Chalcogenide Thin-Film Solar Cells. In *Solar Cell Materials: Developing Technologies* (Vol. 9780470065). https://doi.org/10.1002/9781118695784.ch7

Pickerel, K. (2018). *What is a half-cell solar panel?* https://www.solarpowerworldonline.com/2018/10/what-is-a-half-cell-solar-panel/

Pulli, E., Rozzi, E., & Bella, F. (2020). Transparent photovoltaic technologies: Current trends towards upscaling. *Energy Conversion and Management*, *219*(June), 112982. https://doi.org/10.1016/j.enconman.2020.112982

Pv, E., & Energy, S. (2018). *Presented at the 35th European PV Solar Energy Conference and Exhibition, 24-28 September, 2018, Brussels, Belgium*. *September*, 24–28.

Reinders, A. H. M. E., De La Gree, G. D., Papadopoulos, A., Rosemann, A., Debije, M. G., Cox, M., & Krumer, Z. (2017). Leaf roof - Designing luminescent solar concentrating PV roof tiles. *2017 IEEE 44th Photovoltaic Specialist Conference, PVSC 2017*, 1–5. https://doi.org/10.1109/PVSC.2017.8366810

Ren, G., Ma, G., & Cong, N. (2015). Review of electrical energy storage system for vehicular applications. *Renewable and Sustainable Energy Reviews*, *41*, 225–236. https://doi.org/10.1016/j.rser.2014.08.003

Roncali, J., & Garnier, F. (1984). Photon-transport properties of luminescent solar concentrators: analysis and optimization. *Applied Optics*, *23*(16), 2809. https://doi.org/10.1364/ao.23.002809

Sharma, K., Sharma, V., & Sharma, S. S. (2018). Dye-Sensitized Solar Cells: Fundamentals and Current Status. *Nanoscale Research Letters*, *13*. https://doi.org/10.1186/s11671-018-2760-6

Silvia, C., Sebastian, F. V., & Juan, L. D. (2015). Understanding the Outstanding PowerConversion Efficiency of Perovskite-Based Solar Cells. *Scientific Reports*, *2*, 9757–9759. https://doi.org/10.1038/srep00591

Singh, B. P., Goyal, S. K., & Kumar, P. (2021). Solar PV cell materials and technologies: Analyzing the recent developments. *Materials Today: Proceedings*, *43*, 2843–2849. https://doi.org/10.1016/j.matpr.2021.01.003

Slooff, L. H., Bende, E. E., Burgers, A. R., Budel, T., Pravettoni, M., Kenny, R. P., Dunlop, E. D., & Büchtemann, A. (2008). A Luminescent Solar Concentrator

with 7.1% power conversion efficiency. *Physica Status Solidi - Rapid Research Letters*, *2*(6), 257–259. https://doi.org/10.1002/pssr.200802186

Solar Energy Technology Office. (2019). *Cadmium Telluride | Department of Energy*. https://www.energy.gov/eere/solar/cadmium-telluride

Solaredge. (2010). *Technical Note Bypass Diode Effects in Shaded Conditions*. https://www.google.fr/search?q=http://www.solaredge.com/files/pdfs/se_technical_bypass_diode_effect_in_shading.pdf&ie=utf-8&oe=utf-8&aq=t&rls=org.mozilla:fr:official&client=firefox-a#client=firefox-a&hs=kMb&hl=fr&rls=org.mozilla:fr:official&sclient=psy-ab

Soltecture. (n.d.). *Soltecture » CIS = CIGS & CIGSe*. Retrieved May 19, 2021, from http://www.soltecture.com/technology/cis-cigs-cigse.html

Sophie, V. (2021, April 20). *ClearVue completes world's first solar glass greenhouse in Perth | RenewEconomy*. https://reneweconomy.com.au/clearvue-completes-worlds-first-solar-glass-greenhouse-in-perth/

Spectra, P. (2021). *10.6: Photoluminescence Spectroscopy*. 1–11.

Stadler, A. (2012). Transparent Conducting Oxides—An Up-To-Date Overview. *Materials*, *5*(12), 661–683. https://doi.org/10.3390/ma5040661

Subtil Lacerda, J., & Van Den Bergh, J. C. J. M. (2016). Diversity in solar photovoltaic energy: Implications for innovation and policy. *Renewable and Sustainable Energy Reviews*, *54*, 331–340. https://doi.org/10.1016/j.rser.2015.10.032

Traverse, C. J., Pandey, R., Barr, M. C., & Lunt, R. R. (2017). Emergence of highly transparent photovoltaics for distributed applications. *Nature Energy*, *2*(11), 849–860. https://doi.org/10.1038/s41560-017-0016-9

Tummeltshammer, C., Taylor, A., Kenyon, A. J., & Papakonstantinou, I. (2016). Losses in luminescent solar concentrators unveiled. *Solar Energy Materials and*

Solar Cells, *144*, 40–47. https://doi.org/10.1016/j.solmat.2015.08.008

Ubiquitous Energy. (2020, April 9). *INSTALLATION AT UBIQUITOUS ENERGY HQ; REDWOOD CITY CA*. https://ubiquitous.energy/example-installations/

UNEP, (United Nations Environmental Programme), ILO, (International Labor Organization), IOE, (International Organisation of Employers), & Confederation), I. (International T. U. (2008). *Green Jobs: Towards Decent Work in a Sustainable, Low Carbon World, United Nations Office at Nairobi (UNON), Nairobi*.

van Sark, W. G. J. H. M. (2013). Luminescent solar concentrators - A low cost photovoltaics alternative. *Renewable Energy*, *49*, 207–210. https://doi.org/10.1016/j.renene.2012.01.030

Vernon, G. (2021, April 28). *New solar greenhouse with a window to the future opens in Perth | Farm Online | Australia*. https://www.farmonline.com.au/story/7227658/a-world-first-greenhouse-with-a-clear-view-to-the-future/

Weber, & John, L. (1976). *Luminescent greenhouse collector for solar radiation*. *15*(10), 3–4.

Weniger, J., Tjaden, T., & Quaschning, V. (2014). Sizing of residential PV battery systems. *Energy Procedia*, *46*, 78–87. https://doi.org/10.1016/j.egypro.2014.01.160

Wilson, L. R., & Richards, B. S. (2009). Measurement method for photoluminescent quantum yields of fluorescent organic dyes in polymethyl methacrylate for luminescent solar concentrators. *Applied Optics*, *48*(2), 212–220. https://doi.org/10.1364/AO.48.000212

Xue, Q., Xia, R., Brabec, C. J., & Yip, H.-L. (2018). Recent advances in semi-transparent polymer and perovskite solar cells for power generating window applications. *1688 | Energy Environ. Sci*, *11*, 1688.

https://doi.org/10.1039/c8ee00154e

Yamaguchi, M. (2020). High-Efficiency GaAs-Based Solar Cells. *Post-Transition Metals*. https://doi.org/10.5772/INTECHOPEN.94365

Yang, C., & Lunt, R. R. (2017). Limits of Visibly Transparent Luminescent Solar Concentrators. *Advanced Optical Materials*, *5*(8), 1–10. https://doi.org/10.1002/adom.201600851

Zettl, M., Mayer, O., Klampaftis, E., & Richards, B. S. (2017). Investigation of Host Polymers for Luminescent Solar Concentrators. *Energy Technology*, *5*(7), 1037–1044. https://doi.org/10.1002/ente.201600498

Zhao, Y., Meek, G. A., Levine, B. G., & Lunt, R. R. (2014). Near-infrared harvesting transparent luminescent solar concentrators. *Advanced Optical Materials*, *2*(7), 606–611. https://doi.org/10.1002/adom.201400103